Charles University
2nd Faculty of Medicine

Neurosciences

Mgr. Ján Kriška

Úloha Wnt signalizační dráhy v regeneraci ischemicky poškozené nervové tkáně

The role of the Wnt signaling pathway in the regeneration following ischemic brain injury

PhD thesis

Supervisor: Ing. Miroslava Anděrová, CSc.

Prague 2020

Prohlášení

Prohlašuji, že jsem závěrečnou práci zpracoval samostatně a že jsem řádně uvedl a citoval všechny použité prameny a literaturu. Současně prohlašuji, že práce nebyla využita k získání jiného nebo stejného titulu.

Souhlasím s trvalým uložením elektronické verze mé práce v databázi systému meziuniverzitního projektu Theses.cz za účelem soustavné kontroly podobnosti kvalifikačních prací.

V Praze, 23. 3. 2020 Ján Kriška

Identifikační záznam

KRIŠKA, Ján. *Úloha Wnt signalizační dráhy v regeneraci ischemicky poškozené nervové tkáně. [The role of the Wnt signaling pathway in the regeneration following ischemic brain injury]*. Praha, 2020. 154 stran, 3 přílohy. Disertační práce (Ph.D.). Univerzita Karlova, 2. lékařská fakulta. Vedoucí závěrečné práce Ing. Miroslava Anděrová, CSc.

Acknowledgements

I would like to express my sincere thanks to my supervisor, Dr. Miroslava Anděrová, for her help, useful comments, and infinite patience, as well as to my colleagues, who also became my friends, for helping me with the experiments, and for creating such a wonderful and warm working environment in our laboratory. Last but not least, this work would not see the light of day without the financial support provided by the Czech Science Foundation (grant numbers P304/12/G069 and 17-04034S) and the Charles University Grant Agency (grant number 26214).

Author's publications

Publications related to the thesis and contributions of individual co-authors:

1.) **Kriska J**, Honsa P, Dzamba D, Butenko O, Kolenicova D, Janeckova L, Nahacka Z, Andera L, Kozmik Z, Taketo MM, Korinek V, Anderova M. (2016) Manipulating Wnt signaling at different subcellular levels affects the fate of neonatal neural stem/progenitor cells. Brain Res. 2016 Nov 15;1651:73-87. doi: 10.1016/j.brainres.2016.09.026. Epub 2016 Sep 19.; **IF 2.746**

CONTRIBUTIONS:

Animal breeding: Janeckova L, Kozmik Z, Taketo MM, Korinek V

Tissue isolation and cell cultures preparation: Kriska J

Electrophysiological analyses: Kriska J, Honsa P, Dzamba D, Butenko O, Kolenicova D

Immunohistochemical analysis and confocal microscopy: Kriska J, Dzamba D, Butenko O, Janeckova L

Reverse transcription quantitative polymerase chain reaction experiments: Janeckova L

Western blotting experiments: Janeckova L, Nahacka Z

Data analysis and evaluation: Kriska J, Dzamba D, Butenko O, Janeckova L, Nahacka Z, Korinek V, Anderova M

Supervision: Andera L, Korinek V, Anderova M

Manuscript preparation and editing: Kriska J, Dzamba D, Janeckova L, Taketo MM, Korinek V, Anderova M

2.) Honsa P, Valny M, **Kriska J**, Matuskova H, Harantova L, Kirdajova D, Valihrach L, Androvic P, Kubista M, Anderova M. (2016) Generation of reactive astrocytes from NG2 cells is regulated by sonic hedgehog. Glia. 2016 Sep;64(9):1518-31. doi: 10.1002/glia.23019. Epub 2016 Jun 24.; **IF 6.200**

CONTRIBUTIONS:

Animal breeding: Honsa P

Animal surgery: Honsa P, Valny M, Kirdajova D

Tissue isolation and cell cultures preparation: Honsa P, Kriska J, Harantova L

Electrophysiological analyses: Honsa P, Valny M, Kriska J

Immunohistochemical analysis and confocal microscopy: Honsa P, Valny M, Matuskova H

Reverse transcription quantitative polymerase chain reaction experiments: Valihrach L, Androvic P, Kubista M

Data analysis and evaluation: Honsa P, Valny M, Kriska J, Harantova L, Valihrach L, Androvic P, Anderova M

Supervision: Kubista M, Anderova M

Manuscript preparation and editing: Honsa P, Kubista M, Anderova M

3.) Valny M, Honsa P, Waloschkova E, Matuskova H, **Kriska J**, Kirdajova D, Androvic P, Valihrach L, Kubista M, Anderova M. (2018) A single-cell analysis reveals multiple roles of oligodendroglial lineage cells during post-ischemic regeneration. Glia. 2018 May;66(5):1068-1081. doi: 10.1002/glia.23301. Epub 2018 Feb 2.; **IF 5.829**

CONTRIBUTIONS:

Animal breeding: Valny M, Honsa P

Animal surgery: Valny M, Honsa P, Waloschkova E, Matuskova H

Tissue isolation and cell cultures preparation: Valny M, Honsa P, Kriska J, Kirdajova D

Immunohistochemical analysis and confocal microscopy: Valny M, Honsa P, Waloschkova E, Matuskova H

Reverse transcription quantitative polymerase chain reaction experiments: Androvic P, Valihrach L, Kubista M

Data analysis and evaluation: Valny M, Honsa P, Androvic P, Valihrach L, Anderova M

Supervision: Kubista M, Anderova M

Manuscript preparation and editing: Valny M, Anderova M

Other author's publications:

4.) Belov Kirdajova D, **Kriska J**, Tureckova J, Anderova M. (2020) Ischemia-triggered glutamate excitotoxicity from the perspective of glial cells. Front Cell Neurosci. 2020 Mar 19;14(51):1-27. doi: 10.3389/fncel.2020.00051.; **IF (2018) 3.900**

5.) Kolenicova D, Tureckova J, Pukajova B, Harantova L, **Kriska J**, Kirdajova D, Vorisek I, Kamenicka M, Valihrach L, Androvic P, Kubista M, Vargova L, Anderova M. (2020) High potassium exposure reveals the altered ability of astrocytes to regulate their

volume in the aged hippocampus of GFAP/EGFP mice. Neurobiol Aging. 2020 Feb;86:162-181. doi: 10.1016/j.neurobiolaging.2019.10.009. Epub 2019 Oct 22.; **IF (2018) 4.398**

6.) Valny M, Honsa P, **Kriska J**, Anderova M. (2017) Multipotency and therapeutic potential of NG2 cells. Biochem Pharmacol. 2017 Oct 1;141:42-55. doi: 10.1016/j.bcp.2017.05.008. Epub 2017 May 15. Review.; **IF 4.235**

7.) Dzamba D, Honsa P, Valny M, **Kriska J**, Valihrach L, Novosadova V, Kubista M, Anderova M. (2015) Quantitative Analysis of Glutamate Receptors in Glial Cells from the Cortex of GFAP/EGFP Mice Following Ischemic Injury: Focus on NMDA Receptors. Cell Mol Neurobiol. 2015 Nov;35(8):1187-202. doi: 10.1007/s10571-015-0212-8. Epub 2015 May 21.; **IF 2.328**

8.) Anderova M, Benesova J, Mikesova M, Dzamba D, Honsa P, **Kriska J**, Butenko O, Novosadova V, Valihrach L, Kubista M, Dmytrenko L, Cicanic M, Vargova L. (2014) Altered astrocytic swelling in the cortex of α-syntrophin-negative GFAP/EGFP mice. PLoS One. 2014 Nov 26;9(11):e113444. doi: 10.1371/journal.pone.0113444. eCollection 2014. Erratum in: PLoS One. 2015;10(3):e0119744.; **IF 3.234**

9.) Honsa P, Pivonkova H, Harantova L, Butenko O, **Kriska J**, Dzamba D, Rusnakova V, Valihrach L, Kubista M, Anderova M. (2014) Increased expression of hyperpolarization-activated cyclic nucleotide-gated (HCN) channels in reactive astrocytes following ischemia. Glia. 2014 Dec;62(12):2004-21. doi: 10.1002/glia.22721. Epub 2014 Jul 14.; **IF 6.031**

Table of contents

List of abbreviations

4OHT	(Z)-4-hydroxytamoxifen
A-NG2 cells	astrocyte-like NG2 cells
A488/594/660	Alexa Fluor (hydrazide) 488/594/660
AA	acrylamide
aCSF	artificial cerebrospinal fluid
Actb	gene encoding β-actin
AF488	Alexa Fluor 488 hydrazide
Aldh1l1	gene encoding 10-formyltetrahydrofolate dehydrogenase
AMPA	α-amino-3-hydroxy-5-methyl-4-isoxazolepropionic acid
APC	adenomatous polyposis coli
Aqp4	gene encoding aquaporin-4
ATP	adenosine triphosphate
β-act	β-actin
β-cat	β-catenin
βIIItub	β III tubulin
B27	supplement B27
BBB	blood–brain barrier
BCL9	B cell lymphoma 9
BF-NG2 cells	*bona fide* NG2 cells
bFGF	fibroblast growth factor-basic
BIS	bisacrylamide
BL	basal lamina
BMP	bone morphogenetic protein
BP	band-pass
BrdU	5-bromo-2'-deoxyuridine
BSA	bovine serum albumin
BV	blood vessel
c.p.	current pattern
Ca^{2+}	calcium
CBF	cerebral blood flow
CC1	adenomatous polyposis coli clone CC1
Ccnd1	gene encoding cyclin D1

cDNA	complementary DNA
Ck1	casein kinase 1
Cldn11	gene encoding claudin-11
C_m	membrane capacitance
Cnp	gene encoding 2',3'-cyclic nucleotide 3'-phosphodiesterase; CNPase
CNS	central nervous system
CO	corn oil
CO_2	carbon dioxide
com	cells with a complex current pattern/profile
Cre	Cre recombinase
CreERT2	Cre recombinase fused with a mutated form of estrogen receptor
CreEsr1	Cre recombinase fused with a mutated form of estrogen receptor
Cspg4	chondroitin sulfate proteoglycan 4
Cspg4$^+$	chondroitin sulfate proteoglycan 4-positive
C_t	cycle threshold
Ctnnb1	gene encoding β-catenin
CTRL	control (non-operated)
Cy3	cyanine dye 3
Cyc	cyclopamine
D3/4/7/14	day 3/4/7/14
DAPI	4′,6-diamidino-2-phenylindole
DCX	doublecortin
del	deletion
Dkk1	Dickkopf 1
DMEM/F12	Dulbecco's Modified Eagle Medium/Nutrient Mixture F12
dn	dominant negative
DNA	deoxyribonucleic acid
DNase	deoxyribonuclease
Dvl	dishevelled
E2-10	exon 2-10
EAAT1	excitatory amino acid transporter 1
EAAT2	excitatory amino acid transporter 2
ECL	enhanced chemiluminescence
EDTA	ethylenediaminetetraacetic acid

EdU	5-ethynyl-2´-deoxyuridine
EGF	epidermal growth factor
EGFP	enhanced green fluorescent protein
EGFR	epidermal growth factor receptor
EGTA	ethylene glycol-bis(β-aminoethyl ether)-N,N,N′,N′-tetraacetic acid
ERT2	mutant form of estrogen receptor
Esr1	estrogen receptor 1
EtOH	ethanol (controls)
Ex3	exon 3
F	fluorescence intensity
F_0	baseline fluorescence intensity
FACS	fluorescence-activated cell sorting
FBS	fetal bovine serum
FCI 3/4/7/14	focal cerebral ischemia, after 3/4/7/14 days
FGF	fibroblast growth factor
FP	forward primer
GABA	gamma-aminobutyric acid
GAPDH	gene encoding glyceraldehyde-3-phosphate dehydrogenase
GCI	global cerebral ischemia
GFAP	glial fibrillary acidic protein
GLAST-1	glutamate aspartate transporter 1
GLI	glioma-associated oncogene
GLT-1	glutamate transporter 1
Glu	glutamate
Glul	gene encoding glutamate-ammonia ligase (glutamine synthetase)
Gria2/3	glutamate ionotropic receptor AMPA type subunit 2/3
Grik1/3	glutamate ionotropic receptor kainate type subunit 1/3
Grin1/2d/3a	glutamate ionotropic receptor NMDA type subunit 1/2d/3
Grm3/5/7	glutamate metabotropic receptor 3/5/7
GS	glutamine synthetase
GSK-3β	glycogen synthase kinase 3β
HEPES	4-(2-hydroxyethyl)-1-piperazineethanesulfonic acid
Hes1	gene encoding transcription factor *hairy and enhancer of split-1*
Hsp90	heat shock protein 90

i.p.	intraperitoneal
Id2	gene encoding *inhibitor of DNA binding 2*
IgG	immunoglobulin G
iPSC	induced pluripotent stem cells
IR	input resistance
K^+	potassium
K_A	fast activating and inactivating outwardly rectifying K^+ current
K_A/C_m	current density of K_A
K_{DR}	delayed outwardly rectifying K^+ current
K_{DR}/C_m	current density of K_{DR}
Ki67	gene encoding marker of proliferation (Mki67)
Kif7	kinesin-4 family protein 7
K_{IR}	inwardly rectifying K^+ current
K_{IR}/C_m	current density of K_{IR}
LEF	lymphoid enhancer factor
Lgr5	leucine-rich repeat-containing G-protein-coupled receptor 5
LP	long-pass
Lrp	low density lipoprotein receptor-related protein
LV	lateral ventricle
M	microglia
MAP2	microtubule-associated protein 2
MBP	myelin basic protein
MCA	middle cerebral artery
MCAO	middle cerebral artery occlusion
mDach1	mouse homologue of drosophila dachshund gene
Mki67	gene encoding marker of proliferation
MOSP	myelin/oligodendrocyte-specific protein
mRNA	messenger RNA
n	number of (cells, animals, sections, measurements)
Na	Na^+ current
Na^+	sodium
Na/C_m	current density of Na
Nes	gene encoding nestin
NeuN	neuronal nuclei

NeuroD	gene encoding transcription factor *neuronal differentiation*
NG2	neuron-glial antigen 2
Nkd1	gene encoding naked cuticle homolog 1
NMDA	N-methyl-D-aspartate
NMDG	N-Methyl-D-glucamine
non-P β-cat	active, non-phosphorylated β-catenin
NS/PC	neural stem/progenitor cell
NSC	neural stem cell
O4	oligodendrocyte antigen O4
OB	olfactory bulb
OD	optical density
OGB-1	Oregon-Green Bapta-1, AM calcium indicator
OL	oligodendrocyte
OL-NG2 cells	oligodendrocyte-like NG2 cells
OLIG2	oligodendrocyte transcription factor OLIG2
OPC	oligodendrocyte precursor cell
out	cells with an outwardly rectifying current pattern/profile
p	phosphorylation OR p-value (according to the context)
P-NG2 cells	proliferating NG2 cells
pA	polyadenylation site
PAGE	polyacrylamide gel electrophoresis
pas	cells with a passive current pattern/profile
pβ-cat	phosphorylated β-catenin
PB	phosphate buffer
PBS	phosphate-buffered saline
PCA	principal component analysis
PC	principal component
PCNA	proliferating cell nuclear antigen
PDGFα	platelet-derived growth factor alpha
PDGFαR	platelet-derived growth factor alpha receptor
PDGFβR	platelet-derived growth factor beta receptor
Pdgfra	gene encoding platelet-derived growth factor alpha receptor
Pdgfrb	gene encoding platelet-derived growth factor beta receptor
PFA	paraformaldehyde

PGK-Neo	neomycin resistance cassette
PKA	protein kinase A
PLL	poly-L-lysine
PMSF	phenylmethylsulfonyl fluoride
PSA	antibiotics penicillin/streptomycin/amphotericin
PTB	pentobarbital
Ptch	patched
Rack1	receptor for activated C kinase
RIPA	radio immunoprecipitation assay buffer
RMS	rostral migratory stream
RNA	ribonucleic acid
RNA-Seq	RNA sequencing
RNAi	RNA interference
ROI	region of interest
RP	reverse primer
RT-qPCR	reverse transcription quantitative polymerase chain reaction
Ryk	related to receptor tyrosine kinase
S.D.	standard deviation
S.E.M.	standard error of the mean
SAG	smoothened agonist
SDS	sodium dodecyl sulfate
sFRPs	secreted frizzled-related proteins
SGZ	subgranular zone
Shh	sonic hedgehog
siRNA	small interfering RNA
Slc1a2	gene encoding solute carrier family 1 member 2
Slc1a3	gene encoding solute carrier family 1 member 3
Smo	smoothened
SOM	self-organizing maps
SOX10	transcription factor SOX10
Sp1	transcription factor Sp1
Sp5	gene encoding SP5 transcription factor (transcriptional repressor)
SUFU	supressor of fused
SVZ	subventricular zone

TAM	tamoxifen
TCF	T-cell factor
Tcf7l2	gene encoding transcription factor 7-like 2 (Tcf4)
td	tandem dimeric, tandem dimer
Tom	fluorescent protein Tomato
$Tomato^{+}$	tomato-positive
Troy	tumor necrosis factor receptor superfamily, member 19
Trpv4	transient receptor potential cation channel subfamily V member 4
TTC	2,3,5-triphenyltetrazolium chloride
TTX	tetrodotoxin
Tuj1	class III β-tubulin
Ubb	gene encoding ubiquitin
Vim	gene encoding vimentin
V_m	membrane potential
VZ	ventricular zone
Wnt	Wingless/Integrated
Wnt3a	Wnt signaling ligand 3a
Wnt4-10b	genes encoding Wnt signaling ligands 4-10b
Wnt11	gene encoding Wnt signaling ligand 11

1 INTRODUCTION

Injuries to the brain belong to one of the leading causes of death worldwide, affecting a great number of people in developed countries and thus imposing a considerable economic burden on the society (Rajsic et al., 2019). Insufficient blood flow during cerebral ischemia, with resultant cell death, adds to neurological disorders that torment human race (Verma et al., 2018; Tannenberg et al., 2004).

Therefore, regenerative medicine looks up to new strategies for treatment or replacement of diminishing numbers of neural cells. A good example of such strategies could be the potential utilization of precursor cells, naturally residing in the brain (Groves et al., 2019; Ravanelli et al., 2018), and capable of differentiating to other cell types (Vancamp et al., 2019; Honsa et al., 2016; Kriska et al., 2016). Additionally, the proteins of the Wnt (Wingless/Integrated) and Shh (Sonic hedgehog) families regulate a number of cellular processes during embryonic development (Borday et al., 2018; Carballo et al., 2018), but they also play important roles in the cell cycle progression, differentiation of precursors, establishment of neurogenic niches, and programmed cell death after birth (Marinaro et al., 2012; Zhang et al., 1998).

The goal of the thesis was to analyze the role of cellular signaling pathways in gliogenesis and neurogenesis in the postnatal central nervous system. These signaling pathways may refine and boost the differentiation potential of precursor cells during ischemia and subsequent reperfusion, and thus enhance the regeneration of affected nervous tissue.

1.1 Ischemic brain injury

The chapters about ischemia have been already published (Belov Kirdajova et al., 2020), and the text is adapted to the nature of this thesis.

Stroke, or cerebral infarction, is one of the most common causes of mortality worldwide, as it is responsible for approximately six million deaths every year, with the lifetime risk for stroke estimated at around 9% (Woodruff et al., 2011; Seshadri et al., 2006), and ~15% mortality (Marini et al., 1999). Aging, genetic polymorphisms, and presentations of unhealthy lifestyle, such as hypertension, obesity, smoking, or shift work, are all among risk factors (Boehme et al., 2017; Brown et al., 2009). It has been reported that age-specific stroke rates are higher in men; however, women suffer from higher total number of stroke events due to their longer life expectancy and overall higher incidence

at greater age. Additionally, it has been proven that women have worse post-stroke outcomes than their male counterparts (Etherton et al., 2017; Reeves et al., 2008). Characteristic symptoms of stroke range from mild to severe and may encompass dizziness, impairments in vision or body movement, difficulty speaking, and unconsciousness (Nadarajan et al., 2014).

Ischemic stroke due to a blocked artery comprises more than 85% of all stroke incidents, while cerebral hemorrhage accounts for the rest (Woodruff et al., 2011). The most frequently affected vessel of the brain is the middle cerebral artery and its occlusion causes poor blood flow, followed by glucose and oxygen deprivation resulting in cell death, in a large lateral surface area of the brain (Puig et al., 2018) (Figure 1).

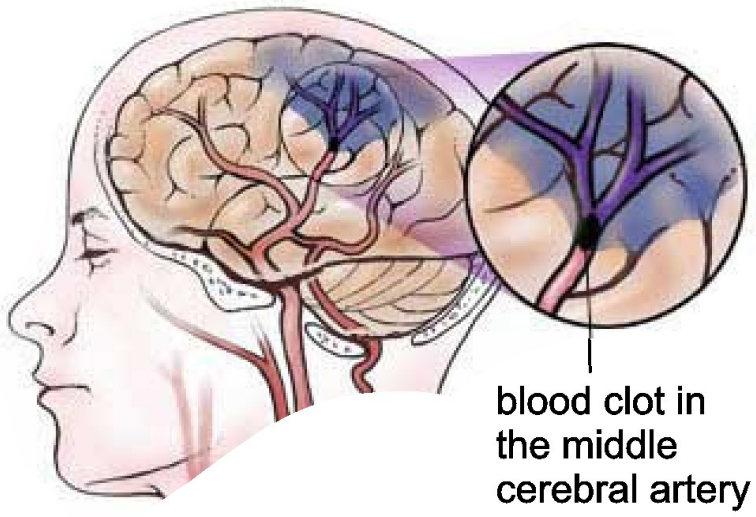

Figure 1. Ischemic stroke. Local cerebral ischemia occurs when the blood flow to the brain is restricted because of a blood clot, typically thrombus or embolus. The most frequently occluded artery is the middle cerebral artery, causing ischemic stroke, with symptoms such as sensory loss, ataxia, or speech impairments (adapted from http://brainmind.com/Stroke.html).

An apparent fall in the number of cells in the brain parenchyma is caused by its high demand of aerobic metabolism. The adult human brain represents a relatively small proportion of the body weight (only ~2%); however, it accounts for more than 20% of the whole-body energy budget (Doyle et al., 2008). Physiological cerebral blood flow (CBF) is at ~50 ml/100 g/minute and ischemic injury occurs once the CBF drops to less than 40% of its normal values (Baron, 2001; Heiss et al., 2004). As the CBF gets below 10 ml/100 g/minute, rapid irreversible damage to neurons ensues (Matsumoto et al., 1990). These irreversible changes involve a decrease in oxidative phosphorylation, adenosine triphosphate (ATP) depletion, and homeostatic imbalance of intracellular and

extracellular molecules (Figure 2), which results in excitotoxicity, oxidative stress, acidification, inflammatory response and apoptosis.

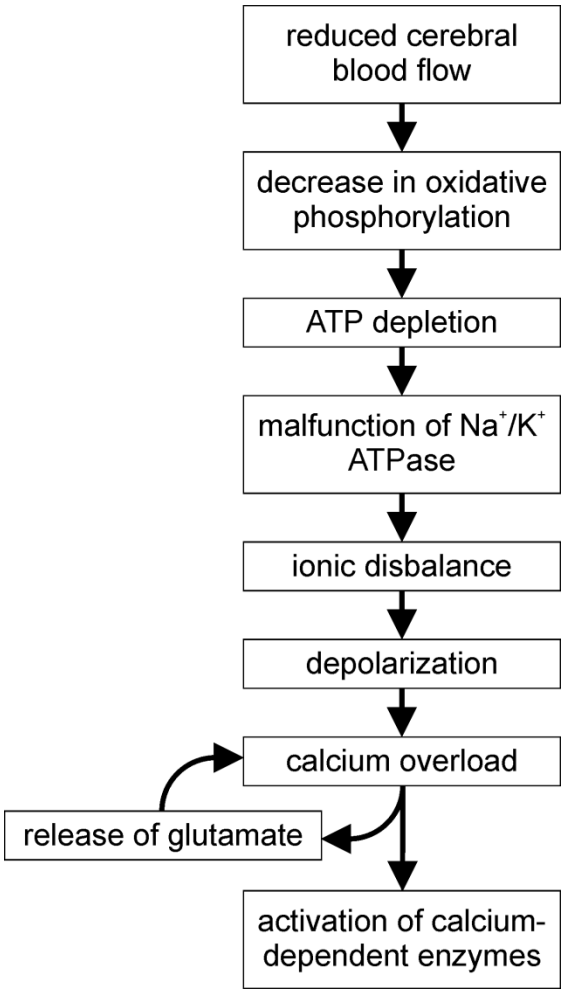

Figure 2. Ischemic cascade. Compromised blood flow to the brain causes a decrease in the adenosine triphosphate (ATP) production. Low concentration of ATP in turn negatively influences the activity of sodium-potassium (Na^+/K^+) pump, which leads to depolarization due to ionic imbalance in the intra- and extracellular space. As a result, high concentration of calcium (Ca^{2+}) triggers glutamate release and glutamate activates calcium-transmitting channels, forming thus a vicious circle of excitotoxicity. This results in the activation of downstream Ca^{2+}-dependent enzymes that are involved in processes such as inflammation and apoptosis (adapted from Rama and García (2016)).

Based on the duration of ischemia, neuronal cells die first, followed by glial cells – oligodendrocytes, astrocytes, and polydendrocytes (Caltana et al., 2009; Doyle et al., 2008; White et al., 2000). Ischemic brain injury leads to motoric, sensoric, and cognitive dysfunctions and it is accompanied by elevated neurogenesis in the hippocampus and the subventricular zone (SVZ) of the lateral ventricles (LV). Glial cells also react to ischemic injury. Astrocytes and polydendrocytes undergo reactive gliosis, which is characterized by higher proliferation rate and hypertrophy, followed by glial scar formation, which impedes regenerative axonal growth in the central nervous system (CNS), but also prevents detrimental factors from entering the compromised area (Anderova et al., 2011; Pivonkova et al., 2010; Komitova et al., 2006). Moreover, microglial cells activate and transform into phagocytic cytotoxic cells. Oligodendrocytes undergo degenerative

changes that result in the degradation of the myelin sheath covering axons (Bu et al., 2004).

Immediate restoration of blood flow with clot-dissolving (thrombolytic) drugs remains the most utilized approach trying to limit the extent of brain injury after stroke (Wardlaw et al., 2014). Nevertheless, recent studies attempt to take advantage of cell therapy, in which stem cells from various sources are used to replace damaged or dead cells in the neural tissue (Ruzicka et al., 2017). It is worth mentioning that the study of multipotent precursor cells, namely neural stem/progenitor cells (NS/PCs) and neuron-glial antigen 2 (NG2)-positive glia (also called polydendrocytes), that give rise to other cell types in the mature CNS, may provide new data on the role of these cells in the regeneration after ischemic injury of nervous tissue.

1.1.1 Focal cerebral ischemia

Based on the extent and localization, ischemic injury can be divided into two subtypes: focal and global ischemia. While global cerebral ischemia (GCI) stems from an overall decrease in blood flow in the whole parenchyma of the brain due to transient cardiac arrest, focal cerebral ischemia (FCI) is a result of an occlusion of specific arteries that supply the brain with oxygen and glucose (Yao et al., 2018).

As the name implies, FCI, or stroke, is confined to a locally defined region of the brain. This type of ischemia is usually a result of thrombosis (caused by a blood clot) or embolism (caused by a dislodged and relocated thrombus) (VanGilder et al., 2012; Figure 1). Focal cerebral ischemia may be either transient (CBF reestablished) or permanent; nevertheless, both types cause only a local decrease in the CBF. In the vicinity of the occluded vessel, two distinct zones can be distinguished: a zone of severe ischemia – the infarction core, and a zone of moderate ischemia – the penumbra (Rossi et al., 2007). While at the onset of ischemia, the size of both zones is almost equivalent (Ginsberg, 2003), the ischemic core spreads at the expense of penumbra as the ischemic injury progresses (Zhao et al., 1997).

On the one hand, the infarction core is characterized by insufficient amounts of ATP, pathological concentrations of ions, increased concentrations of glutamate, and tissue acidosis – all features typical of excitotoxicity (Figures 3 and 4). Cell death already occurs within the first minutes after the onset of ischemic injury (Wetterling et al., 2016).

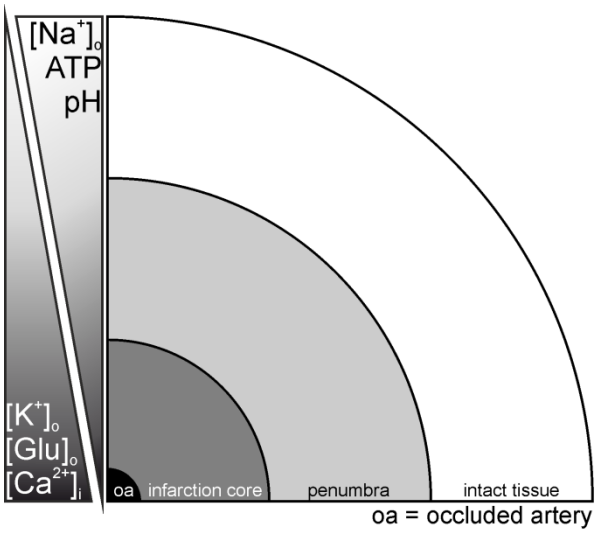

Figure 3. Focal cerebral ischemia. There are two distinguishable zones in the close vicinity of an occluded artery – infarction core and penumbra. The infarction core is characterized by high concentrations of extracellular potassium (K^+) and glutamate (Glu), and intracellular calcium (Ca^{2+}) as well as low values of extracellular sodium concentration (Na^+), stored adenosine triphosphate (ATP), or pH. The farther from the ischemic core, the more physiological values of above-mention variables are observed, while the penumbra serves as a transition zone between the ischemic core, with necrotic tissue, and intact, healthy tissue (author's own scheme; drawn according to information from Rossi et al. (2007)).

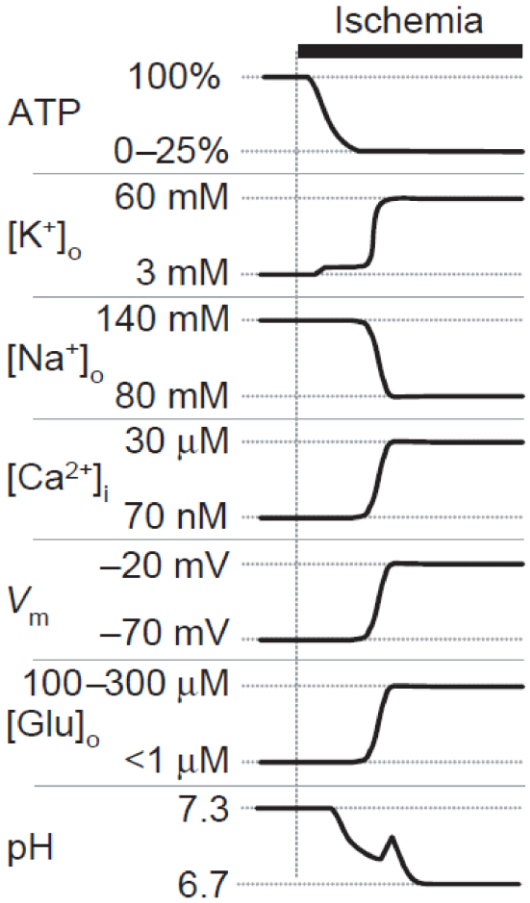

Figure 4. Core of focal cerebral ischemia. A scheme depicting events that occur in the ischemic core. Similar actions may be observed also during global ischemia. A decrease in the adenosine triphosphate (ATP) production inhibits sodium-potassium (Na^+/K^+) ATPase, which changes the transmembrane ion gradients. This causes depolarization and glutamate (Glu) release into the extracellular space. Ischemic injury as well results in extracellular acidification. Abbreviations: Ca^{2+} – calcium; V_m – membrane potential (Rossi et al., 2007).

On the other hand, there is a residual blood flow in the penumbra because of the presence of collateral arteries (Harukuni and Bhardwaj, 2006; Jung et al., 2017), with decreased but still sufficient ATP concentrations, only marginally shifted ionic concentrations and recurrent episodes of cortical spreading depression also called peri-infarct depolarization (Hinzman et al., 2015; Oliveira-Ferreira et al., 2019; Figure 3 and 5), and apoptosis as typical cellular death (Doyle et al., 2008; Rossi et al., 2007).

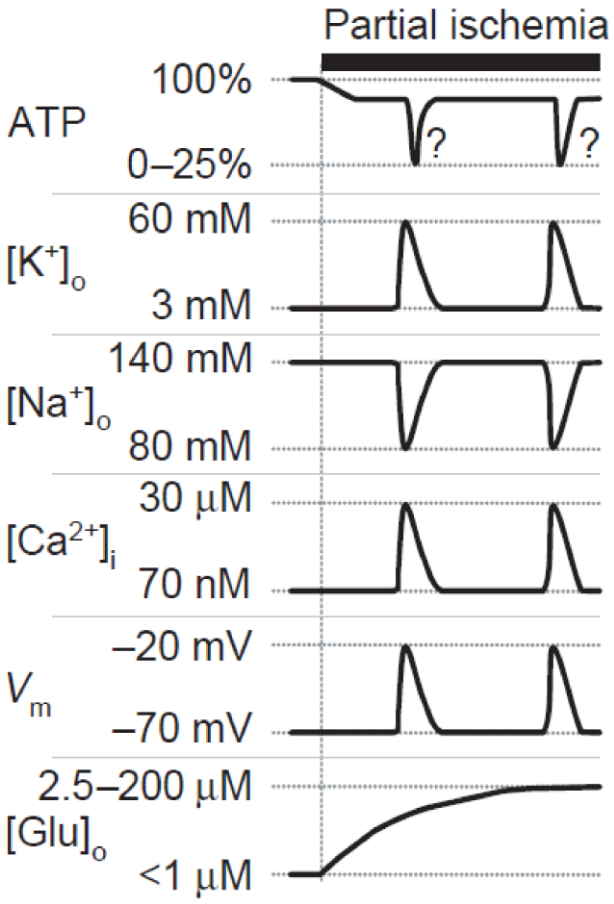

Figure 5. Penumbra of focal cerebral ischemia. A scheme showing events in the penumbral region of focal brain injury. A decrease in adenosine triphosphate (ATP) is less severe; nevertheless, it triggers recurrent transient depolarizations coupled with ion shifts, while glutamate (Glu) concentrations rise slowly but steadily. Upon early reperfusion, penumbral tissue may be spared. However, during longer-lasting ischemia, the penumbra is 'devoured' by the ischemic core and necrosis occurs also in this region. Abbreviations: Ca^{2+} – calcium; K^+ – potassium; Na^+ – sodium; V_m – membrane potential (Rossi et al., 2007).

Another factor that may add to the spared nervous tissue in the penumbral region of focal ischemia is the presence of the circle of Willis that creates a sort of redundancy for collateral circulation in the brain (Figure 6). It has been reported that abnormalities in the circle of Willis are often present in ischemic stroke localized in the middle cerebral artery territory (Husson et al., 2016; Du et al., 2011).

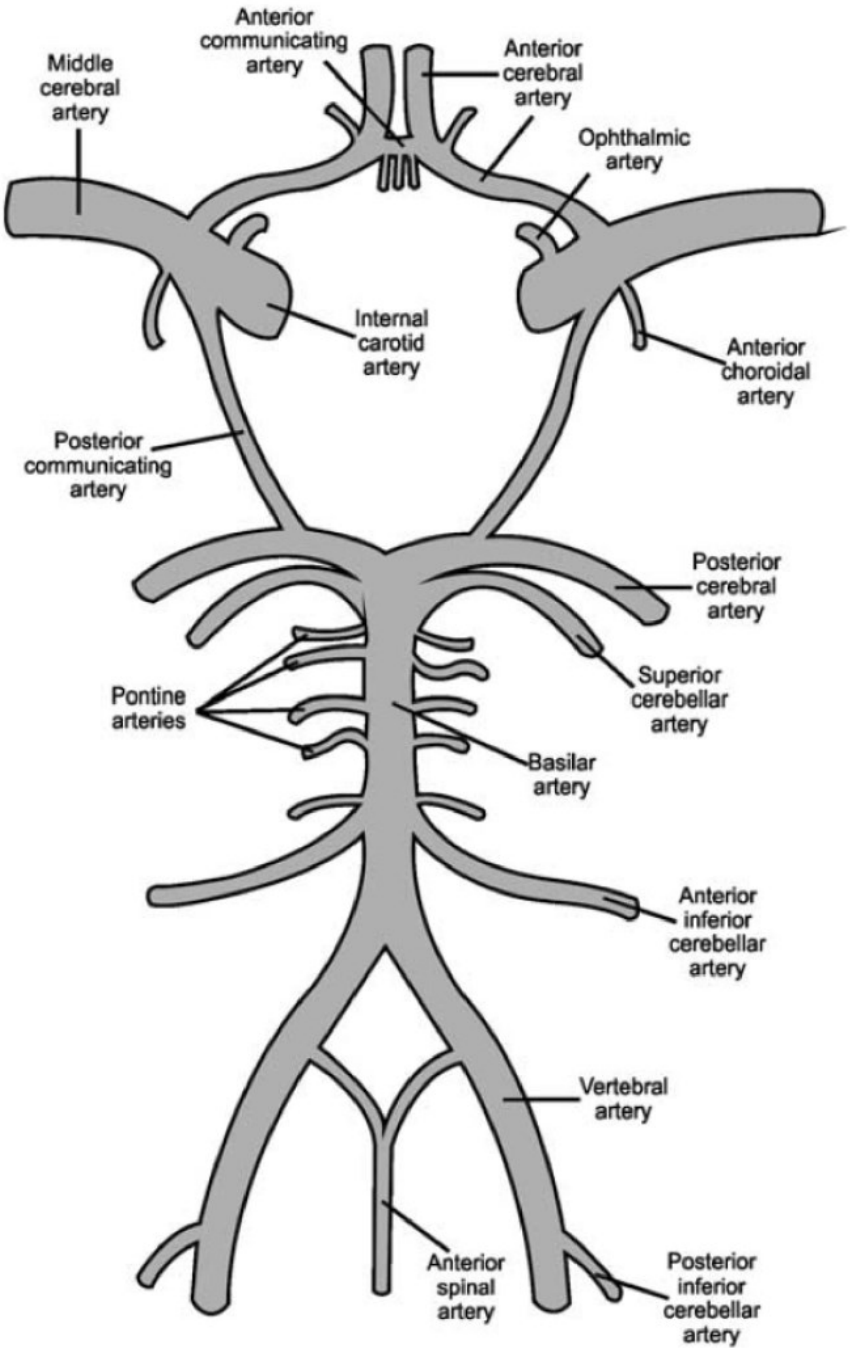

Figure 6. Anatomy of the circle of Willis. Schematic illustration of blood vessels supplying the rodent brain, where the posterior cerebral artery, posterior communicating artery, internal carotid artery, middle cerebral artery, anterior cerebral artery, and anterior communicating artery form the circle of Willis. This structure is named after Thomas Willis, who believed that it was a compensatory mechanism for a blocked brain vessel. The middle cerebral artery is prone to the occlusion, and together with variations in the circle of Willis, focal ischemia may occur to various extents (Vrselja et al., 2014).

The penumbra also draws attention of regenerative medicine, since it is believed that normal functions might be restored especially in this zone (Jung et al., 2017).

Nevertheless, residual or even newly formed viable neurons have been also detected in the ischemic core (Jiang et al., 2017).

All the processes listed before take place at the site of injury – in the cerebral cortex; however, in our experiments on NS/PCs, we focused on a region distant from the cortex, specifically on the SVZ. This zone is localized around the LV in the medial region of the brain. It has been documented that the induction of focal ischemia has a consistent impact also on the physiological functions of cells residing there (Ginsberg, 2003).

1.2 Postnatal neurogenesis

The process of transition from NS/PCs to matured neurons and glial cells is called neurogenesis and gliogenesis, respectively. Neurogenesis occurs predominantly at embryonic stages of the mammalian ontogenetic development. During embryogenesis, neurons are produced from embryonic neural stem cells (NSCs) in the neural tube, while gliogenesis is suppressed and increases at the perinatal stage and continues postnatally (Miller and Gauthier, 2007). Over the course of neurogenesis, radial glial cells in the ventricular zone (VZ) act as primary NSCs and are the main source of newly formed neuronal cells in many CNS regions (Lui et al., 2011). Another source of neurons is a pool of radial-glia-derived intermediate progenitors, also termed basal progenitor cells, occupying the SVZ (Noctor et al., 2004; Haubensak et al., 2004). After several waves of symmetric and asymmetric divisions, NSCs differentiate to neurons. However, neurons do not form neural circuits immediately as they first migrate relatively long distances to the forming cortex and mature there (Rakic, 1995).

Nerve cells are post-mitotic, which means that they do not divide, and for many years, a premise saying that neurogenesis ceases after birth was set. However, not all neurons are generated during embryogenesis, since there are precursor cells that proliferate in the postnatal CNS and might potentially differentiate and mature into functional neurons and glial cells (Gage et al., 1995; Ramasamy et al., 2013). These two main endogenous sources of new neurons in the mammalian brain are NS/PCs (Butti et al., 2019) and polydendrocytes (also named NG2 glia) (Kirdajova and Anderova, 2019; Tsoa et al., 2014; Belachew et al., 2003).

1.2.1 Neural stem/progenitor cells

In 1960s, postnatal neurogenesis in the CNS was documented for the first time (Altman and Das, 1965). Under physiological conditions, adult neurogenesis takes place in two distinct regions of the mammalian brain – the subgranular zone (SGZ) of the dentate gyrus in the hippocampus, and the SVZ of the LV, which is adjacent to the striatum (Figure 7) (Vukovic et al., 2011; Ihrie and Alvarez-Buylla, 2008; Doetsch et al., 1999). These two regions are considered *bona fide* neurogenic zones of the adult brain, as they have been shown to comprise NS/PCs that possess the trait of generating distinct cell types *in vitro* as well as *in vivo* (Lie et al., 2005; Bizen et al., 2014). These NS/PCs also self-renew *in vitro* and *in vivo* indefinitely, and thus meeting the definition of "stem cells" (Malatesta et al., 2008). However, they proliferate at a much slower pace than during embryogenesis (Furutachi et al., 2013). Besides the two neurogenic regions of the adult CNS, there is a body of evidence that during ischemia, multiple neurogenic sites within the brain parenchyma are activated, lasting for more than one month after the induction of ischemic injury (Kokaia et al., 2006).

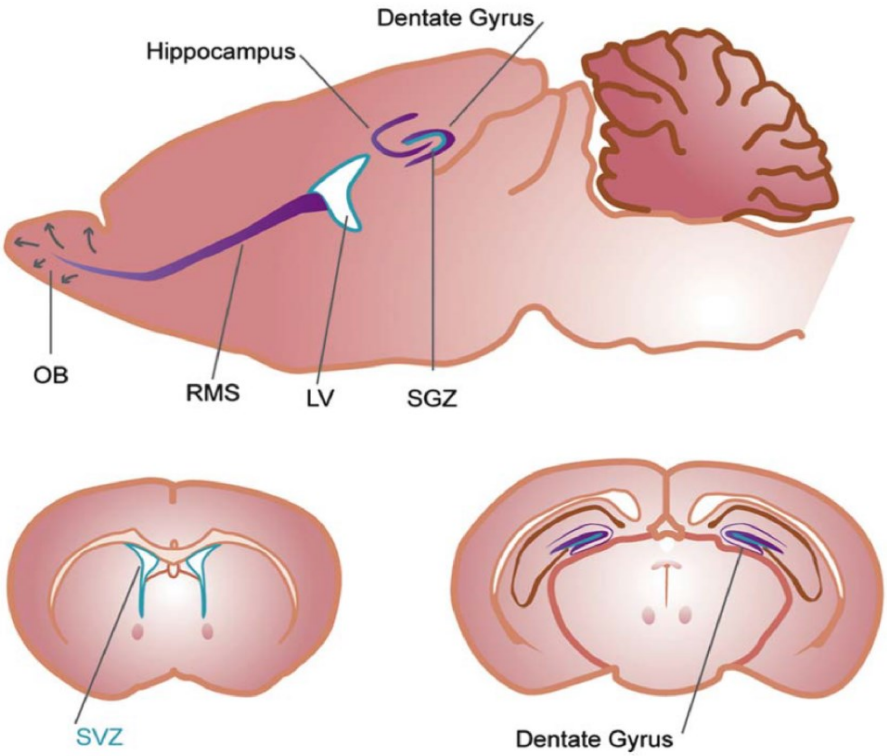

Figure 7. Neurogenic niches of the mature mouse brain. The illustrations depicting sagittal **(top)** and coronal **(bottom)** sections of the brain. There are two distinct regions of the rodent brain where adult neurogenesis takes place (depicted in blue) – the subgranular zone (SGZ) of the dentate gyrus in the hippocampus, and the subventricular zone (SVZ) of the lateral ventricles (LV). The SGZ produces neurons that incorporate in the hippocampus, while the neurons derived

from the SVZ migrate along the so-called rostral migratory stream (RMS) to the olfactory bulb (OB) and mature there (adapted from Vukovic et al. (2011)).

Adult NS/PCs share some common properties with astrocytes, which could be a reason why they were discovered just recently. Both cell types express glial fibrillary acidic protein (GFAP) and vimentin (Vim), are interconnected with gap junctions, and their membranes possess glutamate transporters. Moreover, they also resemble each other morphologically (Namba et al., 2005; Doetsch, 2003). Despite these similarities between astrocytes and stem cells, adult neurogenesis is presumably maintained by the local microenvironment, or niche, and the presence of specific factors and molecules is the most crucial difference separating NS/PCs from astrocytes (Lee et al., 2012).

In our study, we focused on NS/PCs residing in the SVZ, of which the architecture is well described in mice (Figure 8). This region contains three main cell types (A-, B-, and C-type cells): astrocytes (B-type), being *bona fide* stem cells, and giving rise to highly proliferative transient amplifying cells (C-type) that, in turn, generate migratory neuroblasts (A-type). These neuroblasts eventually differentiate to mature neurons in the olfactory bulb (OB), where they incorporate into the existing neuronal circuit (Ihrie and Alvarez-Buylla, 2008; Gil-Perotin et al., 2013).

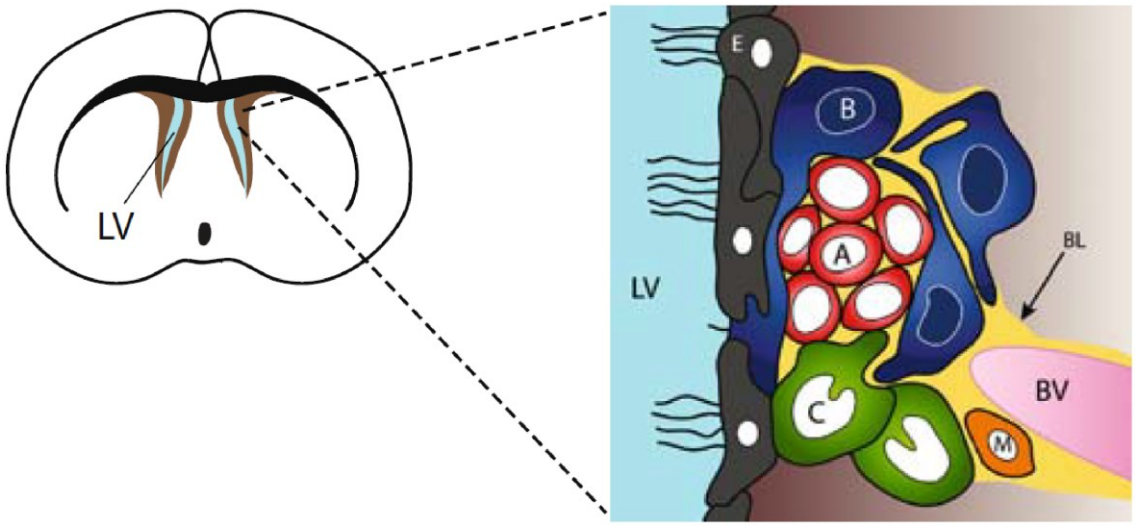

Figure 8. Architecture of the subventricular zone (SVZ) in mice. The illustration showing coronal section of the brain **(left)** and the cellular composition of the neurogenic niche **(right)**. This region is adjacent to the walls of the lateral ventricles (LV) and is composed of B-type cells, corresponding to *bona fide* astrocytic stem/progenitor cells, rapidly dividing C-type cells, derived from the B-type cells, and their progeny – A-type cells that represent neuroblasts migrating to the olfactory bulb where they differentiate to neurons. The SVZ cells contact ependymal cells (E), the

basal lamina (BL), and microglia (M) and are in the vicinity of blood vessels (BV) (Ihrie and Alvarez-Buylla, 2008).

However, adult neurogenesis in humans is rather disputable, since no significant presence of postnatally generated neurons has been observed in many studies (Sorrells et al., 2018; Coletti et al., 2018). This could be due to the fact that in humans, newly generated neuronal precursors from the SVZ do not migrate to the olfactory bulb unlike in rodents (Bergmann et al., 2012). On the other hand, there is evidence of neurogenesis in the striatum of the postnatal human brain (Ernst et al., 2014).

In the adult brain, a subpopulation of NS/PCs at neurogenic niches expresses mouse homologue of drosophila *dachshund* gene (mDach1) that is also expressed in the embryo (Machon et al., 2002). In the experimental setting, these stem cells differentiated under physiological conditions only to glial cell types. However, after FCI, enhanced neurogenesis was observed and newly-derived neuronal precursors migrated to the OB, where they matured (Honsa et al., 2013). When mDach1-expressing NS/PCs were transplanted into the lesioned brain, they also differentiated to neurons with characteristics similar to those found in the intact brain. This might favour this type of stem cells to replace lost cells in the damaged or diseased brain in regenerative therapies (Prajerova et al., 2010a).

1.2.2 NG2 glia

At the beginning of 1980s, the very first reference to NG2 glia was made. These cells were described in immunofluorescent double-labeling experiments as a cell type that has some properties associated with neuronal cells and some characteristics common with glia (Stallcup, 1981). Presumably, their name stems from this discovery, as it is an abbreviation of neuron-glial antigen 2. This antigen is also called chondroitin sulfate proteoglycan 4 and is encoded by the *Cspg4* gene. Additionally, these cells can be also identified by the expression of platelet-derived growth factor alpha receptor (PDGFαR), of which ligand is responsible for their survival and proliferation (Rivers et al., 2008; Calver et al., 1998).

NG2 cells enjoy various pseudonyms as they exercise many functions in the CNS. They are oligodendrocyte precursor cells (OPCs) because their subpopulation gives rise to oligodendrocytes under physiological conditions (Boshans et al., 2019; Figure 9). They are also termed polydendrocytes because they possess many elaborate, highly branched

processes (Chittajallu et al., 2004). Especially in grey matter they thus resemble astrocytes; however, the processes of NG2 cells are not that well-developed and bushy. Last but not least, they are also termed synantocytes because they often contact neurons at their synapses and nodes of Ranvier (Serwanski et al., 2017; Bergles et al., 2000).

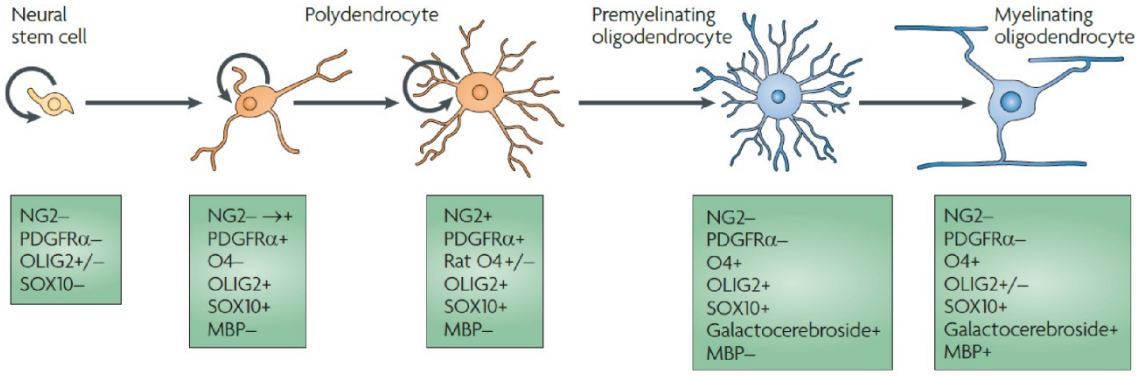

Figure 9. NG2 cells in the oligodendrocyte lineage. A scheme depicting development of polydendrocytes **(top)** with markers characterizing different developmental stages **(bottom)**. There are two markers, neuron-glial antigen 2 (NG2) and platelet-derived growth factor alpha receptor (PDGFαR), that are expressed only in polydendrocytes and not in neural stem cells or oligodendrocytes. As NG2 cells differentiate to myelinating cells, the expression of specific proteins commences. Abbreviations: MBP – myelin basic protein; O4 – oligodendrocyte antigen O4; OLIG2 – oligodendrocyte transcription factor OLIG2; SOX10 – transcription factor SOX10 (Nishiyama et al., 2009).

Synantocytes also display a complex membrane current pattern composed of passive potassium (K^+) conductance, with inwardly and outwardly rectifying K^+ currents (Lin and Bergles, 2002). During development, NG2 cells are densely packed at neurogenic areas occupied by stem cells (Spassky et al., 1998). Conversely, polydendrocytes in the adult CNS are spread within both white and grey matter and are almost as numerous as astrocytes. They form 8-9% of all cells in white matter, while they comprise only 2-3% of all cells in grey matter (Dawson et al., 2003). Especially in grey matter, they populate the nervous tissue in territories, meaning that every single NG2 cell has its own space and 'monitors' the neighboring tissue with its processes (Nakano et al., 2017).

It is now well established that NG2 glia is a mature macroglial cell type in the adult CNS, distinct from astrocytes and oligodendrocytes. Polydendrocytes persist throughout the postnatal CNS and proliferate slowly. Nevertheless, they are considered the most proliferative glial cell type in the adult mammalian brain (Dawson et al., 2000).

NG2 cells that express the gene *2',3'-cyclic nucleotide 3'-phosphodiesterase* (*Cnp*), also known as CNPase, were shown to differentiate also to neurons *in vitro*. The same was also confirmed in *in vivo* experiments, where these proliferative precursors of the adult CNS gave rise to functional neurons that propagated action potentials (Belachew et al., 2003). Moreover, postnatal NG2 cells from the SVZ migrated to the OB and differentiated to interneurons or oligodendrocytes. On the other hand, polydendrocytes from the cortex differentiated to oligodendrocytes or astrocytes. This diverse differentiation potential of NG2 cells from various regions of the postnatal brain implies a region-specific variance within this cell type (Aguirre and Gallo, 2004), which has also been confirmed by the finding that grey and white matter NG2 cells show distinct membrane properties (Chittajallu et al., 2004). It has been demonstrated that early postnatal NG2 cells from the SVZ show characteristics similar to those of transient amplifying multipotent cells of C-type (Aguirre et al., 2004), while another study claimed that NG2 cells definitely represent a cell population that is distinct from NS/PCs in the postnatal SVZ (Komitova et al., 2009). Moreover, similarly to the moot point in NS/PCs, there is also a strong disagreement about the neurogenic potential of NG2 cells (Kang et al., 2010).

Although NG2 cells are known to provide the CNS with oligodendrocytes during development and normal functioning of the mature CNS, or with remyelinating cells in demyelinated lesions, the situation is completely different after ischemia (Valny et al., 2017). A proportion of the resident NG2-expressing cell population in the vicinity of the lesion promptly responds to ischemic injury, which includes migration towards the site of injury, cell proliferation and reactive gliosis (Bonfanti et al., 2017; Tanaka et al., 2001). The alteration in the differentiation potential of NG2 cells induced by CNS injury is also a subject for discussion. Recent fate-mapping experiments showed that NG2 glia acquire a multipotent phenotype after the occlusion of the middle cerebral artery. These precursors differentiated to reactive astrocytes (Valny et al., 2018; Honsa et al., 2016; Honsa et al., 2012). Differentiation to this cell type may promote the survival of spared neurons as GFAP-positive reactive astrocytes contribute to the formation of glial scar and thus prevent detrimental substances from entering the affected tissue. Nevertheless, glial scar can act as a double-edged weapon, since in later stages of ischemic injury, it inhibits neurite outgrowth and CNS regeneration (Pekny et al., 2014). However, despite the findings that the NG2 molecule inhibits the growth of axons, some studies indicated that NG2 cells provide an adhesive substrate and facilitate axonal growth (Yang et al., 2006).

Additionally, there is some evidence that NG2 glial cells isolated from adult rodents are progenitors of newly derived doublecortin (DCX)-positive neuronal cells (Honsa et al., 2012). Neuronal fate of polydendrocytes after CNS injury had been already challenged. However, the experiments were performed in a model of amyotrophic lateral sclerosis rather than in a model of FCI (Kang et al., 2010). And since the fact that polydendrocytes react differently to various types of CNS injuries is well-accepted, the results from the above-mentioned publications do not contradict each other. For example, after a stab wound injury, only a small subpopulation of reactive astrocytes was generated from NG2 glia (Komitova et al., 2011), which was not the case in the ischemic brain (Honsa et al., 2012).

The reported neurogenic potential of NG2 cells after ischemia or in other CNS pathologies might increase the recuperation of the damaged tissue and thus better the overall outcome.

1.3 Cellular signaling pathways

Neurogenesis, hand in hand with gliogenesis, largely depends on molecular and genetic inputs such as growth factors and cellular signaling pathways, but these processes are also modulated during pathological states (Lamus et al., 2020; O'Keeffe et al., 2009).

In our study, we focused on two highly influential signaling cascades that modulate the fate of cells from the embryo, throughout the life of an organism until its demise. These two cellular pathways are called the Wnt and the Shh signaling pathway. Their role in the development of the brain has been well established, since both of them were identified as survival factors for embryonic NS/PCs (Kalani et al., 2008; Komada et al., 2008). Nevertheless, recent research riveted its attention more on the function of these morphogens in neurogenesis and in the modulation of progenitor cells properties after birth (Lie et al., 2005; Lai et al., 2003).

1.3.1 Wnt signaling pathway

Neural progenitors are strongly influenced by their microenvironment. Among many transcription factors, growth factors and small molecules affecting the regulation of cell precursors, it is Wnt signaling that steps into the limelight (Bowman et al., 2013; Bonnert et al., 2006).

The Wnt ligands belong to a large group of secreted cysteine-rich glycosylated proteins that are involved in many cellular processes, such as embryonic cell patterning, cell proliferation and differentiation, synaptic plasticity, or programmed cell death (Chodelkova et al., 2018; Clevers et al., 2014; Lim and Nusse, 2013; Alvarez et al., 2004). There are 19 distinct Wnt genes in the mammalian genome and three major Wnt signaling pathways have been identified: the canonical Wnt (β-catenin) pathway and two non-canonical pathways – the planar cell polarity and Wnt/calcium (Ca^{2+}) pathways. Since in our experiments, we focused on canonical Wnt signaling, non-canonical pathways are only briefly described in this literary review. The planar cell polarity pathway orchestrates the orientation of the cells that reside in the tissue. It does not involve β-catenin and signals through the frizzled receptor and activates small proteins and kinases that regulate cytoskeleton. In the Wnt/Ca^{2+} pathway, the signal is relayed through phospholipase C, which triggers the Ca^{2+} release from the endoplasmic reticulum. Elevated intracellular Ca^{2+} concentration activates Ca^{2+}-dependent enzymes that regulate cell adhesion and migration (van Amerongen, 2012).

The signaling relay of the canonical Wnt (β-catenin) pathway starts at the cytoplasmic membrane and ends in the nucleus. In the absence of a Wnt signal, the multi-protein destruction complex is formed in the cytoplasm. Kinases of this complex put a molecular tag on β-catenin, the key factor of the whole cascade, and thus mark it for degradation in the proteasome. Nevertheless, activation of the canonical Wnt pathway stabilizes β-catenin. This stabilization is achieved via a negative regulation of glycogen synthase kinase 3β (GSK-3β), followed by accumulation of β-catenin in the cytoplasm and its subsequent translocation to the nucleus, where it binds to the transcription factors T-cell factor/lymphoid enhancer factor (TCF/LEF), and thus influences the expression of Wnt target genes (Wiese et al., 2018; Nusse, 2008; Hamada et al., 1999; Figure 10). Many of these genes are implicated in proliferation and differentiation of neural precursors, or in self-regulation of the pathway, with its numerous negative feedback loops (ten Berge et al., 2008; Mikels and Nusse, 2006).

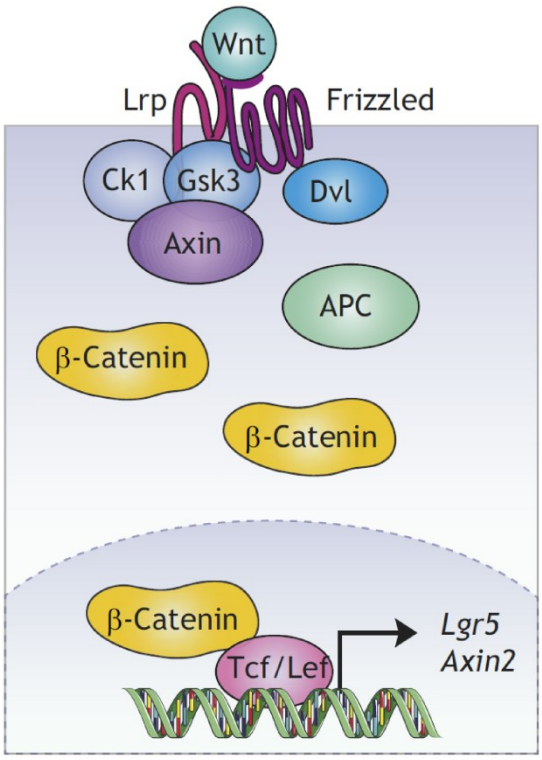

Figure 10. Canonical Wnt signaling pathway. In the absence of wingless and integrated (Wnt) ligand, the so-called destruction complex is formed in the cytoplasm, consisting of axin, casein kinase 1 (Ck1), dishevelled (Dvl), adenomatous polyposis coli (APC), and glycogen synthase kinase 3 (Gsk3), which marks β-catenin, the key protein of the pathway, for degradation in the proteasome. However, once the Wnt signal binds the receptors frizzled and low density lipoprotein receptor-related protein (Lrp), no destruction complex is formed, β-catenin accumulates in the cytoplasm and subsequently translocates to the nucleus where it binds to transcription factors T-cell factor/lymphoid enhancer factor (Tcf/Lef), which activates Wnt target genes such as leucine-rich repeat-containing G-protein-coupled receptor 5 (Lgr5) and Axin2 (adapted from Wiese et al. (2018)).

As it was already indicated above, the Wnt pathway exercises a plethora of functions during embryogenesis. As an example, in mice with disrupted Wnt signaling, a part of the midbrain did not develop, indicating that the Wnt cellular relay is essential for the survival of stem cells that form this part of the brain, as well as for their differentiation (Brault et al., 2001). Conversely, stabilized β-catenin protein in NS/PCs led to enlarged brains with enlarged lateral ventricles, which was caused by higher numbers of precursor cells in this region (Chenn and Walsh, 2002). The key element of canonical Wnt signaling, β-catenin, plays a crucial role in gene transcription and cell adhesion (Mosimann et al., 2009; Nelson and Nusse, 2004). All these data support the notion that the Wnt signaling pathway regulates the activity of stem cells in embryogenesis.

However, the role of Wnt signaling is indisputable also in the postnatal stages of ontogenesis. Activation of β-catenin-dependent signaling promoted proliferation of precursor cells in the SVZ, while its inhibition reduced the number of newly generated cells (Adachi et al., 2007). Similar effects of Wnts were observed also in the other neurogenic niche of the adult brain, the SGZ, where the Wnt3 ligand was specifically responsible for an increase in neurogenesis *in vitro* as well as *in vivo*, while in the presence of Wnt inhibitors, neurogenesis was almost extinguished (Lie et al., 2005). Moreover, components of Wnt signaling have been shown to interact with a variety of other molecules such as fibroblast growth factor (FGF) or retinoic acid and influence thus the pool of NS/PCs (ten Berge et al., 2008; Jacobs et al., 2006).

Additionally, it has been shown that hypoxia and FCI increase the number of NS/PCs in the hippocampus and GFAP-positive neural progenitors in the SVZ, respectively, and also promote the expansion of neuroblasts one month after middle cerebral artery occlusion (MCAO), and canonical Wnt signaling is involved in this process (Zhang et al., 2014a; Cui et al., 2011). Similarly, the impact of β-catenin on the ability of NS/PCs to give rise to neurons, as well as to oligodendrocytes, in ischemic conditions was confirmed also in another study (Zhang et al., 2016). Moreover, Wnt signaling contributed to functional recovery following focal ischemia in mice (Shruster et al., 2012).

The output of the Wnt pathway can be regulated in many ways and at many subcellular levels. For example, the activity of Wnt signaling can be attenuated by ribonucleic acid interference (RNAi). Small interfering RNA (siRNA), inhibiting the *related to receptor tyrosine kinase* (Ryk), caused a significant decrease in TCF-driven transcription (Lu et al., 2004). Another approach may be the addition of small molecules, since this has been shown to either inhibit or activate Wnt signaling to various degrees. Pai et al. (2004) used deoxycholic acid that induced stabilization of β-catenin and its subsequent translocation to the nucleus, which, in turn, led to a higher expression of cyclin D1, one of the Wnt signaling target genes. Others utilized purified natural compounds, or their synthetically developed derivates, to disrupt the β-catenin/Tcf protein-protein interaction, and thus inhibit the Wnt pathway (Chen et al., 2009; Lepourcelet et al., 2004). Moreover, treatment with andrographolide, a competitive inhibitor of GSK-3β, increased NS/PCs proliferation and the number of newborn neurons in the hippocampus (Varela-Nallar et al., 2015). Another way of manipulating Wnt signaling at different subcellular levels could represent microinjections of messenger

ribonucleic acid (mRNA) into the blastomeres of an embryo (Glinka et al., 1998; Molenaar et al., 1996). However, the current method of choice is employing animal models, especially various transgenic mouse strains (Kriska et al., 2016; Korinek et al., 1998).

All the above-described findings show the importance of the Wnt/β-catenin pathway in proliferation and differentiation of NS/PCs in the adult brain, especially during different pathophysiological conditions involving ischemia. Additionally, knowing that neural progenitors have the capacity to differentiate to other cell types of the CNS, altering this signaling may ameliorate or even overcome the difficulties associated with the diseased CNS.

1.3.2 Sonic hedgehog signaling pathway

Another cellular pathway that affects neurogenesis and gliogenesis is Shh signaling. This pleiotropic secreted protein, which acts as morphogen and mitogen in embryogenesis, belongs to the hedgehog family, together with two other ligands – indian hedgehog and desert hedgehog (Xia et al., 2019). Nevertheless, our work was dedicated only to Shh, major activating ligand in the brain, which has an irreplaceable role in the organization of the developing brain and is required for the formation of precursor cells (Merkle et al., 2014; Rash and Grove, 2011).

In the absence of a Shh signal, protein kinase A (PKA) phosphorylates transcription factors glioma-associated oncogenes (GLIs) that are subsequently proteolytically processed by the proteasome and act as transcriptional repressors. However, once a Shh ligand is attached to its receptor patched (Ptch), abolishing thus its inhibiting modulation on the transmembrane receptor smoothened (Smo), the expression of Smo is increased and the protein starts to accumulate at the primary cilium of the cell. This in turn causes a decrease in the activity of PKA (Callejo et al., 2007). Downstream GLI proteins can be then modified and translocated to the nucleus where they activate so-far inhibited target genes (Ho and Scott, 2002; Figure 11).

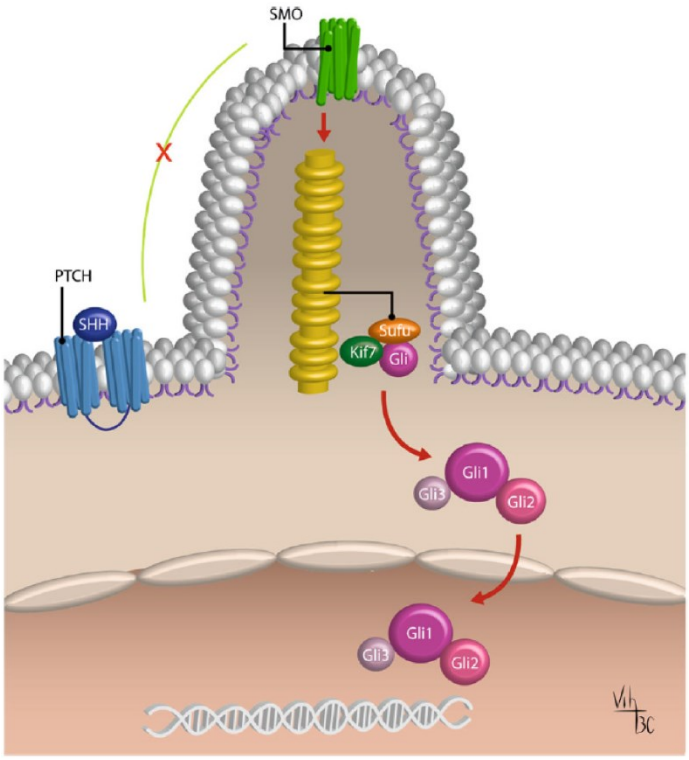

Figure 11. Sonic hedgehog (Shh) signaling pathway. Once the Shh ligand binds to the patched (Ptch) receptor at the cell membrane, the signaling pathway is activated. The receptor no longer inhibits smoothened (Smo) as this protein accumulates at the primary cilium, a microtubule-based organelle, and promotes the downstream relay of signals. Smo activates glioma-associated oncogene (Gli), which enters the nucleus and binds to the Shh target genes. Abbreviations: Kif7 – kinesin-4 family protein 7; SUFU – supressor of fused (Carballo et al., 2018).

The Shh pathway promotes NS/PCs survival and proliferation, since its disruption caused deficient formation of the telencephalon (Komada et al., 2008). Studies also revealed that Shh is necessary for the production of oligodendrocytes from neural progenitors during embryogenesis, while a decrease in the population of oligodendrocytes after the deletion of the Shh signaling effector Smo was compensated by increased proliferation of NG2 cells (Winkler and Franco, 2019).

This signaling is active also postnatally, especially in the neurogenic niches, where its activation resulted in enhanced proliferation of precursor cells in these regions (Lai et al., 2003). The experiments performed in the SVZ indicated that B-cells (stem cells), followed by C-cells (transient amplifying cells), were the major Shh-responding populations, and that inhibition of this pathway led to decreased numbers of new neurons (Palma et al., 2005).

Moreover, higher activity of Shh signaling has been also observed during acute brain injury, in which this ligand promoted reactive gliosis and cell proliferation

(Amankulor et al., 2009). Similar upregulation of Shh signaling was also identified during brain ischemia, while this mitogen was found to be a mediator contributing to ischemia-induced expansion of NS/PCs *in vitro* and *in vivo* (Androutsellis-Theotokis et al., 2006). Additionally, it was shown that in cerebral ischemia, Shh is necessary and sufficient to trigger the 'multipotency mode' of reactive glia that then acquire the characteristics of stem cells (Sirko et al., 2013). On the other hand, under physiological conditions, neuron-derived Shh had an opposite effect and prevented astrocytes from the transformation to their reactive form (Garcia et al., 2010). Interestingly, it has been proven that the SVZ is organized in microdomains of NS/PCs that differentiate to distinct types of neurons, while various components of the Shh pathway are specifically expressed in these microdomains (Ihrie et al., 2011).

Another work on Wnt as well as Shh signaling showed that these pathways altered the differentiation potential of neonatal NS/PCs, as they both increased neurogenesis and suppressed gliogenesis. Moreover, these two signaling relays influenced proliferation and differentiation of stem cells differently. Only Wnt enhanced the formation of cellular processes and increased proliferation at the early stage of *in vitro* differentiation, while Shh had no effect on the development of the processes and maintained higher proliferation rate of cells during the entire course of differentiation (Prajerova et al., 2010b). Additionally, a new role of these two signaling pathways emerged recently. They interact with the receptor for activated C kinase (Rack1) to control the accurate mammalian cerebellar morphogenesis (Yang et al., 2019).

2 AIMS OF THE STUDY

The purpose of this study was to elucidate the role of cellular signaling pathways (canonical Wnt signaling and Shh signaling) in gliogenesis and neurogenesis utilizing precursor cells (NS/PCs from the SVZ or NG2 glia from the cortex) isolated from neonatal (up to postnatal day 2) as well as adult (2-month-old and older) transgenic mice with tamoxifen (TAM)-inducible Cre-mediated recombination of deoxyribonucleic acid (DNA).

We assessed the effect of signaling pathways under physiological conditions as well as after the induction of FCI. The phenotype of cells derived from the precursor cells was identified using the patch-clamp technique in the whole-cell configuration, immunochemical analysis, reverse transcription quantitative polymerase chain reaction (RT-qPCR), and Western blotting. For this study, we put together our principal hypothesis saying that the manipulation (either inhibition or activation) of canonical Wnt signaling after FCI may change the differentiation potential of precursor cells and thus ameliorate the negative effects of ischemic brain injury. This hypothesis was subsequently divided into three partial hypotheses and four associated specific aims as follow:

Hypothesis 1: The differentiation potential of NS/PCs isolated from neonatal and adult mice is influenced by Wnt signaling manipulation.

Aim 1: To evaluate three transgenic mouse models that enable Wnt signaling manipulation in *in vitro* experiments employing RT-qPCR, immunocytochemical analysis, and Western blotting.

Aim 2: To assess neonatal and adult NS/PCs under physiological conditions utilizing electrophysiological analyses, immunocyto/histochemical analyses, Western blotting, and RT-qPCR.

Hypothesis 2: Ischemic injury itself triggers proliferation and differentiation of NS/PCs. We assume that the differentiation potential of NS/PCs isolated from the SVZ following permanent FCI is modulated by Wnt signaling manipulation.

Aim 3: To disclose the differentiation potential of adult NS/PCs after ischemic brain injury using electrophysiological and immunohistochemical analyses, RT-qPCR, and Western blotting.

Hypothesis 3: The differentiation potential of polydendrocytes (NG2 glia) isolated from adult mice can be modulated by FCI, and Wnt and Shh signaling pathways.

Aim 4: To evaluate adult NG2 glia after ischemic brain injury employing FACS, single-cell RT-qPCR, immunohistochemical and electrophysiological analyses, and the administration of Shh signaling activators and blockers.

3 MATERIALS AND METHODS

To fulfil the set goals, we employed transgenic mouse strains as a source of neural progenitors (NS/PCs and NG2 glia) and as a tool for manipulating the canonical Wnt signaling pathway, MCAO as a means of inducing FCI, and a series of experimental procedures to prepare the specimens for analyses and to assess the changes in the differentiation potential of NS/PCs and NG2 cells under various experimental conditions.

3.1 Transgenic animal models

In our experiments, we employed transgenic mouse strains that enabled us to alter the activity of cellular signaling pathways in distinct cell types or to track the fate of neural progenitors derived from various regions of the rodent brain. The procedures that involved the employment of laboratory animals were carried out in accordance with the European Communities Council Directive from November 24, 1986 (86/609/EEC) and with the guidelines of the Institute of Experimental Medicine, Czech Academy of Sciences, which was approved by the Animal Care Committee (approval numbers 18/2011, 146/2013, and 2/2017). Additionally, all efforts were made to minimize both the suffering and the numbers of mice assigned to the individual experiments.

3.1.1 Mouse strains for experiments on neural stem/progenitor cells

In our experiments on NS/PCs, neonatal (postnatal day 0-3) mice or adult (postnatal day 50-56) male mice were employed, and three different transgenic mouse strains were utilized. These animals facilitated the manipulation of the canonical Wnt signaling pathway at different subcellular levels, specifically at the nuclear, membrane, or cytoplasmic levels. First, we employed the *Rosa26-Dkk1* mice (Wu et al., 2008), in which after Cre-mediated excision of a transcriptional blocker, the mice produced the extracellular Wnt pathway inhibitor Dickkopf 1 (Dkk1) from the ubiquitous *Rosa26* locus (Figure 12), blocking membrane receptors of the pathway. Next, the $Catnb^{lox(ex3)}$ mice harbored the floxed allele of the *Ctnnb1* gene (the gene that encodes protein β-catenin; Harada et al., 1999). In these mice the allele enabled conditional stabilization of β-catenin (Figure 12). Lastly, the *Rosa26-tdTomato-EGFP/dnTCF4* mice (Janeckova et al., 2016) produced dominant negative (dn)TCF4 protein from the *Rosa26* locus and this protein acted as a nuclear Wnt pathway inhibitor (similarly to the *Rosa26-Dkk1* strain, dnTCF4

expression was triggered upon Cre-mediated excision of a transcriptional blocker that was located upstream of *dnTCF4* complementary DNA (cDNA); Figure 12). Moreover, this strain was designed to produce tandem dimeric (td) red fluorescent protein Tomato (Tom), which was replaced by enhanced green fluorescent protein (EGFP) after Cre-mediated DNA excision. All these mouse strains were individually crossbred with the general Cre deletor mouse *Rosa26-CreERT2* that possessed TAM-inducible Cre recombinase fused with a mutant form of estrogen receptor (ERT2) (Ventura et al., 2007; Figure 12). According to the resulting genotype, the mice enabled inhibition of Wnt signaling either at the nuclear level (genotype $Rosa26^{dnTCF4/CreERT2}$; further termed 'dnTCF4' mice/cells), or at the membrane level (genotype $Rosa26^{Dkk1/CreERT2}$; further termed 'Dkk1' mice/cells). Moreover, $Ctnnb1^{del(ex3)/+}Rosa26^{+/CreERT2}$ mice (where 'del' stands for deletion; further termed 'Ex3' mice/cells), produced a stable form of β-catenin protein that hyper-activated the canonical Wnt signaling pathway upon Cre-mediated excision of the DNA sequence for exon 3 of the *Ctnnb1* gene.

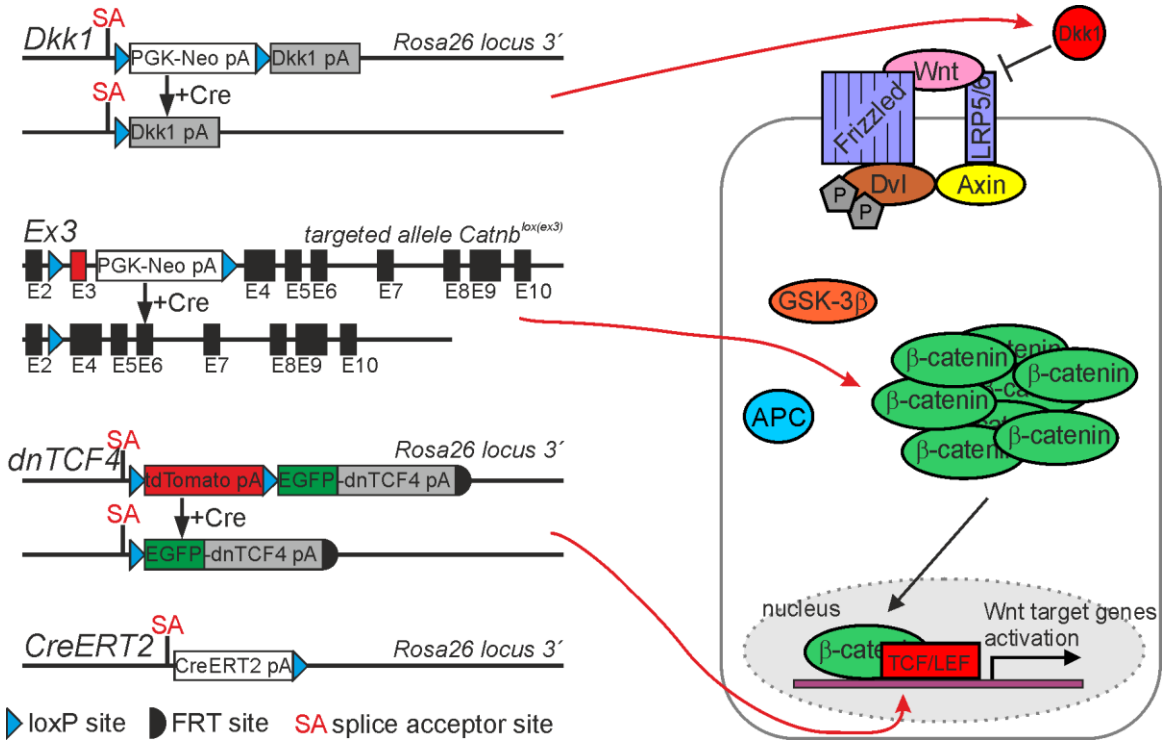

Figure 12. Modulation of the Wnt signaling pathway in transgenic mice. (Left) Schemes depicting genetic modifications present in the mouse strains used in the study of neural stem/progenitor cells. Suppression of Wnt signaling at the membrane level, due to the over-expression of a secreted Wnt inhibitor Dickkopf 1 (Dkk1). Activation of the pathway caused by the production of a stable variant of β-catenin. Cre-mediated excision of exon 3 (E3 or Ex3, red rectangle) removes the amino acid sequence involved in the degradation of the protein, and thus stable β-catenin aberrantly activates Wnt target genes. The Wnt-responsive transcription in the

nucleus is blocked by dominant negative T-Cell factor 4 (dnTCF4). Cre deletor mouse, *Rosa26-CreERT2*, carries the gene encoding tamoxifen-inducible Cre recombinase, fused with a mutated form of the estrogen receptor (CreERT2). **(Right)** Simplified scheme of the canonical Wnt signaling pathway that shows where the alterations take place. Red arrows point to the interference site affected in the transgenic mice used in the study. Abbreviations: APC – adenomatous polyposis coli; Cre – Cre recombinase; Dvl – dishevelled; E2-10 – exon 2-10; EGFP – enhanced green fluorescent protein; GSK-3β – glycogen synthase kinase 3β; LRP5/6 – low-density lipoprotein 5/6; P – phosphorylated site; pA – polyadenylation site; PGK-Neo – neomycin resistance cassette; TCF/LEF – T-Cell Factor/Lymphoid Enhancer Factor; td – tandem dimer; Wnt – Wingless/Integrated (adapted from Kriska et al. (2016)).

The Cre-recombination-mediated manipulation of Wnt signaling was achieved either by addition of 1 μM (Z)-4-hydroxytamoxifen (4OHT; dissolved in ethanol (EtOH); Sigma-Aldrich, St. Louis, MO, USA) into the differentiation medium, or by intraperitoneal (i.p.) injections of TAM (200 mg/kg of the animal's body weight; Toronto Research Chemicals, Toronto, Ontario, Canada) dissolved in corn oil (CO; Sigma-Aldrich, St. Louis, MO, USA). Mice/cells treated only with the vehicle (EtOH or CO) were considered as controls and labeled as 'EtOH' and 'CO', respectively, while mice/cells with manipulated Wnt signaling were labeled as '4OHT' or 'TAM'. Intraperitoneal (i.p.) injections of TAM were delivered in two doses, each once a day of two consecutive days and experiments (MCAO or tissue collection) were performed on the third day after the last TAM injection.

3.1.2 Mouse strain for experiments on NG2 glia

Our experiments on NG2 cells (also termed polydendrocytes) were performed in 3-month-old offspring of *B6.Cg-Tg(Cspg4-cre/Esr1*)BAkik/J* mice crossbred with mice of the strain *B6;129S6-Gt(ROSA)26Sortm14(CAG-tdTomato)Hze/J* (further termed 'Cspg4-Tom' mice/cells; Jackson Laboratory, Bar Harbor, ME, USA; Figure 13). In these mice, the expression of TAM-inducible Cre recombinase was controlled by the *Cspg4* promoter (Zhu et al., 2011). After TAM administration, tdTomato red fluorescent protein was expressed in *Cspg4*-positive (or *Cspg4*$^{+}$) mice/cells, which included mainly NG2 cells and their progeny.

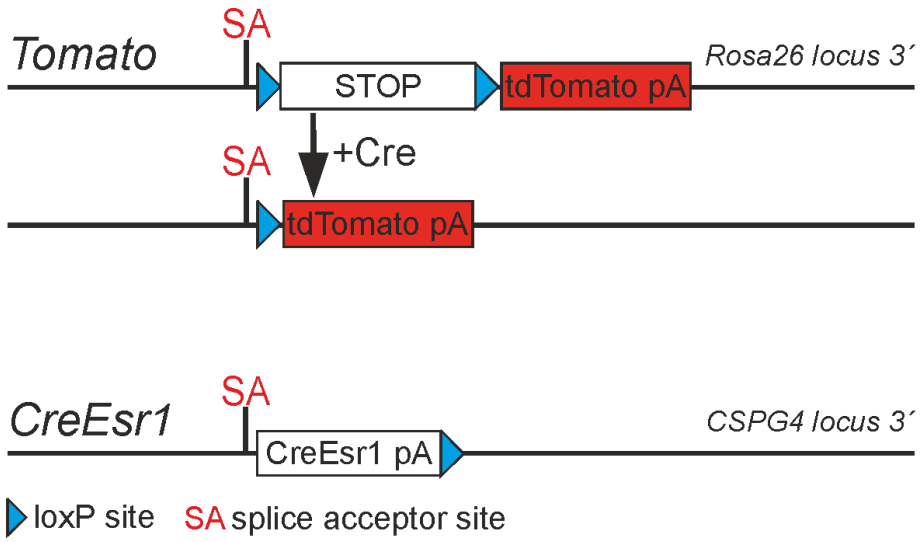

Figure 13. Scheme showing genetic modifications present in the mouse strain used for experiments on NG2 cells. These mice possess deoxyribonucleic acid (DNA) for red fluorescent protein tdTomato, which is blocked by transcriptional blocker (STOP), in all cells of the organism (*Rosa26* locus). At the same time, their genome comprises DNA for Cre recombinase fused with a mutated form of estrogen receptor (CreEsr1) that is expressed in all cells with active *Cspg4* promoter, a hallmark of NG2 cells. However, this fused protein cannot enter the cell nucleus because of its conformation. Nevertheless, upon tamoxifen administration, the protein changes its conformation, allowing thus translocation to the nucleus where it cuts out the STOP sequence. The expression of the fluorescent protein is no longer blocked and Cspg4-positive cells turn red. This procedure creates mice/cells that are further called 'Cspg4-Tom'. Abbreviations: Cre – Cre recombinase; *Cspg4* – chondroitin sulfate proteoglycan 4; Esr1 – estrogen receptor 1; pA – polyadenylation site; td – tandem dimer (author's own scheme).

Tamoxifen was administered in a form of i.p. injections for two consecutive days (200 mg/kg, Sigma-Aldrich, St. Louis, MO, USA) and experiments were carried out 14 days after the last TAM injection, unless stated otherwise. In order to inhibit or activate Shh signaling in these mice, i.p. injections of either specific antagonist cyclopamine (Cyc, 25 mg/kg, LKT Laboratories, St. Paul, MN, USA; Chen et al., 2002) or selective Smo agonist (SAG, 20 mg/kg, VDM Biochemicals, Bedford Heights, OH, USA; Lewis and Krieg, 2014) were administered for 7 consecutive days.

3.2 Induction of focal cerebral ischemia

Adult mice underwent permanent MCAO, a procedure which has become a conventional model of FCI. Mice were anesthetized with 2% isoflurane (Abbot, IL, USA) and maintained at 1% isoflurane using a vaporizer (Tec-3, Cyprane Ltd., Keighley, UK). An incision in the skin between the orbit and the external auditory meatus was made and the temporal muscle was retracted. Afterwards, a ~1.5 mm hole was drilled through the

frontal bone, ~1.0 mm rostrally to the fusion of the zygoma and the squamosal bone, and ~3.5 mm ventrally to the dorsal surface of the brain. After the *dura mater* was opened and removed, the middle cerebral artery (MCA; Figure 14) was exposed and cauterized with a pair of bipolar tweezers (SMT, Czech Republic) at a proximal location.

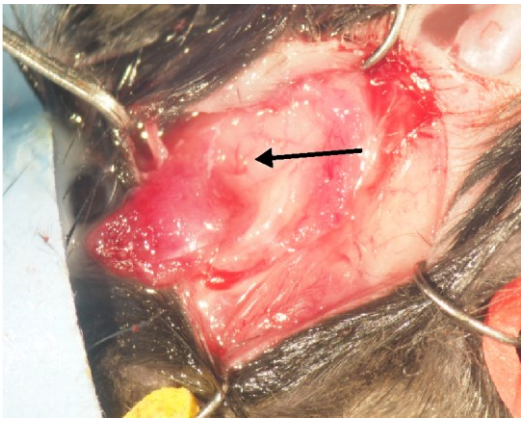

Figure 14. Middle cerebral artery occlusion. The 'Y'-shaped middle cerebral artery (MCA; black arrow) of the left hemisphere is exposed and will be cauterized with a pair of bipolar tweezers, which induces focal cerebral ischemia. Note the retracted temporal muscle to the left to the MCA (photograph by courtesy of author's trainee Hana Bernhardová).

Body temperature of the mouse was maintained at 37 ± 1 °C using a heating pad during the surgery (Honsa et al., 2012). After the operation, the mice were injected 0.5 ml of saline solution subcutaneously. Analgesics were also administered when necessary. Operated mice were labeled as 'MCAO', while non-operated animals were considered as controls and labeled as 'CTRL'. This distal model of MCAO has a high survival rate (>95%) and a good reproducibility, as it typically yields an infarct lesion of a relatively small volume only in the cortical region (Honsa et al., 2013).

For the visualization of ischemic region, we performed staining with 2% 2,3,5-triphenyltetrazolium chloride (TTC; Sigma-Aldrich, St. Louis, MO, USA) at room temperature for 20 minutes (Figure 15).

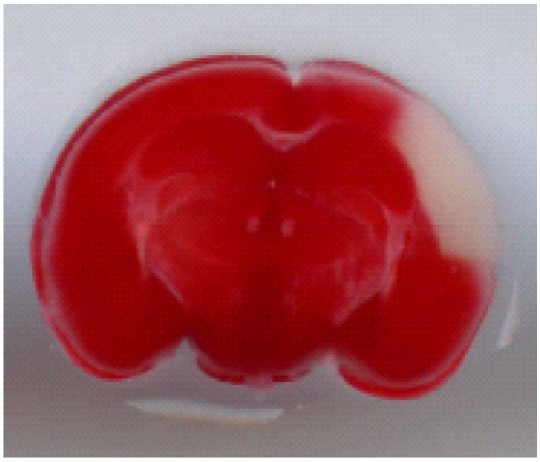

Figure 15. Staining with 2,3,5-triphenyltetrazolium chloride. Coronal section of the mouse brain after middle cerebral artery occlusion. The occluded artery was in the left hemisphere (right side of the photograph), causing focal cerebral ischemia. White area represents tissue of the cortex that was affected by ischemia (photograph by courtesy of author's colleague Zuzana Heřmanová).

3.3 Tissue isolation and cell cultures preparation

To prepare tissue or cell culture specimens for our analyses, we isolated the frontal lobe of neonatal mice or cut coronal sections of the adult mouse brain and cut out specific brain regions for further processing.

3.3.1 Isolation and processing of tissue for cultures of neural stem/progenitor cells

Primary cultures were prepared from NS/PCs isolated from neonatal or adult mouse brains. Neonatal mice were hypothermed, while adult animals were deeply anesthetized first with 4% isoflurane (Abbot, IL, USA) and subsequently with pentobarbital solution (PTB; 100 mg/kg, i.p.; Sigma-Aldrich, St. Louis, MO, USA), and perfused transcardially with ice-cold isolation buffer containing (in mM): 110 N-Methyl-D-glucamine (NMDG)-Cl, 2.5 KCl, 24.5 $NaHCO_3$, 1.25 Na_2HPO_4, 0.5 $CaCl_2$, 7 $MgCl_2$, 20 glucose, osmolality 290 ± 3 mOsmol/kg.

After decapitation, the brains were quickly dissected out and a part of the frontal lobe of the neonatal brain (with the presumptive SVZ region) or the SVZ derived from coronal sections of adult mice was isolated.

Neonatal brain tissue was further processed using a 1 ml pipette. The tissue was mechanically dissociated in a 2-ml-Eppendorf tube with 1 ml of proliferation medium containing Neurobasal-A medium (Life Technologies, Waltham, MA, USA), supplemented with the B27 supplement (B27; 2%; Life Technologies, Waltham, MA, USA), L-glutamine (2 mM; Sigma-Aldrich, St. Louis, MO, USA), antimicrobial reagent primocin (100 µg/ml; Invivogen, Toulouse, France), fibroblast growth factor-basic (bFGF; 10 ng/ml) and epidermal growth factor (EGF; 20 ng/ml; both were purchased from PeproTech, Rocky Hill, NJ, USA). The cells were subsequently filtered through a 70 µm cell strainer, into a 100 mm-diameter Petri dish containing additional 9 ml of proliferation medium. The cells were cultured as neurospheres, at 37 °C and 5% carbon dioxide (CO_2).

After seven days of *in vitro* proliferation, the formed neurospheres (Figure 16, left) were collected and transferred into a 12 ml Falcon tube, and centrifuged at 1020×g for 3 minutes. The supernatant was discarded, and 1 ml of protease trypsin (Sigma-Aldrich, St. Louis, MO, USA) was added to the pelleted neurospheres. After 3 minutes of

trypsin incubation, 1 ml of trypsin inhibitor (Sigma-Aldrich, St. Louis, MO, USA) was added to the dissociated cells, to block the proteolytic effect of trypsin. Subsequently, a negligible portion (~100 μl) of the cell suspension was used to count cells in the hemocytometer. The rest of the cell suspension was centrifuged at 1020×g for 3 minutes. The cells were plated on poly-L-lysine (PLL)-coated (Sigma-Aldrich, St. Louis, MO, USA) coverslips placed in a 24-well plastic plate, at the cell density of 6×10^4 cells/cm^2. The cultures were treated with differentiation medium, which had the same composition as the proliferation medium, but it was devoid of EGF, and with higher (20 ng/ml) concentration of bFGF. The cultivation conditions were maintained at 37 °C and 5% CO_2, with medium exchange on every third day. After 8-9 days of *in vitro* differentiation (Figure 16, right), the cells were used for electrophysiological measurements, immunocytochemistry, Western blotting analysis, and RT-qPCR. To estimate the impact of Wnt signaling inhibition or activation during differentiation of NS/PCs, 4OHT and EtOH cultures were compared.

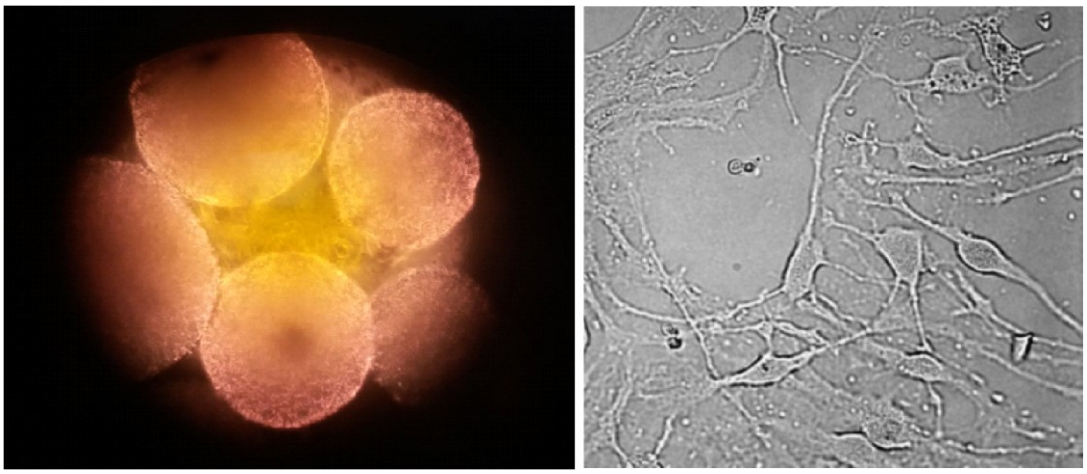

Figure 16. Cultivation of neural stem/progenitor cells *in vitro*. (Left) Neural stem/progenitor cells form neurospsheres during the proliferation stage of *in vitro* cultivation. **(Right)** Neural stem/progenitor cells after 8-9 days of differentiation form relatively highly confluent cell cultures (author's own photographs).

Primary cultures of adult NS/PCs were derived from the SVZ of the LV; from both right and left SVZs from CTRL mice, while only from the SVZ ipsilateral to the site of injury in mice three days after MCAO (Figure 17). After decapitation, brains were quickly removed from the skull and sliced into ~500 μm coronal slices using vibratomes HM 650 V (MICROM International GmbH, Walldorf, Germany) or Leica VT 1200S (Baria s.r.o., Czech Republic), and the SVZs were carefully dissected out and cut into

smaller pieces using a razor. To obtain a single-cell suspension, the tissue was first incubated with continuous shaking at 37 °C for 45 minutes in 1 ml of papain solution (20 U/mL) with 0.2 ml of deoxyribonuclease (DNase; both from Worthington, Lakewood, NJ, USA). After papain treatment, the activity of the enzyme was inhibited with 1 ml of trypsin inhibitor (Sigma-Aldrich, St. Louis, MO, USA), and the tissue was afterwards mechanically dissociated by gentle trituration using a 1 ml pipette and centrifuged at 1020×g for 3 minutes. After centrifugation, the supernatant was discarded and the cells were resuspended in 1 ml of proliferation medium, of which composition was equal to the one used for the cultures derived from neonatal mice; however, the concentration of EGF was higher, at 30 ng/ml. The rest of the procedure was the same as for neonatal mice, with one exception – the cells were cultured as neurospheres for longer period of time to secure enough cells for further analyses, which required ~12 days of *in vitro* proliferation.

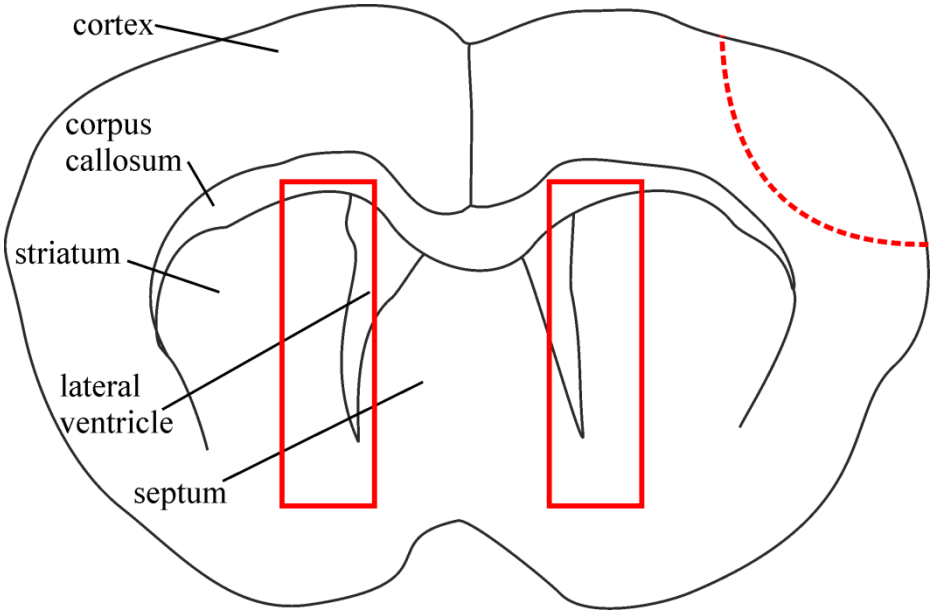

Figure 17. Isolation of the subventricular zone. For the experiments on adult neural stem/progenitor cells, the tissue around the subventricular zones was isolated (red solid lines). After the induction of focal cerebral ischemia (red dashed line), only the subventricular zone ipsilateral to the site of injury was isolated. Some of the major brain structures are labeled in the scheme (author's own scheme).

Tissue for Western blotting or RT-qPCR was also isolated from the SVZs of adult CTRL and MCAO animals. Mice were anesthetized with 4% isoflurane (Abbot, IL, USA) and subsequently with 1% PTB and perfused transcardially with ice-cold isolation buffer. After decapitation, brains were quickly removed from the skull and cut into ~500 μm coronal sections using the vibrating microtome. The SVZs were dissected out and cut into

smaller pieces using a razor. Afterwards, the tissue was transferred into empty 2 ml Eppendorf tubes or tubes containing TRI Reagent (Sigma-Aldrich, St. Louis, MO, USA) for further Western blotting and RT-qPCR analyses, respectively. The tubes containing tissue were immediately placed on dry ice and subsequently stored at -80 °C.

3.3.2 Isolation and processing of tissue for cultures of NG2 glia

Control mice or mice three, four, seven, or fourteen days after FCI were deeply anesthetized with PTB (100 mg/kg, i.p.), and perfused transcardially with ice-cold isolation buffer. The cerebral cortex was cut into ~600 μm coronal sections using the vibratome and the region around the ischemic lesion was carefully dissected out from the white matter tracks. The tissue from CTRL animals was isolated from the same regions. The tissue was incubated with continuous shaking at 37 °C for 45 minutes in 1 ml of papain solution supplemented with DNase. After the incubation in papain, the tissue was gently mechanically dissociated with a 1 ml pipette. Dissociated cells were subsequently layered on top of 5 ml of ovomucoid inhibitor solution (Worthington, Lakewood, NJ, USA) and harvested by low-speed centrifugation (140×g for 6 minutes), with subsequent filtration through a 70 μm cell filter. At this stage, the resulting single-cell suspension could be kept on ice and used for cell counting or fluorescence-activated cell sorting (FACS; BD Influx, San Jose, CA, USA). To prepare primary cell cultures, the cells were plated at the same cell density as NS/PCs and maintained in Dulbecco's Modified Eagle Medium/Nutrient Mixture F12 (DMEM/F12) with antibiotics penicillin/streptomycin/amphotericin (PSA; all from Invitrogen, Carlsbad, CA, USA), 20 ng/ml platelet-derived growth factor alpha (PDGFα; Peprotech, Rocky Hill, NJ) and 4 mM glutamine (Sigma–Aldrich, St. Louis, MO, USA). This DMEM/F12-based medium is further referred to as 'basal medium'. For the first 24 hours of *in vitro* cultivation, the basal medium was supplemented with 15% fetal bovine serum (FBS; HyClone, Thermo Scientific, Waltham, MA, USA). Then, the cell cultures were transferred to the differentiation medium consisting of basal medium with B27 supplement (Invitrogen, Carlsbad, CA, USA). To activate Shh signaling in NG2 cells, Shh (20 ng/ml; Peprotech, Rocky Hill, NJ, USA) or SAG (300 ng/ml, VDM Biochemicals, Bedford Heights, OH, USA) were added, and to block Shh signaling, Cyc (4 mg/ml, LKT Laboratories, St. Paul, MN, USA) was added. Seven days after the onset of *in vitro* differentiation, the

phenotype of differentiated Tom-positive NG2 glia was analyzed using the patch-clamp technique in the whole-cell configuration and immunochemical staining.

3.4 Preparation of coronal tissue sections for immunohistochemical staining

Adult mice were deeply anesthetized with PTB (100 mg/kg, i.p.; Sigma-Aldrich, St. Louis, MO, USA) and perfused transcardially using saline solution (ArdeaPharma, a.s., Sevetin, Czech Republic) with 0.65% heparin (Zentiva Group, a.s., Prague, Czech Republic) at room temperature and subsequently with ice-cold 4% paraformaldehyde (PFA; Sigma-Aldrich, St. Louis, MO, USA). The brain was then left in PFA for 3 more hours for thorough fixation, with subsequent transfer to the sucrose gradient for cryoprotection. The tissue was incubated in 10% sucrose for 12 hours, then in 20% sucrose for 24 hours, followed by 30% sucrose incubation for further 72 hours. Thirty-µm-thick coronal sections were prepared using a cryostat (Leica CM1850, Leica Microsystems, Wetzlar, Germany) and subsequently stored at -20 °C in a cryopreservation solution prepared in the laboratory.

3.5 Patch-clamp measurements

The electrophysiological properties of *in vitro* differentiated cells were recorded using the patch-clamp technique in the whole-cell configuration. Recording micropipettes with a tip resistance of ~10 MΩ were made from capillaries of borosilicate glass (Sutter Instruments, Novato, CA, USA) using a P-97 Brown-Flaming puller (Sutter Instruments, Novato, CA, USA) and subsequently filled with artificial intracellular solution containing (in mM): 10 4-(2-hydroxyethyl)-1-piperazineethanesulfonic acid (HEPES), 130 KCl, 0.5 $CaCl_2$, 2 $MgCl_2$, 5 ethylene glycol-bis(β-aminoethyl ether)-N,N,N′,N′-tetraacetic acid (EGTA), with pH 7.2, and in some cases also mixed with Alexa Fluor hydrazide 488 (A488; Molecular Probes, Carlsbad, CA, USA) for visualization of recorded cells. The measurements were made in artificial cerebrospinal fluid (aCSF) containing (in mM): 122 NaCl, 3 KCl, 1.5 $CaCl_2$, 1.3 $MgCl_2$, 1.25 Na_2HPO_4, 28 $NaHCO_3$, and 10 D-glucose (osmolality 300 ± 5 mmol/kg) and this solution was continuously gassed with 5% CO_2 to maintain a final pH of 7.4. All recordings were made at room temperature on coverslips perfused with aCSF in the recording chamber of an upright Axioscop microscope (Zeiss, Gottingen, Germany) equipped with 2 electronic micromanipulators (Luigs & Neumann,

Ratingen, Germany) and a high-resolution AxioCam HR digital camera (Zeiss, Gottingen, Germany). Electrophysiological data were measured with a 10 kHz sample frequency using EPC9/10 amplifiers controlled by the PatchMaster software (HEKA Elektronik, Lambrecht/Pfalz, Germany) and filtered using a Bessel filter.

The value of the membrane potential (V_m) was measured by switching the EPC9/10 amplifiers to the current-clamp mode. Using the FitMaster software (HEKA Elektronik, Lambrecht/Pfalz, Germany), input resistance (IR) was calculated from the current value at 40 ms after the onset of the depolarizing 10 mV pulse from the holding potential of -70 mV. Membrane capacitance (C_m) was determined automatically from the Lock-in protocol by the software. Current patterns were obtained by hyperpolarizing and depolarizing the cell membrane from the holding potential of -70 mV to the values ranging from -160 mV to 40 mV in 10 mV steps, while the duration of each pulse was 50 ms. The inwardly rectifying K^+ (K_{IR}), the fast activating and inactivating outwardly rectifying K^+ (K_A), and the delayed outwardly rectifying K^+ (K_{DR}) current components were determined as follows. In order to isolate the K_{DR} current components, a voltage step from -70 to -60 mV was used to subtract the time- and voltage-independent currents. To activate the K_{DR} currents only, the cells were held at -50 mV, and the amplitude of the K_{DR} currents was measured at 40 mV, 40 ms after the onset of the pulse. The K_{IR} currents were determined analogously at -140 mV, also 40 ms after the onset of the pulse, while the cells were held at -70 mV. The K_A currents were measured at 40 mV and were isolated by subtracting the current traces, clamped at -110 mV from those clamped at -50 mV, and its amplitude was measured at the peak value. While measuring tetrodotoxin (TTX)-sensitive sodium (Na^+) currents, the cells were held at -70 mV and the current amplitudes were isolated by subtracting the current traces measured in solution containing 1 μM TTX (Alomone Labs, Jerusalem, Israel) from those measured in the absence of TTX in aCSF. The Na^+ current amplitudes were measured at the peak value. The current densities were calculated by dividing the maximum current amplitudes by the corresponding C_m values for each individual cell. The action potentials were obtained in the current-clamp mode. The current values in the protocol ranged from 50 to 1000 pA, at 50 pA increments, and the pulse duration was 300 ms. A more detailed description can be found in the publications of our department (Anderová et al., 2006; Neprasova et al., 2007).

After recording, the cells on the coverslips were fixed in 4% PFA dissolved in 0.2 M phosphate buffer (PB; pH 7.4) for 9 minutes, then transferred to 10 mM phosphate-

buffered saline (PBS; pH 7.2) and stored at 4 °C for post-recording identification using immunofluorescence staining.

3.6 Immunocyto/histochemistry and confocal microscopy

The primary cultures on coverslips or 30-µm-thick coronal brain slices (in this section both further referred to as 'specimens') were washed 3 times for 10 minutes in PBS. Afterwards, they were rinsed for 2 hours and at 4 °C in blocking solution containing 5% Chemiblocker (Millipore, Billerica, MA, USA) and 0.5% Triton X-100 (Sigma-Aldrich, St. Louis, MO, USA) diluted in 10 mM PBS. The same blocking solution was also used as the diluent for all primary and secondary antibodies. The specimens were incubated overnight at 4 °C with primary antibodies. The following primary antibodies were used: rabbit polyclonal anti-GFAP (1:800; Sigma-Aldrich, St. Louis, MO, USA), mouse monoclonal anti-GFAP conjugated to A488 (1:300; Thermo Fisher Scientific, Waltham, MA, USA), mouse monoclonal anti-GFAP (1:800; Sigma-Aldrich, St. Louis, MO, USA) conjugated to cyanine dye 3 (Cy3), rabbit polyclonal anti-PDGFαR (1:200; Santa Cruz Biotechnology, Dallas, TX, USA), rabbit polyclonal anti-DCX (1:1000; Abcam, Cambridge, UK), rabbit polyclonal anti-DCX (1:500; Santa Cruz Biotechnology, Dallas, TX, USA), mouse monoclonal anti-microtubule-associated protein 2 (MAP2; 1:800; Merck Millipore, Billerica, MA, USA), mouse monoclonal anti-proliferating cell nuclear antigen (PCNA; 1:1000; Abcam, Cambridge, UK), mouse anti-adenomatous polyposis coli clone CC1 (CC1; 1:200; Merck, Frankfurt, Germany), rabbit anti-Ki67, a marker of proliferation (1:1000; Abcam, Cambridge, UK), rabbit anti-CNPase (1:100; Sigma-Aldrich, St. Louis, MO, USA), mouse anti-myelin/oligodendrocyte-specific protein (MOSP; 1:400; Merck Millipore, Billerica, MA, USA), rabbit anti-NG2 (1:400; Merck Millipore, Billerica, MA, USA), rabbit anti-platelet-derived growth factor β receptor (PDGFβR; 1:200; Santa Cruz, Dallas, TX, USA). On the following day, the specimens were washed 3 times for 10 minutes with PBS, which was followed by incubation with secondary antibodies for two more hours at 4 °C. The secondary antibodies were goat polyclonal anti-rabbit/mouse immunoglobulin G (IgG) conjugated to A488, or Alexa Fluor 594 or 660 (A594/660; 1:200; Molecular Probes, Carlsbad, CA, USA). The specimens were afterwards again washed 3 times for 10 minutes in PBS and rinsed for 5 more minutes, this time at room temperature, in 300 nM 4′,6-diamidino-2-phenylindole (DAPI; Molecular Probes, Carlsbad, CA, USA) diluted in PBS for cell nuclei

visualization. At the end of the procedure, the specimens were mounted onto microscope slides using Aqua Poly/Mount (Polysciences Inc., Eppelheim, Germany). Once the mounting medium solidified, the specimens were ready to be analyzed by confocal microscopy.

To evaluate the proliferation rate of precursor cells, 5-ethynyl-2´-deoxyuridine (EdU; 0.2 mg/ml; Sigma-Aldrich, St. Louis, MO, USA) or 5-bromo-2'-deoxyuridine (BrdU; 1 mg/ml; Sigma-Aldrich, St. Louis, MO, USA) were added to the drinking water and administered to the mice for three or seven days. For EdU visualization, we used the AlexaFluor-647 Click-iTEdU Cell Proliferation Assay Kit (Sigma-Aldrich, St. Louis, MO, USA) and then washed the specimens in PBS. The mouse anti-BrdU primary antibody (1:200, Abcam, Cambridge, UK), in the combination with one of the secondary antibodies mentioned above, was utilized for BrdU visualization.

An LSM 5 DUO confocal fluorescence microscope (Zeiss, Gottingen, Germany) equipped with an Arg/HeNe laser was used for immunofluorescence analysis and, furthermore, the fluorescence signals were analyzed using the ImageJ software (NIH, Bethesda, MD, USA). For NS/PCs analysis, superimposed images of GFAP, PDGFαR, DCX or MAP2 stainings were obtained by overlaying several individual confocal planes. The images were subsequently digitally filtered and the immunopositive areas were used for quantification. The areas corresponding to the immunoreactivity of the cells were calculated in random regions of interest and divided by DAPI-positive area to normalize them to the cell number. At least six random regions of interest (ROIs) from two independent cultures with similar confluence were used for the quantification of each immunostaining. An example of such ROI that corresponds to DCX staining is shown in Figure 18.

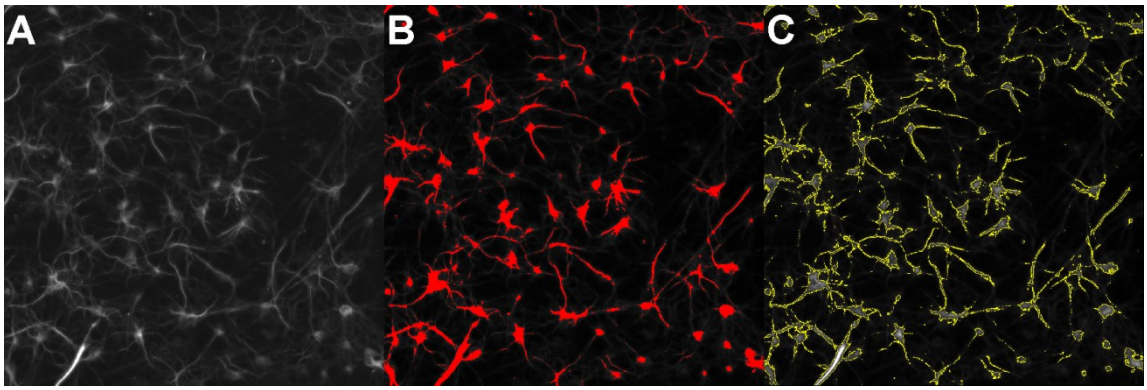

Figure 18. Quantification of immunopositive areas. (A) Superimposed image of doublecortin (DCX) staining, obtained by overlaying 4 individual confocal planes (each 318.2 µm x 318.2 µm

large). **(B, C)** Digitally filtered image (red area) outlined in yellow was used for the quantification of the fluorescent signal (Kriska et al., 2016).

Immunocytochemical staining against β-catenin was similar to the previous staining and more detailed description may be found elsewhere (Doubravska et al., 2011). In short, cells were fixed for 10 minutes in 4% PFA, permeabilized with 0.25% Triton X-100 for another 10 minutes and washed in PBS. Overnight incubation with primary mouse monoclonal antibody (1:2000; BD Transduction Laboratories, San Jose, CA, USA) at 4 °C was followed by incubation with goat anti-mouse secondary antibody conjugated to A488 dye for 1 hour at room temperature. Finally, DAPI (Sigma-Aldrich, St. Louis, MO, USA) was used for counterstaining. Fluorescent microscopy images (n=12) were taken from EtOH and 4OHT cultures. The A488 and DAPI fluorescence signals were analyzed with the ImageJ software and the intensity of β-catenin staining was normalized to the cell number in every image. Obtained data were evaluated by Student's t-test.

To assess the differentiation potential of progenitor cells of the SVZ *in situ* in coronal sections, we utilized a spinning disc confocal fluorescent microscope Dragonfly 530 Andor (Oxford Instruments, Oxford, UK), equipped with Zyla 4.2 PLUS sCMOS camera and Fusion acquisition system. Superimposed images of GFAP, DCX, and PCNA stainings were obtained by overlaying 6-12 individual confocal planes that were beforehand digitally fused using the Fusion stitching tool. Obtained images were processed in the Imaris visualization software (Oxford Instruments, Oxford, UK). The immunopositive SVZ areas were dissected and quantified using the Fiji ImageJ software (NIH, Bethesda, MD, USA). The areas corresponding to immunopositive cells of the SVZ were calculated and normalized to DAPI-positive area. Together six SVZ sections from two biological replicates were analyzed in each immunostaining data set.

The LSM 5 DUO confocal microscope with 40× oil objective was also used for immunochemical analysis of NG2 glia. Stacks of consecutive confocal images at the thickness of 3 μm were acquired sequentially with two lasers to avoid any crosstalk between the channels. The background noise of each confocal image was reduced by averaging four input images. The co-localization of fluorescence signals was assessed by employing the maximum Z-projection feature in the Zeiss LSM Image Browser (Zeiss, Gottingen, Germany). The assessment of the cells in the glial scar was performed in confocal images of coronal brain sections of at least three mice and the cell counts were

estimated from superimposed images generated in the GSA Image Analyzer (Bansemer & Scheel GbR, Rostock, Germany).

3.7 Reverse transcription quantitative polymerase chain reaction

For the NS/PCs experiments, the tissue was isolated and stored as described at the end of section 3.3.1. Furthermore, RNA was purified using TRI Reagent (Sigma-Aldrich, St. Louis, MO, USA) or RNA Blue (Top-Bio, Prague, Czech Republic) according to the manufacturers' protocols. The reverse transcription of RNA and RT-qPCR were performed using LightCycler® 480 SYBR Green I Master (Roche Diagnostics, Indianapolis, IN, USA; Lukas et al., 2009). The primers for RT-qPCR are listed in Table 1.

Since the RT-qPCR analysis was performed on Tom-expressing NG2 glia, we were able to take advantage of the single-cell approach. A negligible amount of the fluorescent dye Hoechst 33258 (Life Technologies, Carlsbad, CA, USA) was added to the cell suspension to identify and subsequently discard damaged or dead cells. Individual cells were collected employing FACS (BD Influx, San Jose, CA, USA). The cell sorter was set to place one cell in each well of 96-well microtiter plates (Life Technologies, Carlsbad, CA, USA) filled with 5 µl of nuclease-free water mixed with bovine serum albumin (BSA; 1 mg/ml; Fermentas, Rockford, IL, USA) and RNaseOut (20 U; Life Technologies, Carlsbad, CA, USA). The expression of almost one hundred genes was assessed and the lists of primers for RT-qPCR can be found in Honsa et al. (2016) and Valny et al. (2018). The mRNA was reverse-transcribed into cDNA with SuperScript III (ThermoFisher Scientific, Waltham, MA, USA), with further pre-amplification and analysis in the BioMark platform (Fluidigm, San Francisco, CA, USA). The data were analyzed using the GenEx 6 software (MultiD, Sweden).

Self-organizing maps (SOM) that divided Tom-positive cells into four subpopulations were trained in the GenEx 6 software (MultiD, Sweden), while 0.60 learning rate, 4 neighbors, and 5,000 iterations were all used as the settings. The subpopulations were expressed as groups of cells in the principal component analysis (PCA).

Table 1. Sequences of primers used for reverse transcription quantitative polymerase chain reaction experiments.

Gene symbol	Sequence
Actb	FP: 5'-GATCTGGCACCACACCTTCT-3' RP: 5'-GGGGTGTTGAAGGTCTCAAA-3'
Axin2	FP: 5'-TAGGCGGAATGAAGATGGAC-3' RP: 5'-CTGGTCACCCAACAAGGAGT-3'
Ccnd1	FP: 5'-AGTGCGTGCAGAAGGAGATT-3' RP: 5'-CTCTTCGCACTTCTGCTCCT-3'
GAPDH	FP: 5'-AACTTTGGCATTGTGGAAGG-3' RP: 5'-ATCCACAGTCTTCTGGGTGG-3'
Nkd1	FP: 5'-AGGACGACTTCCCCCTAGAA-3' RP: 5'-TGCAGCAAGCTGGTAATGTC-3'
Sp5	FP: 5'-GGACAGGAAACTGGGTCGTA-3' RP: 5'-AATCGGGCCTAGCAAAAACT-3'
Troy	FP: 5'-GCTCAGGATGCTCAAAGGAC-3' RP: 5'-CCAGACACCAAGACTGCTCA-3'
Ubb	FP: 5'-ATGTGAAGGCCAAGATCCAG-3' RP: 5'-TAATAGCCACCCCTCAGACG-3'
Wnt4	FP: 5'-AACGGAACCTTGAGGTGATG-3' RP: 5'-TCACAGCCACACTTCTCCAG-3'
Wnt5a	FP: 5'-AGGAGTTCGTGGACGCTAGA-3' RP: 5'-ACTTCTCCTTGAGGGCATCG-3'
Wnt5b	FP: 5'-CGCTTTGGAAGATGTTGGTC-3' RP: 5'-ACATCTCCGGTCTCTGCACT-3'
Wnt7a	FP: 5'-GCCTGGACGAGTGTCAGTTT-3' RP: 5'-TGGTACTGGCCTTGCTTCTC-3'
Wnt7b	FP: 5'-AGTGCCAGCACCAGTTCC-3' RP: 5'-CCTTCCGCCTGGTTGTAGTA-3'
Wnt9a	FP: 5'-TCGTGGGTGTGAAGGTGATA-3' RP: 5'-TGGCTTCATTGGTAGTGCTG-3'
Wnt10b	FP: 5'-CTTCGACATGCTGGAGGAG-3' RP: 5'-CCCAGCTGTCGCTTACTCAG-3'

Abbreviations: Actb – β-actin; Ccnd1 – cyclin D1; FP – forward primer; GAPDH – glyceraldehyde-3-phosphate dehydrogenase; Nkd1 – naked cuticle homolog 1; RP – reverse primer; Sp5 – SP5 transcription factor; Troy – tumor necrosis factor receptor superfamily, member 19; Ubb – ubiquitin; Wnt4-10b – Wingless/Integrated 4-10b (adapted from Kriska et al. (2016)).

3.8 Western blotting

Protein analysis employing Western blotting was performed by two different approaches, depending on whether cell cultures or tissue specimens were analyzed. If cell cultures cultivated *in vitro* on plastic dishes were assessed, cells were lysed in standard 1x radio immunoprecipitation assay (RIPA) buffer, containing 25 mM Tris-HCl, pH 8.0; 150 mM NaCl; 1% NP-40; 1% sodium deoxycholate; 0.1% sodium dodecyl sulfate (SDS); 1 mM ethylenediaminetetraacetic acid (EDTA), and supplemented with inhibitors of proteases (Roche, Basel, Switzerland) and phosphatases (20 mM NaF; 1 mM Na3VO4). The total protein content in the homogenates was determined using the Pierce BCA™ protein assay kit (Thermo Fisher Scientific, Waltham, MA, USA). Equal amounts of proteins, supplemented with 100 mM dithiothreitol, were subjected to SDS-polyacrylamide gel electrophoresis (PAGE; 10 – 15%). The proteins were then transferred onto nitrocellulose membrane (Hybond ECL 0.45 µM; Little Chalfont, Amersham, UK) and detected by specific primary antibodies as follows: anti-β-actin (1:1000; Santa Cruz Biotechnology), anti-β-catenin (1:2000; BD Biosciences), anti-phosphorylated (p)β-catenin (1:300; Cell Signaling), anti-β III tubulin (1:400; Sigma-Aldrich). The primary antibodies were combined with horseradish peroxidase-conjugated secondary antibodies (1:5000; Jackson Immunoresearch, West Grove, PA, USA). Peroxidase activity was detected using enhanced chemiluminescence (ECL) detection reagents (Little Chalfont, Amersham, UK).

Tissue was isolated and stored as described at the end of section 3.3.1. Frozen tissue specimens were homogenized with steel balls (Quiagen, Germantown, MD, USA) in 10 µl/mg of ice-cold lysis buffer (50 mM HEPES/KOH, pH 7.4, 1% Triton X-100, 50 mM NaF, 5 mM $Na_2H_2P_2O_7$, 400 mM NaCl, 40 mM β-glycerophosphate, 12.5 mM EGTA, 1.5 mM $MgCl_2$, 1 mM Na_3VO_4, 0.5 mM serine protease inhibitor phenylmethylsulfonyl fluoride (PMSF) and 10 µl/ml of protease inhibitor cocktail containing 1 mM benzamidin, 0.28 mM leupeptin, 0.2 mM pepstatin, 0.22 mM antipain). The lysates were cleared by high-speed centrifugation (30000×g, 30 minutes), combined with Laemmli sample buffer and the samples were incubated for 20 minutes at 70 °C. Total amount of 50 µg of proteins were loaded per lane. The proteins were separated on SDS-PAGE (8.2% acrylamide (AA) with 0.2% bisacrylamide (BIS), or 6% AA with 0.2% BIS for MAP2 protein) and transferred to Immobilon-P^{SQ} membrane (Millipore, Billerica, MA, USA) using Trans-Blot SD Semi-dry Transfer Cell (BioRad, Hercules,

CA, USA). The usual Towbin transfer buffer was used with the exception of the 6% gel for MAP2 protein for which the Bjerrum-Schaffer-Nielsen buffer (48 mM Tris, 39 mM glycine, 0.0375% SDS, pH 9.2.) was used. Samples were blocked for 1 hour with 5% non-fat milk and then incubated with following primary antibodies: mouse monoclonal anti-β-catenin (1:2000; ExBio), rabbit anti-non-phospho (active) β-catenin (1:500; Cell Signaling), rabbit monoclonal anti-GFAP (1:500; Cell Signaling), rabbit anti-DCX (1:500; Cell Signaling), rabbit monoclonal anti-MAP2 (1:500; Cell Signaling), mouse monoclonal anti-β III tubulin (1:400; Sigma-Aldrich), and rabbit monoclonal anti-heat shock protein 90 (Hsp90) (1:1500; Cell Signaling). After one hour of incubation with the primary antibodies (diluted in 5% BSA in PBS with 0.2% Tween 20) at room temperature, the membranes were washed five times for 15 minutes with PBS with 0.2% Tween 20, and incubated with either anti-rabbit IgG or anti-mouse horseradish peroxidase-conjugated antibody (1:3500; Cell Signaling) for one hour at room temperature. Peroxidase activity was detected using ECL detection reagent LumiGlo (Cell Signaling, Leiden, The Netherlands).

3.9 Calcium imaging measurements

Coverslips with cell cultures were incubated for 45 minutes in 0.5 ml of differentiation medium containing 4.5 μM Oregon-Green Bapta-1, AM (OGB-1) and 0.09% Pluronic F-127 (Life Technologies, Waltham, MA, USA) in an incubator at 37 °C and 5% CO_2. The coverslips were then transferred to the microscope superfusion chamber and three measurements were made on each coverslip with a sufficient distance between the measurement regions. During the measurements, the microscope superfusion chamber was continually perfused at room temperature at a flow rate of 2.5 ml/minute with HEPES-based aCSF containing (in mM): 135 NaCl, 2.7 KCl, 1 $MgCl_2$, 2.5 $CaCl_2$, 1 Na_2HPO_4, 10 glucose, 10 HEPES (pH 7.4, osmolality 305 mOsm/kg, equilibrated with O_2). The solutions of ATP, L-glutamic acid (glutamate) (both from Sigma-Aldrich, St. Louis, MO, USA) and HEPES-based aCSF, in which part of NaCl was replaced for KCl to reach 50 mM concentration of K^+ (H-aCSF$_{50K+}$), were applied through a capillary (internal diameter of 250 μm) located 0.5-1 mm from the measurement region and connected to a Perfusion Pressure Kit pressurized application system (flow rate 600 μl/minute) controlled by a ValveBank II controller (AutoMate Scientific, Inc. Berkeley, CA, USA). The HEPES-based aCSF was applied before and after the applications with

the same flow rate so that the responses were not influenced by the application itself. The OGB-1 fluorescence was detected with a TILL Photonics Imaging System installed on a Zeiss Axioskop 2 FS Plus microscope equipped with a long-distance 40x lens (IR Achroplan 0.8 W, Zeiss, Gottingen, Germany). A digital camera (PCO Sensicam, Kelheim, Germany) was controlled by the TILLvisION software. The excitation light (484 nm) was generated by a Polychrome V (TILL Photonics GmbH, Grafelfing, Germany), filtered by a band-pass (BP) 450-490 excitation filter, reflected by a FT 510 beam splitter and the emitted light was filtered by a long-pass (LP) 515 filter (Filter Set 09, Zeiss, Gottingen, Germany). Images were acquired at 0.83 Hz and were analyzed offline. Fluorescence intensity (F) was measured in the cell bodies and expressed as $\Delta F/F_0$, where F_0 is the baseline fluorescence intensity before drug application. The threshold for Ca^{2+} responses was 110% of the baseline fluorescence and the maximum intensity, which occurred within 1 minute from the onset of application, was taken into account. After the measurements, immunocytochemical stainings for GFAP, DCX, MAP2, and PDGFαR were performed to confirm the identity of the measured cells.

3.10 Data analysis

The data are presented as means ± standard error of the mean (S.E.M.) or as means ± standard deviation (S.D.) for a number (n) of cells. Student's t-test was used to determine significant differences between two experimental groups, and one-way or two-way ANOVA with Tukey's *post hoc* test was performed to determine significant differences among more experimental groups, unless indicated otherwise. The significance was calculated in the GraphPad Prism software (San Diego, CA, USA), and the values of $p < 0.05$ were considered significant (*/$^{\#}$/°, one asterisk, hashtag, or circle), $p < 0.01$ very significant (**/$^{\#\#}$/°°, two asterisks, hashtags, or circles), and $p < 0.001$ extremely significant (***/$^{\#\#\#}$/°°°, three or more asterisks, hashtags, or circles).

4 RESULTS

In the present work, we assessed the differentiation potential of precursor cells. The gathered results are divided into three more or less successive chapters. Initially, we performed experiments on NS/PCs derived from neonatal mice. Further, we carried out similar experiments on adult animals, in which we also looked into the impact of Wnt signaling on the differentiation potential of NS/PCs following the induction of FCI. Finally, we aimed to elucidate the effects of cellular signaling pathways (Wnt and Shh) and ischemia on the differentiation potential of NG2 glia. The chapters treating NS/PCs were composed of the results published in Kriska et al. (2016) together with so far unpublished data, while the chapters about NG2 cells were compiled based on two other publications (Valny et al., 2018; Honsa et al., 2016) on which the author collaborated.

4.1 The differentiation potential of neonatal neural stem/progenitor cells

Initial experiments on NS/PCs were commenced in neonatal mice since young animals are more easily available, the processing of the tissue is less time-consuming and, most importantly, they enable higher yields of cells. Moreover, our goal was to compare three transgenic mouse strains in our hands and decide which ones would be employed in further experiments on adult NS/PCs. We utilized several approaches evaluating cellular changes at mRNA, protein, and functional levels.

4.1.1 Expression of Wnt signaling pathway components

Since all the experiments on NS/PCs derived from neonatal mice were conducted *in vitro*, we first analyzed which of the 19 identified mammalian Wnt ligands were present in our cultures. The RT-qPCR analysis revealed the presence of *Wnt4*, *Wnt5a*, *Wnt5b*, *Wnt7a*, *Wnt7b*, *Wnt9a* and *Wnt10b* ligands, while the expression of the other Wnt ligands was very low or they were not expressed at all. The most abundant ligands were *Wnt5a*, *Wnt7a*, and *Wnt7b* and we observed no differences in the expression pattern among mouse strains (Figure 19).

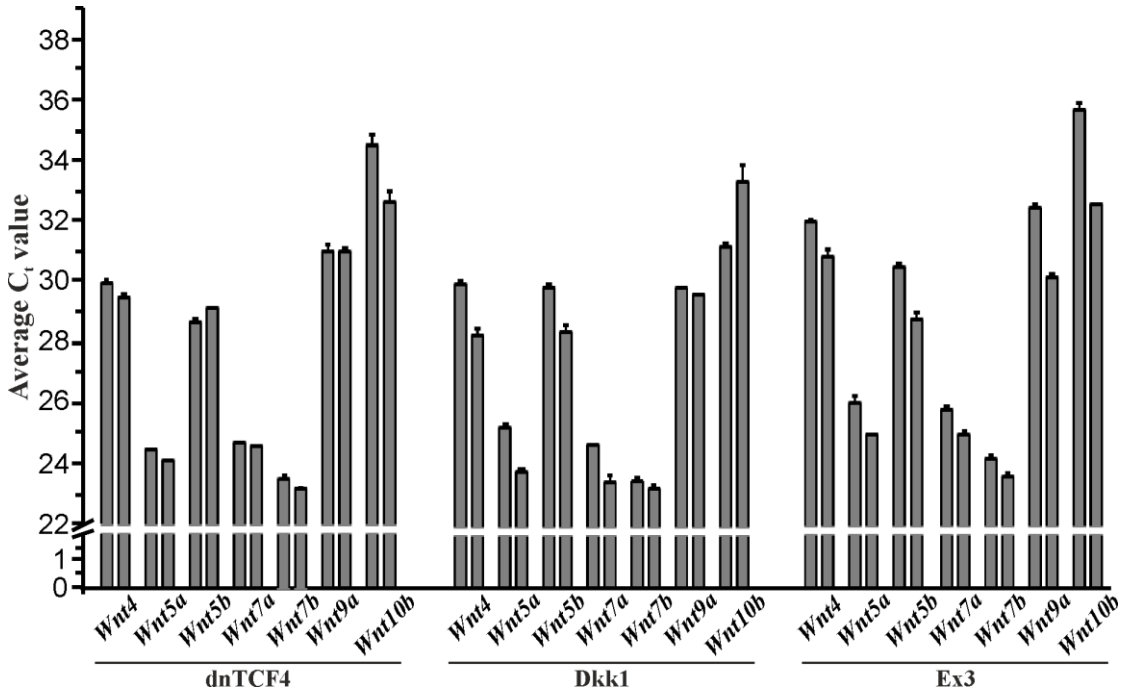

Figure 19. Expression of Wnt ligands in *in vitro* cultures. For each neonatal mouse strain, the expression of Wnt ligands was analyzed in two independent control samples (each performed in technical triplicates) that were void of 4OHT treatment. Four founder mice were used to derive NS/PCs for each mouse strain and the analysis was performed in technical triplicates. The average cycle threshold (C_t) values were normalized to the ubiquitin and β-actin housekeeping genes. The cells were analyzed eight days after the onset of *in vitro* differentiation. Abbreviations: 4OHT – (Z)-4-hydroxytamoxifen; Dkk1 – Dickkopf 1; dnTCF4 – dominant negative T-cell factor 4; Ex3 – exon 3; *Wnt4-10b* – Wnt signaling ligands (Kriska et al., 2016).

Furthermore, we analyzed several Wnt signaling pathway components in order to confirm that our *in vitro* setting with three distinct transgenic mouse strains (Figure 12) represents a suitable tool for manipulating the Wnt signaling pathway. We carried out immunocytochemical staining (Figure 20) and Western blotting analysis (Figure 21) of β-catenin, the main effector of the canonical Wnt pathway. After inhibiting the signaling in the nucleus via the production of dnTCF4, there was no significant difference in the levels of β-catenin protein (Figure 20A, D). Nevertheless, suppression of Wnt signaling by Dkk1 resulted in a marked decrease in the amount of β-catenin (Figure 20B, D). Conversely, the expression of the stabilized β-catenin form led to its higher abundance in Ex3 cells (Figure 20C, D).

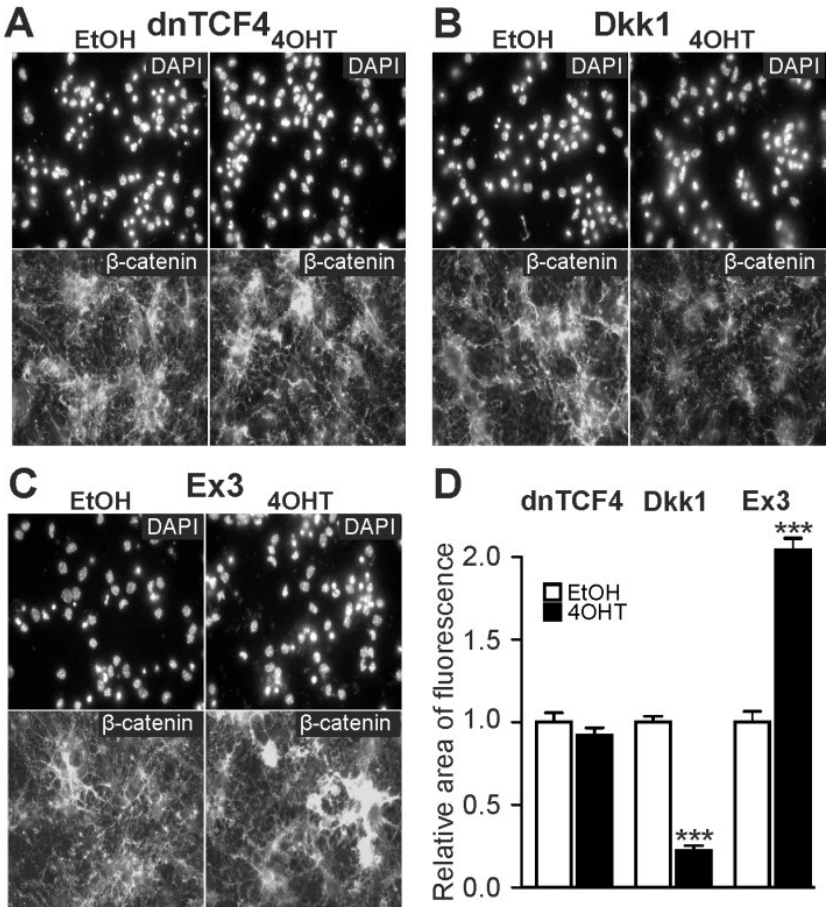

Figure 20. Immunocytochemical staining of β-catenin. (A-C) Representative fluorescent images of DAPI and β-catenin staining in differentiated neonatal neural stem/progenitor cells with inhibited (dnTCF4, Dkk1), or activated (Ex3) Wnt signaling. Cells were treated either with ethanol (EtOH) or with (Z)-4-hydroxytamoxifen (4OHT) and analyzed eight days after the onset of *in vitro* differentiation. **(D)** Quantification of β-catenin expression, showing the proportion of the area of positively-stained cells to the DAPI-positive area (n=12). The area of β-catenin fluorescence in control cells (EtOH) was arbitrarily set to 1. The values are represented as mean ± S.D. (standard deviation). Statistical significance was calculated using t-test; ***, $p < 0.001$. Abbreviations: DAPI – 4',6-diamidino-2-phenylindole; Dkk1 – Dickkopf 1; dnTCF4 – dominant negative T-cell factor 4; Ex3 – exon 3; n – number (adapted from Kriska et al. (2016)).

This stabilized, truncated β-catenin protein in Ex3 cells was also detected on Western blots (Figure 21A, B). Note that β-catenin in Ex3 cultures migrates as a doubled band because of the fact that the mutated variant lacks amino acids encoded by exon 3. As we expected, lower quantity of the N-terminally phosphorylated protein was also observed in these cultures.

Using Quantity One software (Bio-Rad, Hercules, CA, USA), we estimated the β-catenin-to-phosphorylated-β-catenin ratio of the peak heights in control EtOH- and 4OHT-treated cells. In differentiated NS/PCs derived from dnTCF4 and Dkk1 strains, the ratio lowered only negligibly (from 1.27 to 0.84 in Dkk1, and from 1.00 to 0.85 in

dnTCF4 mice). On the contrary, in Ex3 cells the ratio increased considerably from 0.90 in EtOH to 7.46 in 4OHT. Additionally, we performed the densitometric analysis (Figure 21B), which confirmed the changes in the β-catenin expression that corresponded to inhibition or activation of the pathway.

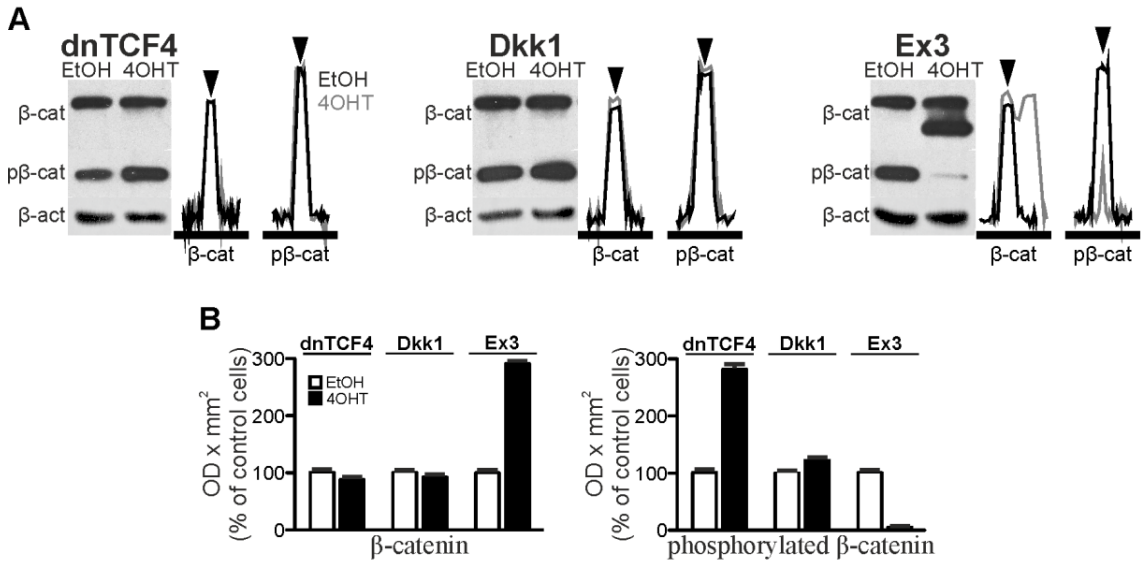

Figure 21. Levels of β-catenin protein in differentiated neonatal neural stem/progenitor cells. (A) Western blotting analysis of total (β-cat) and phosphorylated (pβ-cat) β-catenin, with intensity profiles representing the number and size of the respective bands. Arrowheads mark the molecular weight of β-catenin, which is 92 kDa. Together, four founder mice were used to derive NS/PCs for each mouse strain, and the analysis was performed in technical triplicates. The cells were analyzed eight days after the onset of *in vitro* differentiation. **(B)** Densitometric analysis representing quantification of the Western blots shown in **(A)**. The diagrams show the average optical density (OD) of detected β-catenin and phosphorylated β-catenin bands. Values obtained from cells in controls (EtOH) were arbitrarily set to 100%. The levels of the individual proteins, or their forms, were normalized to the β-actin (β-act) signal. Error bars represent S.D. (standard deviation). Abbreviations: 4OHT – (Z)-4-hydroxytamoxifen; Dkk1 – Dickkopf 1; dnTCF4 – dominant negative T-cell factor 4; Ex3 – exon 3 (adapted from Kriska et al. (2016)).

Additionally, we analyzed the expression of three Wnt signaling target genes, namely *Axin2*, *SP5 transcription factor* (*Sp5*), and *tumor necrosis factor receptor superfamily member 19* (*Troy*; Figure 22). Suppression of Wnt signaling in the nucleus led to lower expression of *Sp5* (average cycle threshold (C_t) value of 34.23 ± 0.37 in EtOH changed to average C_t value of 36.13 ± 0.13 in 4OHT-treated cultures) and *Troy* (28.11 ± 0.06 to 28.47 ± 0.11), while no changes in the expression of Wnt target genes were detected after inhibiting the pathway at the membrane level. Hyper-activation of the Wnt/β-catenin pathway resulted in markedly higher expression of all examined target

genes (32.74 ± 0.14 to 27.49 ± 0.10 in *Axin2*, 35.88 ± 0.17 to 26.55 ± 0.10 in *Sp5*, and 28.86 ± 0.42 to 23.75 ± 0.21 in *Troy*).

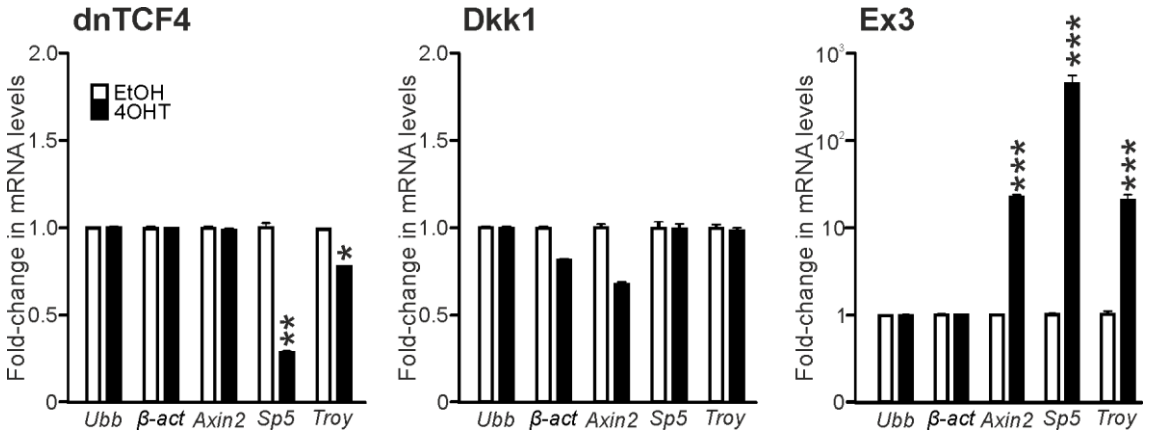

Figure 22. Expression of Wnt target genes in differentiated neonatal neural stem/progenitor cells. Reverse transcription quantitative polymerase chain reaction (RT-qPCR) analysis of Wnt signaling target genes was employed. Together, four founder mice were used to derive NS/PCs for each mouse strain and the analysis was performed in technical triplicates. The average cycle threshold (C_t) values were normalized to *glyceraldehyde-3-phosphate dehydrogenase* (*GAPDH*), and two other housekeeping genes (*ubiquitin* (*Ubb*) and *β-actin* (*β-act*)) are shown in the graph. *Axin2*, *Sp5* and *Troy* are Wnt target genes. The expression level of a given gene in control cells (EtOH) was arbitrarily set to 1. The cells were analyzed eight days after the onset of *in vitro* differentiation. Statistical significance was calculated using t-test; *, $p < 0.05$; **, $p < 0.01$; ***, $p < 0.001$. Abbreviations: 4OHT – (Z)-4-hydroxytamoxifen; Dkk1 – Dickkopf 1; dnTCF4 – dominant negative T-cell factor 4; Ex3 – exon 3; NS/PCs – neural stem/progenitor cells; *Sp5* – SP5 transcription factor; *Troy* – tumor necrosis factor receptor superfamily member 19 (adapted from Kriska et al. (2016)).

Collectively, the analysis of the components of the Wnt pathway described above indicate that employing NS/PCs from the neonatal brain of the three transgenic mouse strains may represent a suitable *in vitro* system for manipulating Wnt signaling. In these experiments, we showed that activation of the pathway resulted in higher amounts of β-catenin protein with a consequent increase in the expression of Wnt target genes in differentiated NS/PCs. The analysis of inhibited pathway at the membrane level or in the nucleus revealed lower quantities of β-catenin protein and decreased expression of Wnt target genes, respectively.

4.1.2 Cell types generated from neonatal NS/PCs and their incidence

In the following series of experiments, we first aimed to identify cellular types generated from NS/PCs in our *in vitro* system, and then to evaluate their incidence in EtOH- and

4OHT-treated cultures. In order to estimate the impact of Wnt signaling inhibition or activation on neonatal NS/PCs differentiation, we employed the patch-clamp technique in the whole-cell configuration and with this approach, we assessed the current profiles of cells differentiated *in vitro*. The measurement of electrophysiological properties was supplemented with immunocytochemical staining. Together, we identified three distinct subpopulations of cells in EtOH- (n=347) and 4OHT-treated (n=380) cultures. These cell types were subsequently divided into three groups according to their electrophysiological and immunochemical properties (Figure 23A-G). Flat-shaped GFAP-positive cells (n=242; Figure 23D) predominantly displayed passive time- and voltage-independent K^+ currents (Figure 23A), their average V_m was -86.38 ± 0.26 mV, and their IR was 81.62 ± 1.91 MΩ. Round DCX/MAP2-positive cells (n=289; Figure 23F, G), expressing K_A and K_{DR} currents (Figure 23C), were characterized by V_m of -72.04 ± 0.90 mV, and high values of IR (1649.79 ± 44.05 MΩ). Branched PDGFαR-positive cells (n=196; Figure 23E), with a complex current pattern, expressed K_{IR} currents, in addition to K_{DR} and K_A currents (Figure 23B), their V_m was -85.78 ± 0.45 mV, and IR was 218.56 ± 8.24 MΩ. Additionally, we took advantage of A488-filled glass capillaries and performed post-recording immunocytochemical identification that revealed that the majority of cells expressing passive currents were GFAP-positive, while most of the cells displaying outwardly rectifying currents were positive to DCX or MAP2. Complex currents were associated mainly with PDGFαR-positive cells.

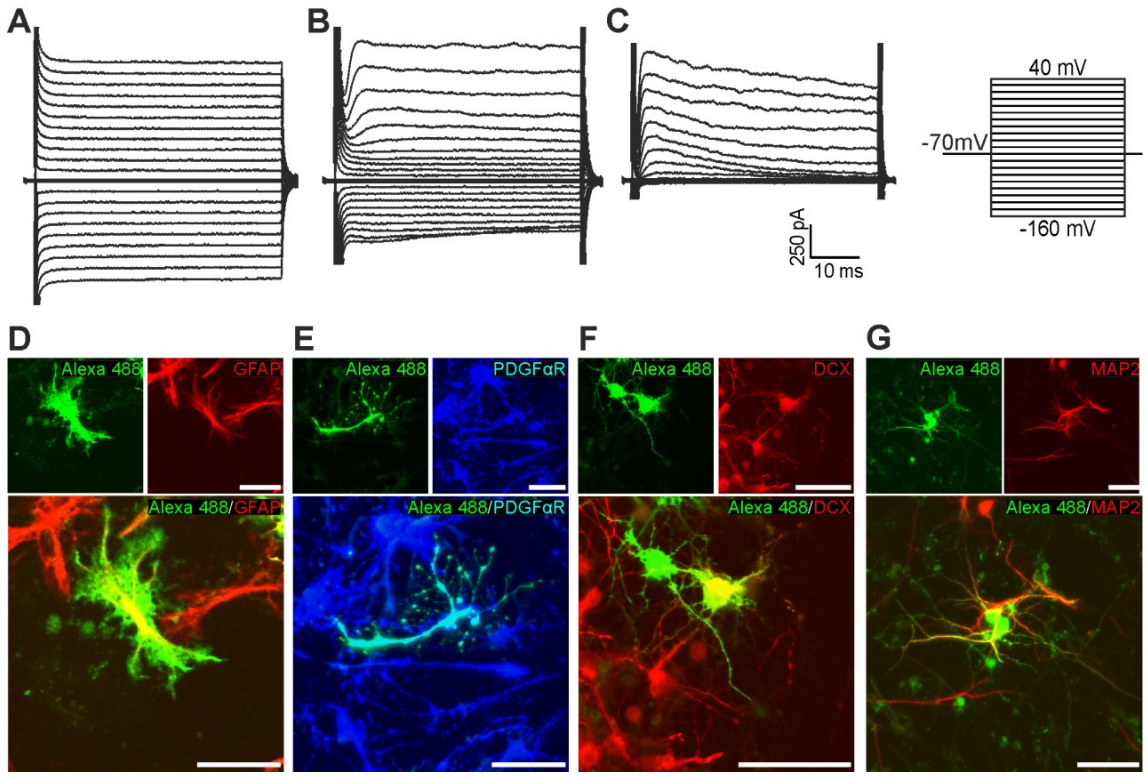

Figure 23. Characterization of cell types identified in the cultures of differentiated neural stem/progenitor cells. Together, three distinct cell types were found in the *in vitro* cultures. Cells with a passive current pattern **(A)** are mostly GFAP-positive and flat-shaped **(D)**. They display predominantly time- and voltage-independent K^+ currents, together with small amplitudes of delayed outwardly rectifying K^+ currents (K_{DR}) and inwardly rectifying K^+ currents (K_{IR}). The majority of cells displaying a complex current profile **(B)** are branched or bipolar, and PDGFαR-positive **(E)**. They express fast activating and inactivating outwardly rectifying K^+ currents (K_A), as well as K_{DR} and K_{IR} currents. Cells with an outwardly rectifying current pattern **(C)** are DCX/MAP2-positive, with a round shape (**F, G**), and express K_A and K_{DR} currents. Current patterns were obtained by hyper- and depolarizing the cell membrane from the holding potential of -70 mV to the values ranging from -160 mV to 40 mV, at 10 mV increments. Scale bar = 50 µm. Abbreviations: DCX – doublecortin; GFAP – glial fibrillary acidic protein; MAP2 – microtubule-associated protein 2; PDGFαR – platelet-derived growth factor alpha receptor (Kriska et al., 2016).

The electrophysiological analyses also showed that Wnt signaling inhibition in both dnTCF4 and Dkk1 cultures markedly lowered the incidence of cells displaying outwardly rectifying currents, and also marginally raised the incidence of cells with a passive current profile (Figure 24). On the other hand, activation of the pathway (Ex3) led to decreased numbers of cells with a passive current profile, and to increased numbers of cells with an outwardly rectifying current pattern. However, neither of these changes in the cell incidence was significant (Figure 24). Any manipulation of the pathway caused

an increase in the incidence of cells displaying complex currents. Nevertheless, such increase was statistically significant only in dnTCF4 cells (Figure 24).

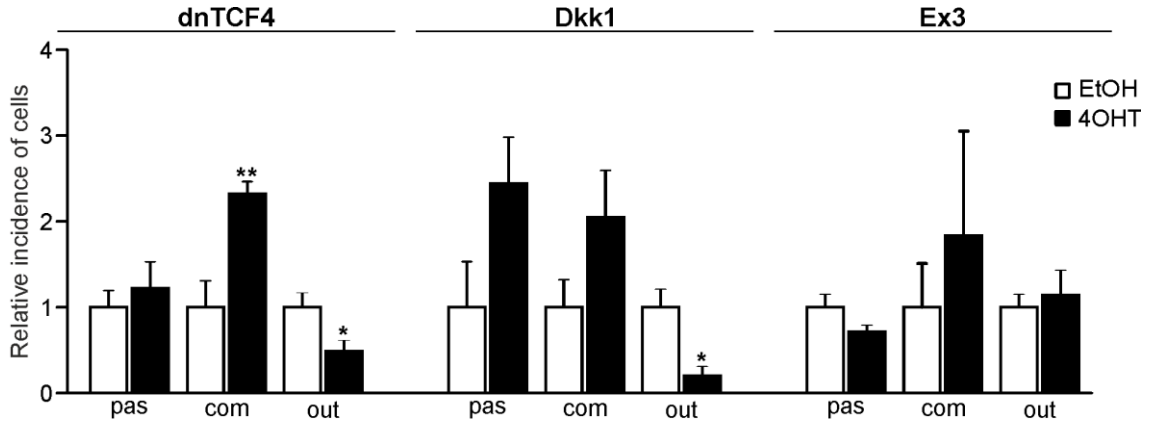

Figure 24. Alterations in the incidence of distinct cell types after Wnt signaling manipulation. The incidence of cells displaying passive (pas), complex (com) or outwardly rectifying (out) current profiles in neonatal cell cultures was assessed. Four (Dkk1 mice) or three (dnTCF4 and Ex3 mice) founder mice were used to derive NS/PCs, and the incidence was quantified from the following total number of cells (in brackets): dnTCF4-EtOH (149), dnTCF4-4OHT (184), Dkk1-EtOH (97), Dkk1-4OHT (101), Ex3-EtOH (101), and Ex3-4OHT (95). The relative incidence of cells in controls (EtOH) was arbitrarily set to 1; *, $p < 0.05$; **, $p < 0.01$. Abbreviations: 4OHT – (Z)-4-hydroxytamoxifen; Dkk1 – Dickkopf 1; dnTCF4 – dominant negative T-cell factor 4; Ex3 – exon 3; NS/PCs – neural stem/progenitor cells (adapted from Kriska et al. (2016)).

Immunocytochemical analysis confirmed lower expressions of DCX and MAP2 in the cultures with suppressed Wnt signaling and decreased expression of GFAP in the cultures with activated Wnt signaling (Figure 25A, B). Furthermore, Western blotting revealed higher β III tubulin expression in the cultures with hyper-activated pathway (Figure 25B, inset).

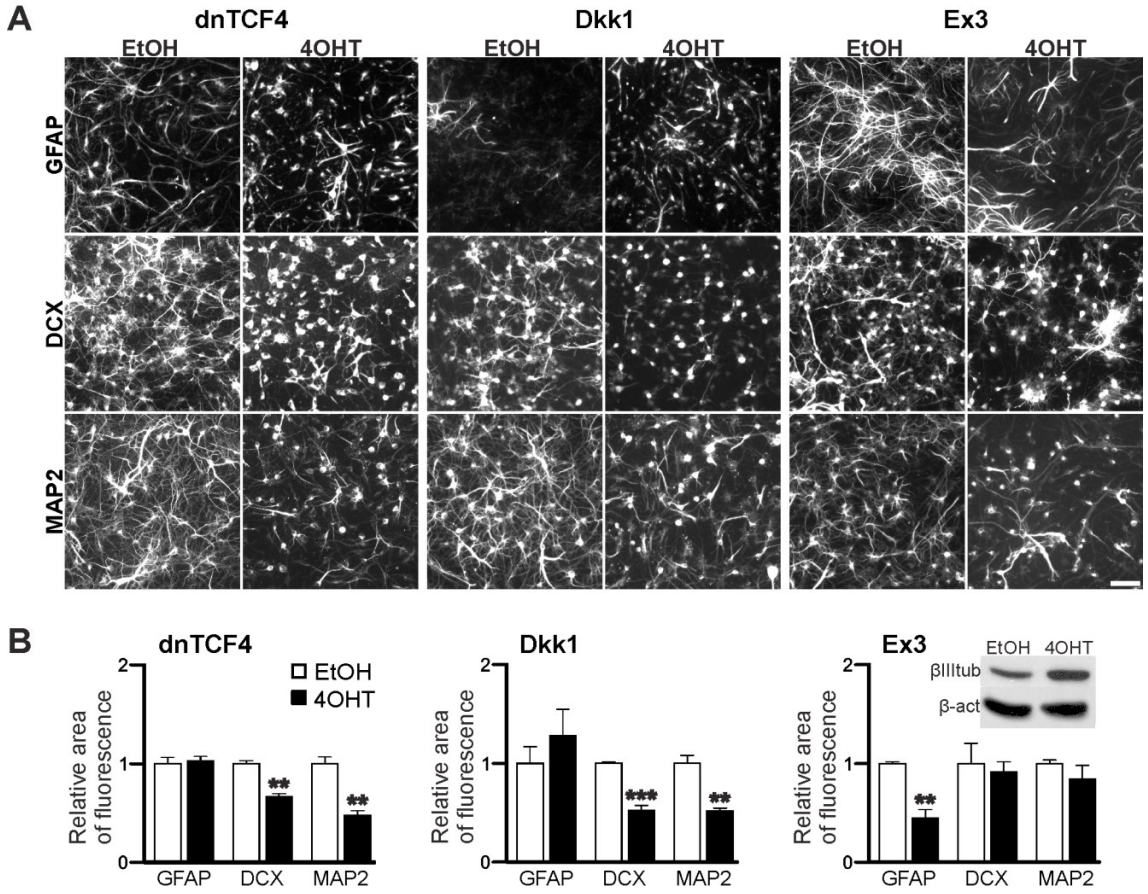

Figure 25. Immunocytochemical staining of cell-type-specific proteins. (A) Representative images of stainings against glial fibrillary acidic protein (GFAP; **top**), doublecortin (DCX; **middle**) and microtubule-associated protein 2 (MAP2; **bottom**). Scale = 50 µm. **(B)** Quantification of GFAP, DCX and MAP2 expression showing the area of positively stained cells within 318.2 µm x 318.2 µm large inspected region (n=6). The area of immunopositive fluorescence in control cells (EtOH) was arbitrarily set to 1. Western blotting analysis of β III tubulin (βIIItub; see inset); **, $p < 0.01$; ***, $p < 0.001$. Abbreviations: 4OHT – (Z)-4-hydroxytamoxifen; β-act – β-actin; Dkk1 – Dickkopf 1; dnTCF4 – dominant negative T-cell factor 4; Ex3 – exon 3; n – number (adapted from Kriska et al. (2016)).

Hence, activation of the Wnt signaling pathway increases the expression of β III tubulin, a neuronal marker, and decreases the incidence of GFAP-positive glial cells displaying passive time- and voltage-independent K^+ currents. In contrast, upon suppression of the Wnt pathway, the incidence of GFAP-positive cells is increased. At the same time, the number of DCX/MAP2-positive neuronal cells showing outwardly rectifying K^+ currents is decreased. Taken together, all these findings imply that our *in vitro* approach may serve as a suitable tool to study the role of Wnt signaling in neonatal neurogenesis and gliogenesis.

4.1.3 Properties of differentiated neonatal neural stem/progenitor cells

Finally, we tried to characterize the three identified cell types after Wnt signaling manipulation. For this reason, we assessed the membrane properties of differentiated neonatal NS/PCs using the patch-clamp technique in the whole-cell configuration and calcium imaging.

The electrophysiological membrane properties of 1245 differentiated cells were analyzed by the patch-clamp technique. In the cells displaying a passive current pattern, the impact of Wnt signaling pathway manipulation on their electrophysiological properties was minimal (Table 2). Inhibited Wnt signaling affected mainly passive electrophysiological properties (V_m, C_m), as we found that dnTCF4 and Dkk1 expression resulted in hyperpolarized cell membrane, and lower C_m values. However, Wnt/β-catenin signaling had a more profound effect on electrophysiological properties of differentiated progenitors showing a complex current pattern (Table 3). Their C_m decreased after Wnt signaling inhibition, while it was marginally elevated after its activation. Interestingly, current densities of K_{IR} currents were higher regardless of Wnt signaling inhibition/activation. Wnt signaling manipulation also affected electrophysiological properties of cells expressing outwardly rectifying currents (Table 4). Both inhibition and activation of the Wnt pathway caused hyperpolarization of the cell membrane, but only Wnt signaling inhibition resulted in lower C_m values. Current densities of K_{DR} currents were higher in cells with inhibited Wnt signaling.

Table 2. Membrane properties of differentiated neonatal NS/PCs displaying a passive current pattern.

	dnTCF4		**Dkk1**		**Ex3**	
	EtOH	**4OHT**	**EtOH**	**4OHT**	**EtOH**	**4OHT**
V_m [mV]	**-83.3±0.6**	**-86.2±0.4****	**-85.2±0.4**	**-87.0±0.3***	-85.7±0.3	-87.0±0.4
IR [MΩ]	73.6±3.1	73.2±2.3	71.2±2.3	71.6±1.8	69.8±3.2	83.8±5.5
C_m [pF]	34.4±2.2	31.3±1.6	**36.7±2.0**	**28.2±1.2***	35.4±2.4	32.1±2.2
K_{IR} [pA]	74.1±7.6	77.2±5.4	58.0±4.6	56.3±3.3	71.4±6.1	86.7±6.5
K_{IR}/C_m [pA/pF]	**2.3±0.2**	**3.9±0.3****	2.3±0.2	2.7±0.2	**2.7±0.2**	**4.2±0.3****
K_{DR} [pA]	127.0±17.1	119.4±11.4	82.3±7.5	78.6±8.1	116.4±12.2	156.5±18.6
K_{DR}/C_m [pA/pF]	3.8±0.5	4.3±0.4	3.2±0.3	3.9±0.5	4.1±0.4	5.3±0.6
n	74	92	76	110	89	65

Abbreviations: 4OHT – (Z)-4-hydroxytamoxifen; C_m – membrane capacitance; Dkk1 – Dickkopf 1; dnTCF4 – dominant negative T-cell factor 4; EtOH – ethanol; Ex3 – exon 3; IR – input resistance; K_{DR} – delayed outwardly rectifying K^+ currents; K_{IR} – inwardly rectifying K^+ currents; K_{IR}/C_m, K_{DR}/C_m – current densities; n – number of cells; V_m – membrane potential. Values in bold indicate significant differences between EtOH- and 4OHT-treated cultures; *, $p < 0.05$; **, $p < 0.01$ (adapted from Kriska et al. (2016)).

Table 3. Membrane properties of differentiated neonatal NS/PCs displaying a complex current pattern.

	dnTCF4		**Dkk1**		**Ex3**	
	EtOH	**4OHT**	**EtOH**	**4OHT**	**EtOH**	**4OHT**
V_m [mV]	-83.6±1.3	-84.1±0.7	-85.2±0.9	-86.3±0.7	-86.2±1.0	-87.5±0.7
IR [MΩ]	202.9±18.0	214.2±11.4	**185.6±15.2**	**135.8±8.4*****	231.4±27.9	164.3±15.2
C_m [pF]	**21.9±1.7**	**13.7±0.7*****	**22.4±1.2**	**16.7±0.8****	17.4±1.8	23.5±1.8
K_{IR} [pA]	81.2±6.6	87.4±4.7	**83.0±6.6**	**106.7±4.9***	**74.2±8.2**	**141.2±11.2****
K_{IR}/C_m [pA/pF]	**4.2±0.3**	**7.4±0.4*****	**4.0±0.3**	**7.8±0.5*****	**4.3±0.4**	**7.4±0.6****
K_{DR} [pA]	514.9±44.2	463.0±29.4	**659.8±59.3**	**434.6±38.7***	618.5±61.2	605.8±40.9
K_{DR}/C_m [pA/pF]	33.7±4.3	46.9±3.4	38.0±4.4	38.3±4.2	43.3±4.4	36.0±3.5
K_A [pA]	**290.3±35.5**	**205.0±12.4***	369.4±62.3	278.4±22.3	229.8±24.0	275.6±38.3
K_A/C_m [pA/pF]	23.2±4.0	23.1±1.6	28.5±6.1	22.0±2.0	20.5±3.5	13.4±1.6
n	35	95	31	58	19	40

Abbreviations: 4OHT – (Z)-4-hydroxytamoxifen; C_m – membrane capacitance; Dkk1 – Dickkopf 1; dnTCF4 – dominant negative T-cell factor 4; EtOH – ethanol; Ex3 – exon 3; IR – input resistance; K_A – fast activating and inactivating outwardly rectifying K^+ currents; K_{DR} – delayed outwardly rectifying K^+ currents; K_{IR} – inwardly rectifying K^+ currents; K_{IR}/C_m, K_{DR}/C_m, K_A/C_m – current densities; n – number of cells; V_m – membrane potential. Values in bold indicate significant differences between EtOH- and 4OHT-treated cultures; *, $p < 0.05$; **, $p < 0.01$; ***, $p < 0.001$ (adapted from Kriska et al. (2016)).

Table 4. Membrane properties of differentiated neonatal NS/PCs displaying an outwardly rectifying current pattern.

	dnTCF4		Dkk1		Ex3	
	EtOH	4OHT	EtOH	4OHT	EtOH	4OHT
V_m [mV]	-69.1±1.3	-70.7±1.7	**-63.6±1.7**	**-74.9±2.9****	**-67.0±2.1**	**-78.7±1.6*****
IR [MΩ]	1856.0±78.0	1817.7±98.8	1797.7±95.6	1514.3±181.8	**1924.7±82.1**	**1434.3±115.9****
C_m [pF]	**10.6±0.4**	**7.5±0.3*****	**11.3±0.5**	**7.7±0.4****	10.3±0.4	9.9±0.5
K_{DR} [pA]	691.0±23.2	637.3±26.0	830.1±34.6	881.1±79.0	652.7±25.3	695.6±42.1
K_{DR}/C_m [pA/pF]	**72.1±2.2**	**101.0±5.1*****	**87.4±3.8**	**132.3±14.3****	71.2±3.1	75.9±3.6
K_A [pA]	**634.5±27.5**	**479.2±27.7****	**795.1±38.5**	**524.0±49.5****	**675.9±37.6**	**441.8±37.1*****
K_A/C_m [pA/pF]	68.7±3.1	78.9±5.1	92.7±5.1	79.0±9.7	**80.3±5.2**	**55.9±5.0***
n	128	78	90	25	77	63

Abbreviations: 4OHT – (Z)-4-hydroxytamoxifen; C_m – membrane capacitance; Dkk1 – Dickkopf 1; dnTCF4 – dominant negative T-cell factor 4; EtOH – ethanol; Ex3 – exon 3; IR – input resistance; K_A – fast activating and inactivating outwardly rectifying K^+ currents; K_{DR} – delayed outwardly rectifying K^+ currents; K_{DR}/C_m, K_A/C_m – current densities; n – number of cells; V_m – membrane potential. Values in bold indicate significant differences between EtOH- and 4OHT-treated cultures; *, $p < 0.05$; **, $p < 0.01$; ***, $p < 0.001$ (adapted from Kriska et al. (2016)).

Besides the differences in the passive membrane properties, and the expression of K^+ channels, we also identified changes in the expression of voltage-dependent Na^+ channels in DCX/MAP2-positive neuron-like cells that expressed an outwardly rectifying current pattern (Figure 26A). Moreover, we detected changes in the incidence of such cells (Figure 26B), which were also capable of generating action potentials (Figure 26C). Inhibition of the Wnt signaling pathway at the membrane and nuclear level led to the absence of cells expressing Na^+ channels (Figure 26B), while activation of the pathway caused an increase in both the Na^+ current densities and the cell incidence (Figure 26B).

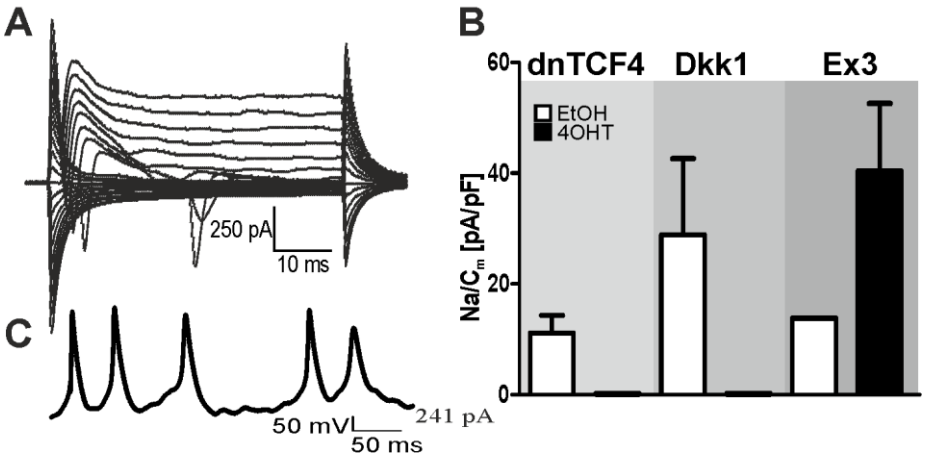

Figure 26. Voltage-gated Na^+ channels in cells with an outwardly rectifying current profile. **(A)** A typical current pattern of a cell expressing outwardly rectifying K^+ currents, together with inwardly rectifying Na^+ currents. **(B)** After Wnt signaling inhibition (dnTCF4 or Dkk1), the incidence of cells expressing Na^+ channels decreased. Conversely, Wnt pathway activation (Ex3) increased the incidence as well as the current densities of voltage-dependent Na^+ channels. The numbers of cells with Na^+ currents identified in the individual cultures were as follow (in brackets): dnTCF4-EtOH (4), dnTCF4-4OHT (0), Dkk1-EtOH (4), Dkk1-4OHT (0), Ex3-EtOH (1), and Ex3-4OHT (3). **(C)** A trace that represents action potentials generated by some of the cells. Abbreviations: 4OHT – (Z)-4-hydroxytamoxifen; C_m – membrane capacitance; Dkk1 – Dickkopf 1; dnTCF4 – dominant negative T-cell factor 4; EtOH – ethanol; Ex3 – exon 3; Na/C_m, current densities of Na^+ currents (adapted from Kriska et al. (2016)).

Finally, measurements of intracellular calcium revealed that after inhibition of the pathway at the cell membrane level, the percentage of MAP2/DCX-positive cells responding to 100 μM glutamate decreased significantly, from ~90% in EtOH to ~20%, and the average amplitude of the glutamate-evoked response decreased by ~66% (Figure 27A). Additionally, Dkk1 over-expression also resulted in a higher response to 50 μM ATP application, when compared to the controls (Figure 27A); however, the average amplitude of responding cells remained unchanged. On the other hand, activation of the pathway led to the lower average amplitude in response to ATP application (Figure 27B), while the Ca^{2+} elevations in response to glutamate application were comparable with those observed in controls (Figure 27B). Inhibition of the pathway in the nucleus (dnTCF4) showed no significant changes in the cell response to glutamate or ATP application.

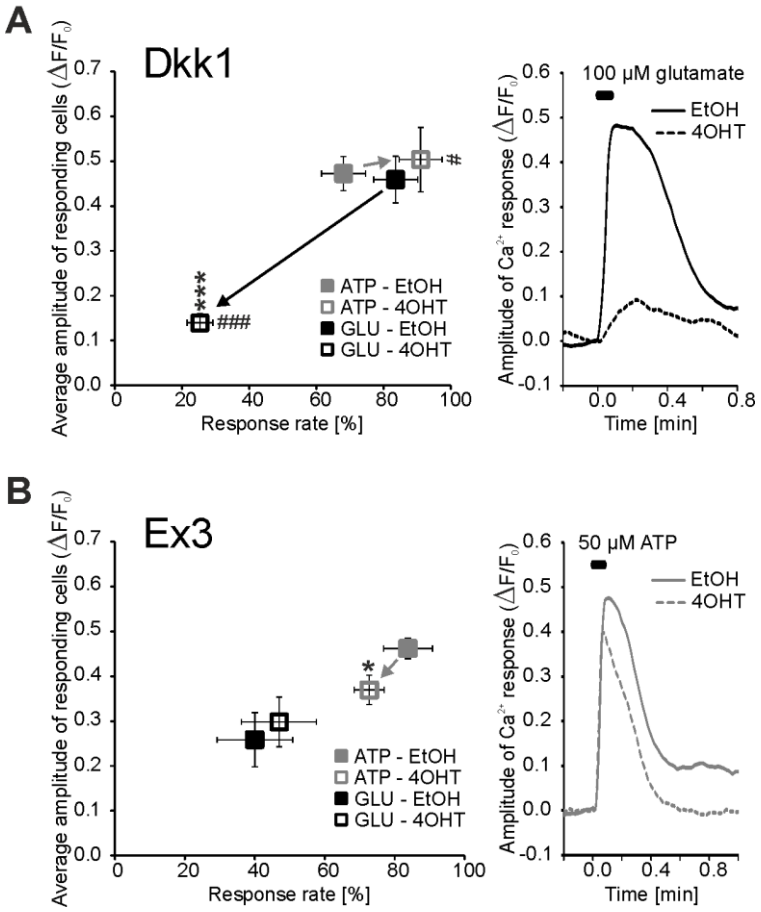

Figure 27. Calcium responses evoked by glutamate and ATP in DCX/MAP2-positive cells. **(A)** Inhibition of Wnt signaling at the membrane level (Dkk1) significantly lowered Ca^{2+} responses (% of responding cells and their average amplitude) to 100 µM glutamate (glu) application, and increased the response rate to 50 µM adenosine triphosphate (ATP) application. **(B)** Activation of the pathway (Ex3) resulted in lower average amplitudes of ATP-responding cells. The number of cells used in this analysis was as follows (in brackets): Dkk1-EtOH (9), Dkk1-4OHT (6), Ex3-EtOH (7), and Ex3-4OHT (7); $^{*/\#}$, $p < 0.05$; $^{***/\#\#\#}$, $p < 0.001$. Abbreviations: 4OHT – (Z)-4-hydroxytamoxifen; DCX – doublecortin; Dkk1 – Dickkopf 1; EtOH – ethanol; Ex3 – exon 3; F_0 – baseline fluorescence intensity; MAP2 – microtubule-associated protein 2 (adapted from Kriska et al. (2016)).

These results show that the alterations in β-catenin signaling influence the distribution of distinct K^+ channels as well as the ability of cells to transport Ca^{2+} after the application of glutamate and ATP. Furthermore, the activation of the Wnt signaling pathway increases the incidence of cells expressing outwardly rectifying K^+ currents together with inwardly rectifying Na^+ currents.

Taken together, the data from our *in vitro* systems modulating the output of the canonical Wnt signaling pathway suggest that hyper-activation of the pathway leads to higher neurogenesis, while gliogenesis is suppressed. Conversely, inhibition of the pathway at

both membrane receptor and nuclear levels showed comparable results and promoted gliogenesis at the expense of neurogenesis. These findings are summarized in the following diagram (Figure 28).

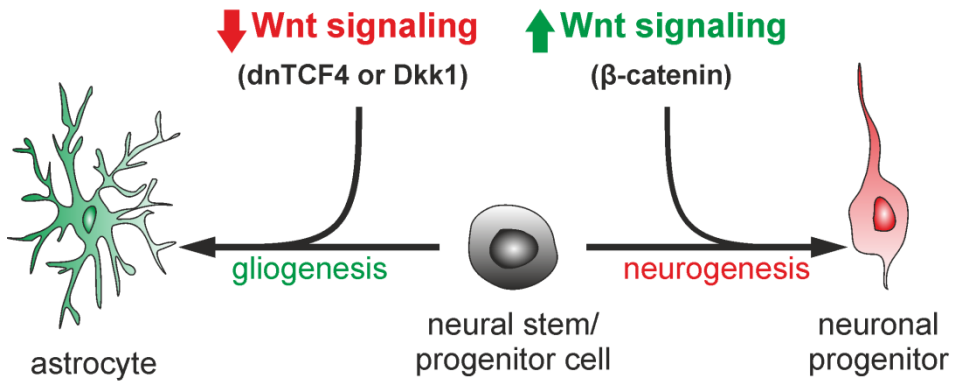

Figure 28. Graphical representation of the changes observed in neonatal mice. According to our analyses, Wnt signaling inhibition (dnTCF4 or Dkk1) led to the differentiation of NS/PCs to the glial phenotype, while activation of the pathway by the stabilization of protein β-catenin (Ex3) promoted neurogenesis. Abbreviations: Dkk1 – Dickkopf 1; dnTCF4 – dominant negative T-cell factor 4; Ex3 – exon 3; NS/PCs – neural stem/progenitor cells (Kriska et al., 2016).

4.2 The differentiation potential of adult neural stem/progenitor cells

The analysis of various Wnt pathway components in neonatal animals taught us that we cannot leave out any of the three mouse strains because each of them behaves slightly differently. Therefore, after we assessed the effect of canonical Wnt signaling on cell cultures derived from neonatal mice, we went on to the experiments on NS/PCs isolated from adult (two-month-old) animals of the same transgenic strains. The purpose of these experiments was to disclose the differentiation potential of NS/PCs also in a model that resembles more the processes occurring in the mature age. To elucidate the impact of the Wnt/β-catenin pathway on the differentiation potential of NS/PCs in non-operated (CTRL) mice and mice after the induction of permanent FCI (MCAO), we compared either *in vitro* cultures treated with 4OHT to their respective controls (EtOH) or tissue specimens from mice with manipulated Wnt signaling (TAM) to control mice with intact Wnt signaling (CO). We employed almost identical set of experiments as in neonatal mice.

4.2.1 Expression of Wnt signaling pathway components

Similarly to the experiments on cells derived from neonatal mice, we aimed to determine the extent to which the components of the canonical Wnt pathway are altered in our models. Initially, we utilized immunocytochemical staining against the principal element of the signaling, i.e. β-catenin (Figure 29). Although we did not detect any changes in the expression of the protein after Wnt signaling inhibition in the cell nucleus (Figure 29A, D), we identified decreased amounts of β-catenin after Wnt signaling inhibition at the membrane receptor level (Figure 29B, D). In cells with hyper-activated Wnt signaling (Ex3), the expression of the protein was increased (Figure 29C, D). All these results correlate well with the findings in neonatal cultures (Figure 20).

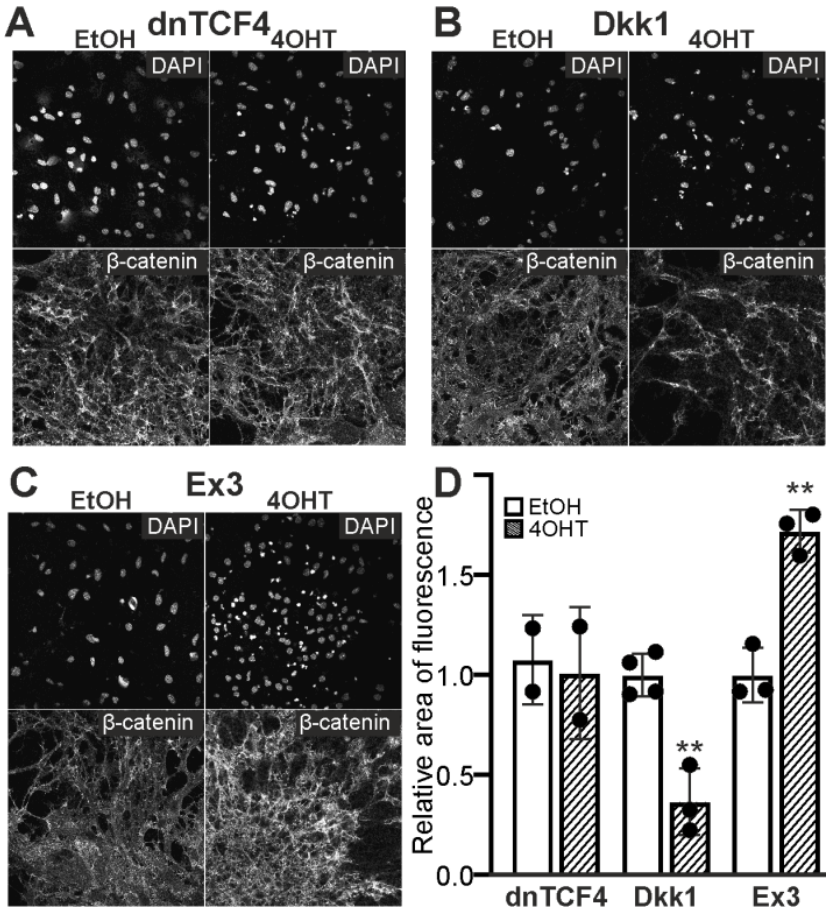

Figure 29. Immunocytochemical staining of β-catenin. (A-C) Representative fluorescent images of DAPI and β-catenin staining in differentiated adult neural stem/progenitor cells with inhibited (dnTCF4, Dkk1), or activated (Ex3) Wnt signaling. Cells were treated either only with ethanol (EtOH) or with (Z)-4-hydroxytamoxifen (4OHT) dissolved in ethanol, and analyzed eight days after the onset of *in vitro* differentiation. **(D)** Quantification of β-catenin expression, showing the proportion of the area of positively-stained cells to the DAPI-positive area (n=12). The area of β-catenin fluorescence in control cells (EtOH) was arbitrarily set to 1. The values are represented as mean ± S.D. (standard deviation). Statistical significance was calculated using t-test; **, p <

0.01. Abbreviations: DAPI – 4',6-diamidino-2-phenylindole; Dkk1 – Dickkopf 1; dnTCF4 – dominant negative T-cell factor 4; Ex3 – exon 3; n – number (unpublished data).

In the following experiments, we evaluated the effect of Wnt signaling manipulation in tissue slices or their lysates. The incentive behind using tissue specimens was the low yield of cells that were derived from adult mice and cultured *in vitro*. First, we assessed the quantities of total β-catenin protein and its non-phosphorylated, active form (Figure 30). However, the results from Western blotting did not correspond well with the findings from immunocytochemistry (Figure 29). We were not able to detect any differences in the expression of total β-catenin. Moreover, the expression of active β-catenin showed no changes in CTRL animals, but we observed significant alterations after the induction of FCI (Figure 30). We identified decreased amounts of this protein after Wnt signaling inhibition in the nucleus (from 6.56 ± 0.56 to 2.70 ± 0.38) and Wnt signaling hyper-activation (from 2.93 ± 0.19 to 1.62 ± 0.16), while inhibition at the cellular membrane increased the expression of active β-catenin (from 2.30 ± 0.07 to 3.93 ± 0.02).

Next, to estimate the activity of β-catenin, we calculated the non-phosphorylated-β-catenin-to-β-catenin ratio. In cells with inhibited Wnt signaling in the nucleus, the ratio decreased from 1.15 to 0.89 in controls and it decreased almost to the half, from 1.01 to 0.52 after FCI. The data from controls correlated well with our findings in neonatal mice and the results from MCAO mice showed that ischemia increased the effect of Wnt signaling. Inhibition at the membrane level led to a slight decrease from 0.42 to 0.31 in CTRL mice, while after FCI, the ratio raised two-fold, from 0.12 to 0.24. The overall low values in Dkk1 cultures were caused by relatively high expression of total β-catenin. Surprisingly, activation of the Wnt pathway resulted in a lower non-phosphorylated-β-catenin-to-β-catenin ratio (from 1.12 to 0.69 in CTRL cells and from 1.02 to 0.88 in MCAO cells). This decrease in the proportion of active protein after Wnt signaling hyper-activation is in a stark contrast to the findings in neonatal cultures, where we detected its eight-fold increase.

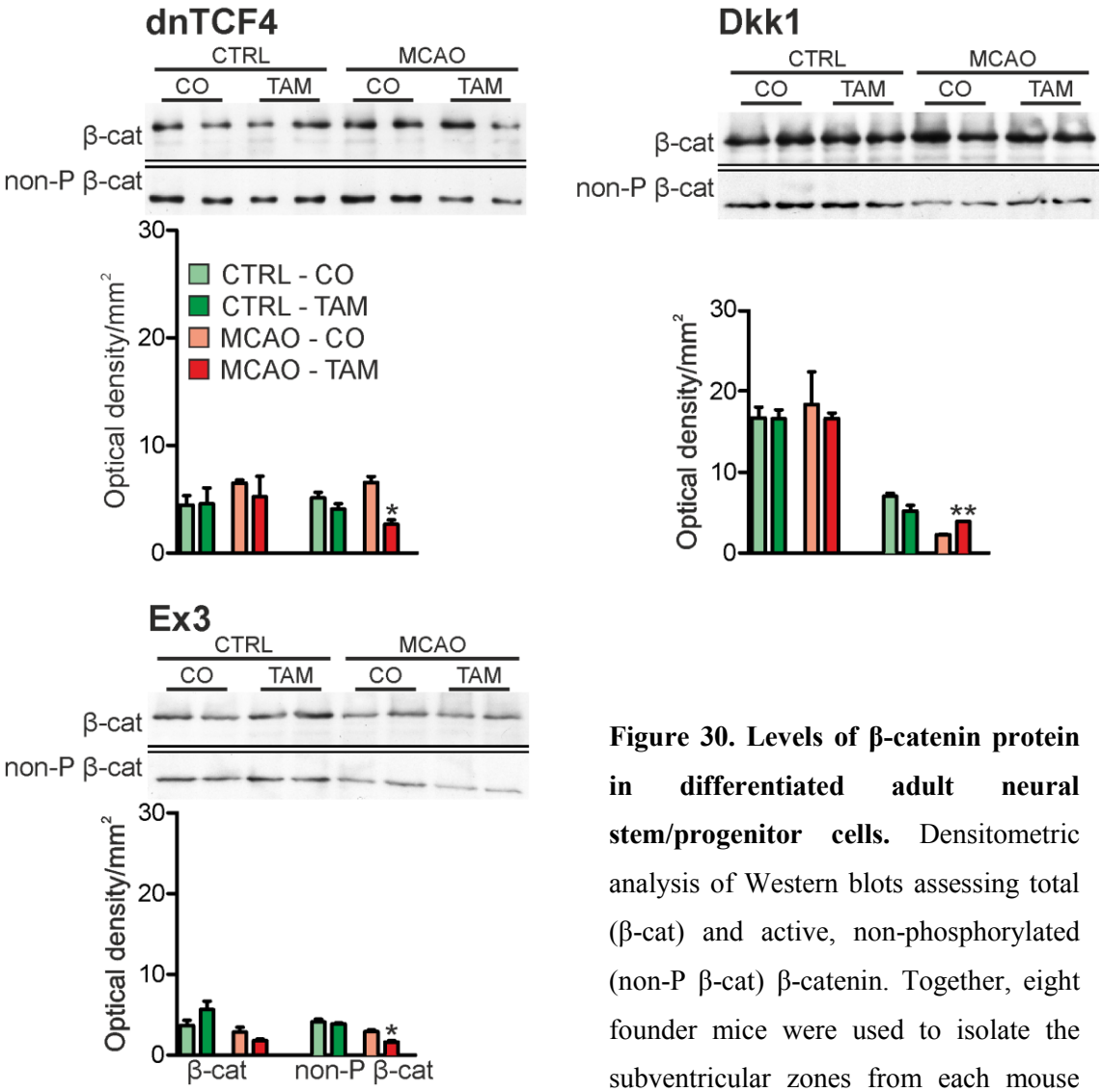

Figure 30. Levels of β-catenin protein in differentiated adult neural stem/progenitor cells. Densitometric analysis of Western blots assessing total (β-cat) and active, non-phosphorylated (non-P β-cat) β-catenin. Together, eight founder mice were used to isolate the subventricular zones from each mouse strain. The tissues were analyzed either in non-operated, control mice (CTRL) or mice after middle cerebral artery occlusion (MCAO), with Wnt signaling either non-manipulated (CO) or manipulated (TAM). Error bars represent S.E.M. (standard error of the mean). Abbreviations: CO – corn oil; Dkk1 – Dickkopf 1; dnTCF4 – dominant negative T-cell factor 4; Ex3 – exon 3; TAM – tamoxifen (unpublished data).

Additionally, we analyzed the expression of Wnt target genes using RT-qPCR (Figure 31). In adult NS/PCs, four different target genes were examined, namely *Axin2*, *naked cuticle homolog 1* (*Nkd1*), *Sp5*, and *Troy*. Their expression was either downregulated or not changed in CTRL mice of all strains. There was one exception, the *Sp5* gene, which was always upregulated. The expression pattern was similar in MCAO mice; however, a striking increase in the expression of Wnt target genes was observed (Figure 31). Interestingly, the expression of the *Sp5* gene was dramatically decreased after the induction of FCI.

Thus, the analysis of the expression of Wnt signaling pathway components revealed several similarities with neonatal cell cultures. The system worked very well *in vitro*. We detected the same expression pattern of β-catenin protein, but different expression of its active form, especially after Wnt signaling hyper-activation. Moreover, the expression of the Wnt target genes was influenced by Wnt signaling manipulation and enhanced following the induction of FCI.

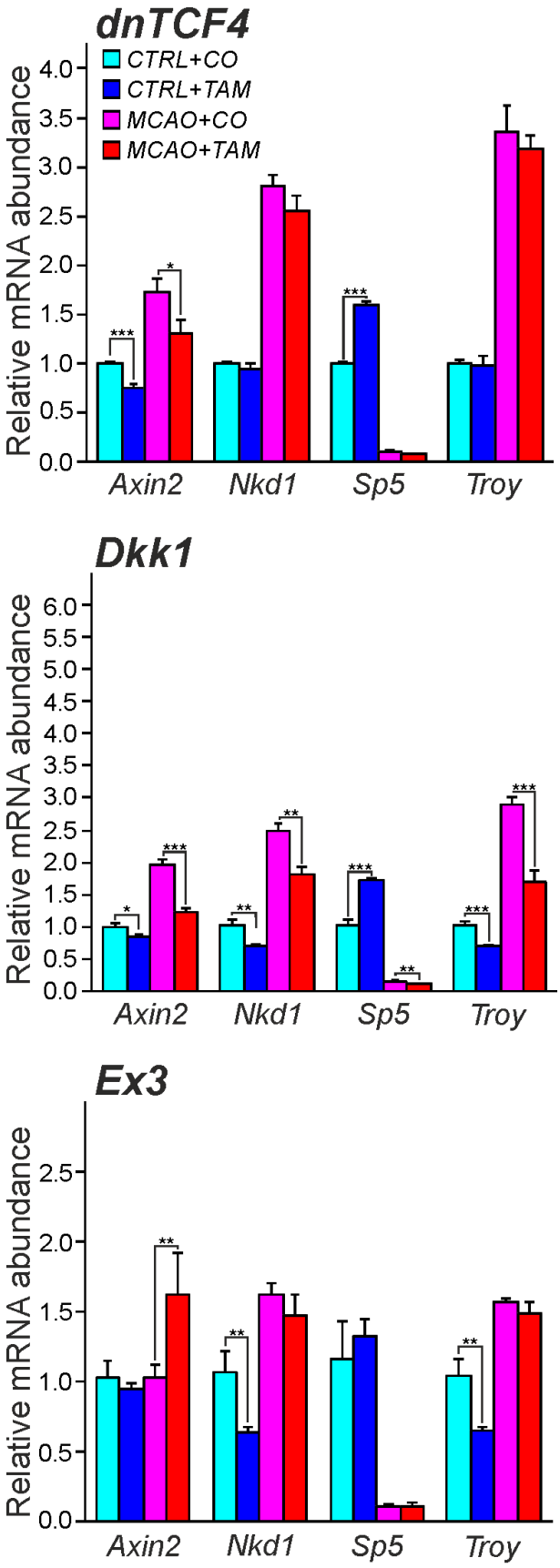

Figure 31. Expression of Wnt target genes in differentiated adult neural stem/progenitor cells. Reverse transcription quantitative polymerase chain reaction (RT-qPCR) analysis was used to assess the mRNA abundance of Wnt target genes. Together, eight founder mice were used to isolate the subventricular zones from each mouse strain, and the analysis was performed in technical triplicates. The average cycle threshold (C_t) values were normalized to *glyceraldehyde-3-phosphate dehydrogenase* (*GAPDH*). *Axin2*, *Nkd1*, *Sp5*, and *Troy* are Wnt target genes. The expression levels of a given gene in control cells (CTRL+CO) were arbitrarily set to 1. The tissues were analyzed either in non-operated control mice (CTRL) or mice after middle cerebral artery occlusion (MCAO), with Wnt signaling either non-manipulated (CO) or manipulated (TAM). Statistical significance was calculated using t-test; *, $p < 0.05$; **, $p < 0.01$; ***, $p < 0.001$. Abbreviations: CO – corn oil; Dkk1 – Dickkopf 1; dnTCF4 – dominant negative T-cell factor 4; Ex3 – exon 3; mRNA – messenger RNA; *Nkd1* – naked cuticle homolog 1; *Sp5* – SP5 transcription factor; TAM – tamoxifen; *Troy* – tumor necrosis factor receptor superfamily member 19 (unpublished data).

4.2.2 Cell types derived from adult NS/PCs and their incidence

In accordance with the study in neonatal mice, we identified the same three cell types that represent differentiated adult NS/PCs (Figure 23). The division into the three groups was based on the electrophysiological and immunocytochemical properties of the cells. Their incidence in *in vitro* cultures derived from adult mice was calculated from the patch-clamp experiments. With this technique, we analyzed the properties of 413 EtOH- and 452 4OHT-treated cells from CTRL mice. In MCAO mice, we assessed 230 EtOH- and 231 4OHT-treated cells. Initially, we failed to identify any alterations in the cell incidence caused by Wnt signaling pathway manipulation in CTRL cells (Figure 32A). This is in contrast with neonatal mice, where we disclosed suppressed neurogenesis after Wnt signaling inhibition. Interestingly, the trend in the incidence of differentiated cells after MCAO resembled the results from neonatal mice. However, significant changes were found only in the cultures with inhibited Wnt signaling at the membrane level (Dkk1 mice; Figure 32B). In these cultures, we observed decreased numbers of cells showing an outwardly rectifying current pattern (from 49.17 ± 3.61% in EtOH to 16.91 ± 5.11% in 4OHT) and increased counts of cells with a complex current profile (from 20.42 ± 3.25% in EtOH to 42.35 ± 4.93% in 4OHT).

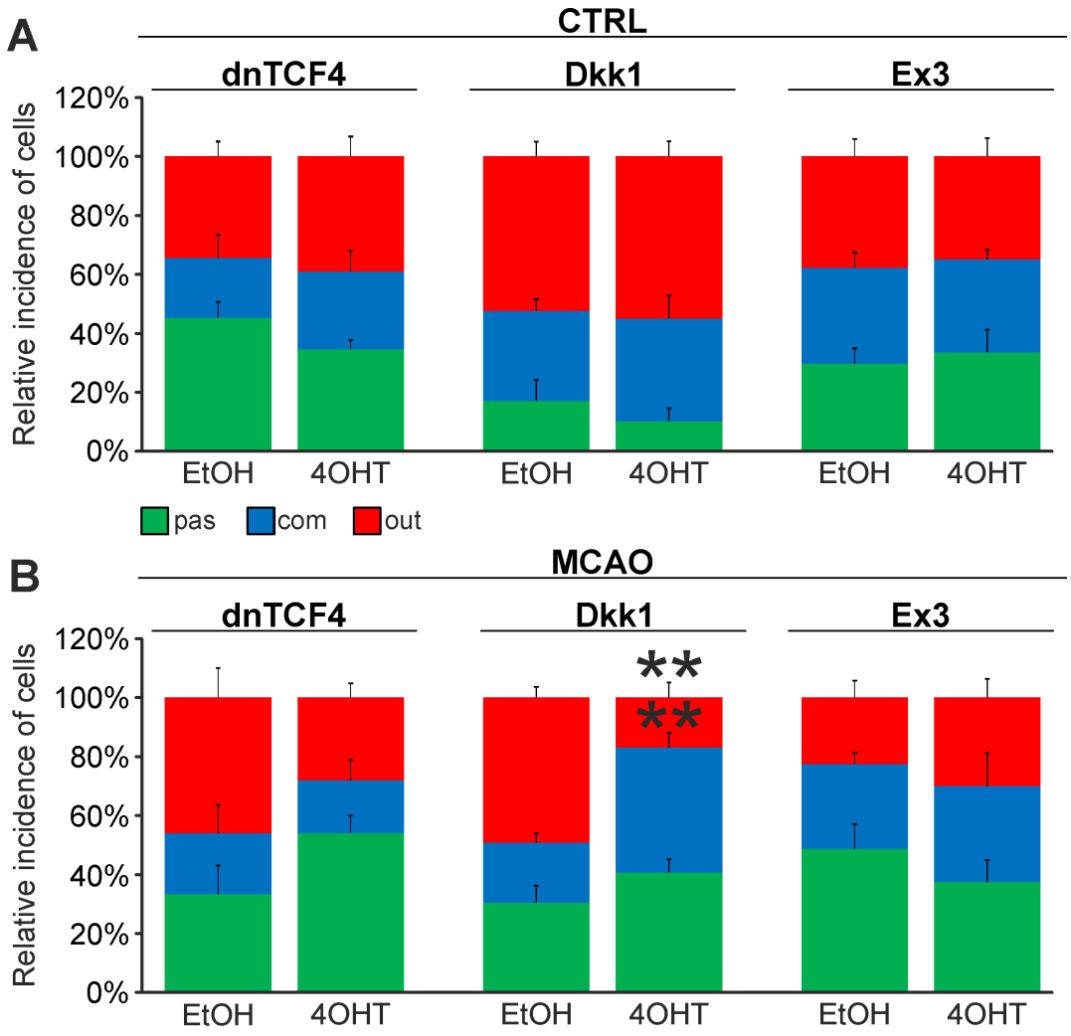

Figure 32. Changes in the incidence of distinct cell types after Wnt signaling manipulation in intact and ischemic mice. The incidence of cells showing passive (pas; in green), complex (com; in blue) or outwardly rectifying (out; in red) current patterns was examined in neural stem/progenitor cell (NS/PC) cultures derived from adult control, non-operated (CTRL) as well as operated (MCAO) mice. Eight founder mice were used to derive NS/PCs from each mouse strain. The incidence was quantified from the following total number of cells (in brackets): CTRL-dnTCF4-EtOH (145), CTRL-dnTCF4-4OHT (141), CTRL-Dkk1-EtOH (116), CTRL-Dkk1-4OHT (114), CTRL-Ex3-EtOH (152), CTRL-Ex3-4OHT (197), MCAO-dnTCF4-EtOH (75), MCAO-dnTCF4-4OHT (72), MCAO-Dkk1-EtOH (75), MCAO-Dkk1-4OHT (79), MCAO-Ex3-EtOH (80), and MCAO-Ex3-4OHT (80). The incidence of cells in controls (EtOH) was compared to the incidence of the same cell types in cells with manipulated Wnt signaling (4OHT) with Student's t-test. **, $p < 0.01$. Abbreviations: 4OHT – (Z)-4-hydroxytamoxifen; Dkk1 – Dickkopf 1; dnTCF4 – dominant negative T-cell factor 4; EtOH – ethanol; Ex3 – exon 3; MCAO – middle cerebral artery occlusion (unpublished data).

Next, we analyzed the expression of cell-type-specific proteins utilizing Western blotting (Figure 33). We evaluated the proteins characteristic of astrocytes (GFAP), neuroblasts (DCX) and mature neurons (MAP2 and β III tubulin) in tissue lysates; however, changes in their expression caused by Wnt signaling manipulation were rare.

After inhibition of the Wnt pathway in the nucleus (dnTCF4), we detected lower expression of β III tubulin in mice after FCI (MCAO). The trend of decreased numbers of neuron-like cells was observed also in the experiments analyzing the incidence of distinct cell types. Surprisingly, after Wnt signaling inhibition due to the over-expression of Dkk1 protein, cells displayed higher expression of MAP2 only after ischemia. Finally, hyper-activated Wnt signaling led to lower expression of DCX in CTRL mice, while the expression of MAP2 increased after FCI. Increased expression of neuronal markers after Wnt signaling activation was identified also in neonatal mice, while together with the induction of FCI, they may have a synergistic effect on the expression of cell-type-specific proteins.

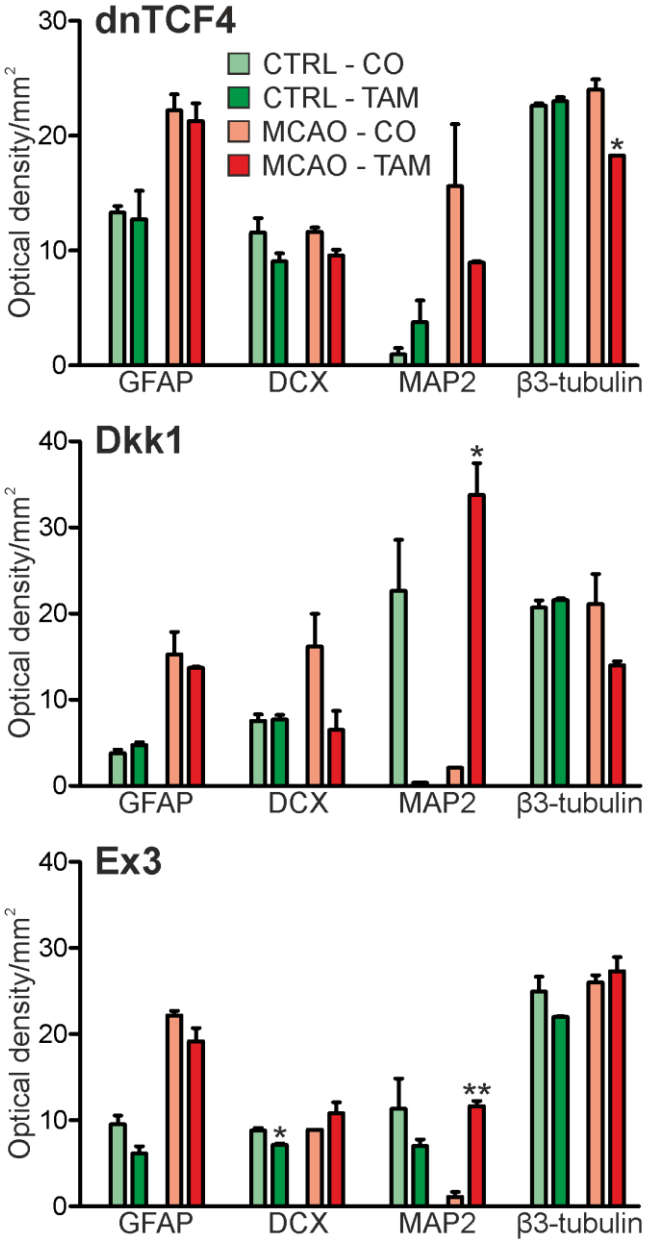

Figure 33. Expression of cell-type-specific proteins in differentiated adult neural stem/progenitor cells. Densitometric analysis of Western blots assessing the abundance of proteins GFAP (marker of astrocytes), DCX (neuroblasts), MAP2, and β3-tubulin (both neurons). The tissues were analyzed either in non-operated, control mice (CTRL) or mice after middle cerebral artery occlusion (MCAO), with Wnt signaling either non-manipulated (CO) or manipulated (TAM). Error bars represent S.E.M. (standard error of the mean); *, $p < 0.05$; **, $p < 0.01$. Abbreviations: CO – corn oil; DCX – doublecortin; Dkk1 – Dickkopf 1; dnTCF4 – dominant negative T-cell factor 4; Ex3 – exon 3; GFAP – glial fibrillary acidic protein; MAP2 – microtubule-associated protein 2; TAM – tamoxifen (unpublished data).

Additionally, we performed immunohistochemical analysis *in situ* in coronal brain sections where we analyzed the expression of DCX (marker of neuroblasts), GFAP (marker of astrocytes), and PCNA (marker of dividing cells) in the SVZ (Figure 34). We observed higher overall immunopositivity after the induction of FCI (Figure 34A, B, C, D), which is a hallmark of ischemia-induced changes in the brain and corresponds well with the results obtained from RT-qPCR analysis (Figure 31) and to some extent also with the data from Western blotting experiments (Figure 33). Furthermore, Wnt signaling inhibition caused higher expression of GFAP and lower expression of DCX in both CTRL and MCAO mice, while the immunopositivity of PCNA was decreased only in MCAO mice. These observations were more significant after Wnt signaling inhibition in the cell nucleus (Figure 34B, C). Conversely, Wnt signaling hyper-activation resulted in the overexpression of PCNA and DCX in CTRL mice, while this effect was diminished after FCI. Moreover, activation of the pathway resulted in the decreased expression of GFAP only after the induction of FCI (Figure 34D).

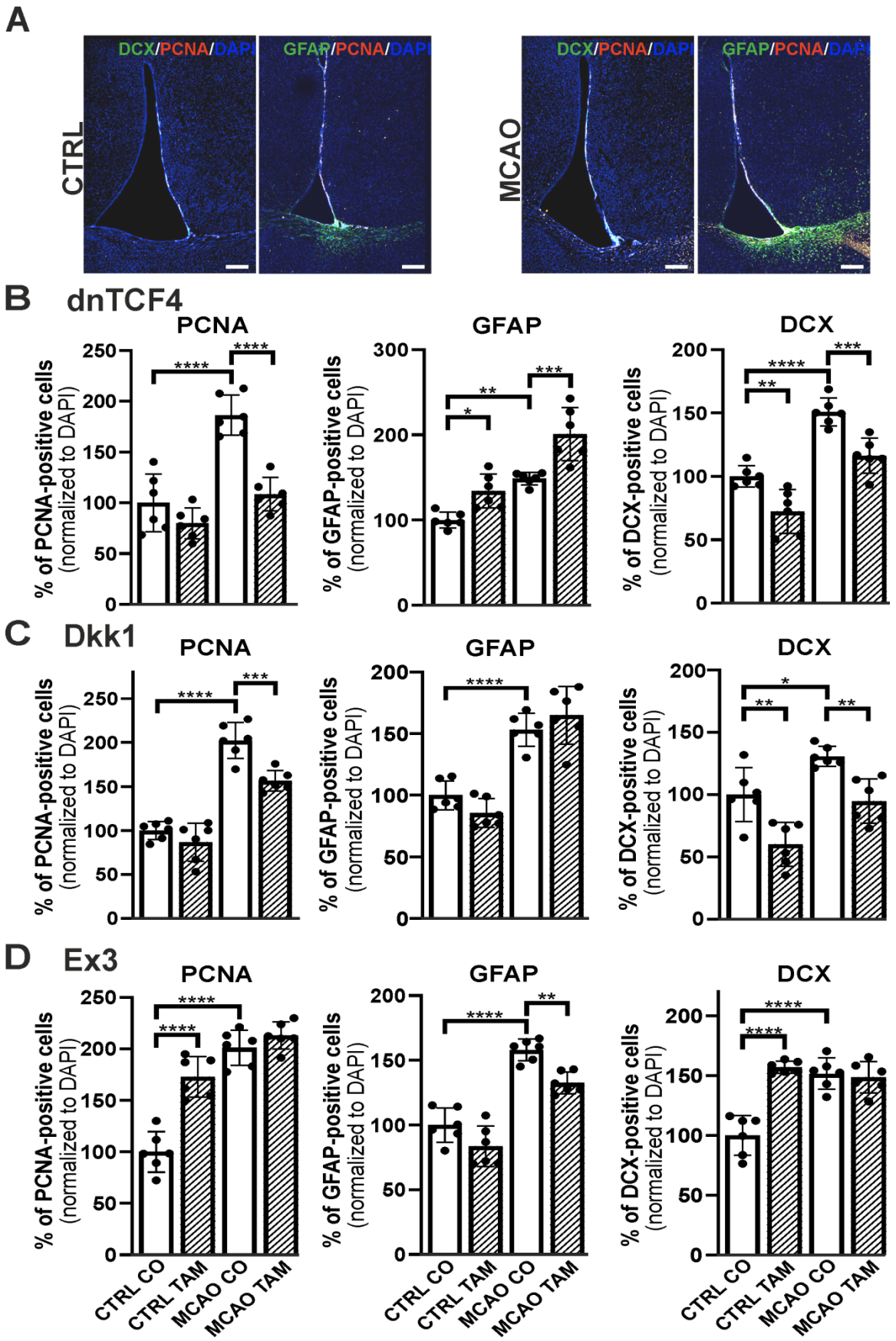

Figure 34. Immunohistochemical analysis of the subventricular zone of adult mice. Inhibition or activation of the canonical Wnt signaling pathway changes the incidence of cell types in the

adult mouse subventricular zone (SVZ) under control, physiological conditions (CTRL) as well as upon focal cerebral ischemia induced by middle cerebral artery occlusion (MCAO). (**A**) Representative images of the SVZ isolated from CTRL and MCAO mice. Increased stainings of neuroblasts marked by doublecortin (DCX), glial fibrillary acidic protein (GFAP)-positive astrocytes, and dividing cells harboring proliferating cell nuclear antigen (PCNA) were recorded 3 days after the induction of ischemia. Scale bar = 0.2 mm. (**B-D**) Quantification of immunohistochemical staining in the SVZ of CTRL and MCAO mice treated either with tamoxifen (TAM) or vehicle, corn oil only (CO). Tamoxifen-induced production of dominant negative human TCF4 protein (dnTCF4; **B**) and Dickkopf-1 Wnt inhibitory protein (Dkk1; **C**) were used to achieve Wnt signaling inhibition and, conversely, production of constitutively active β-catenin (Ex3; **D**) was initiated in order to obtain Wnt pathway activation. Experiments were performed using two biological replicates and three technical replicates for each treatment (n = 6). Average values of the control mice (CTRL CO) were arbitrary set to 100% of immunogenic signal. Error bars represent standard deviation (S.D.) and one-way ANOVA was used to determine significant differences among the experimental groups; *, $p < 0.05$; **, $p < 0.01$; ***, $p < 0.001$; ****, $p < 0.0001$. Abbreviations: DAPI – 4',6-diamidino-2-phenylindole; Ex3 – exon 3; n – number; TCF4 – T-cell factor (unpublished data).

Taken together, our data showed that Wnt signaling influences the incidence of distinct cell types; however, various experimental approaches proved this to various extents. Electrophysiological measurements revealed alterations in the incidence only after FCI induction (Figure 32), while the immunohistochemical analysis showed a wide variety of changes caused by Wnt signaling manipulation in both non-ischemic and ischemic tissue (Figure 34).

4.2.3 Properties of differentiated adult neural stem/progenitor cells

The electrophysiological characterization of membrane properties was conducted also in adult mice as we utilized the patch-clamp technique measurements on *in vitro* differentiated NS/PCs. Together 1,355 cells were analyzed and the effect of Wnt signaling manipulation in CTRL and MCAO mice was investigated in cells with a passive, complex and outwardly rectifying current profile (Tables 5-10).

Cells with a passive current profile

In cells with a passive current pattern, the changes in the membrane properties were sporadic (Tables 5 and 6). Wnt signaling manipulation affected only the passive electrophysiological properties and the strongest effect was identified in the V_m after the induction of FCI. We found that after Wnt signaling inhibition, the cells became hyperpolarized. In dnTCF4 mice, the V_m changed from -84.9 ± 0.7 mV in EtOH to -87.1

± 0.4 mV in 4OHT, while in Dkk1 mice, its value changed from -86.0 ± 0.6 mV in EtOH to -89.1 ± 0.3 mV in 4OHT. Such hyperpolarization under ischemic conditions was observed in all analyzed cell types.

Table 5. Membrane properties of differentiated adult NS/PCs isolated from CTRL mice, and showing a passive current profile.

	dnTCF4		**Dkk1**		**Ex3**	
	EtOH	**4OHT**	**EtOH**	**4OHT**	**EtOH**	**4OHT**
V_m [mV]	-84.5±0.7	-83.0±1.0	-86.8±0.9	-85.5±1.0	**-85.4±0.7**	**-87.6±0.6***
IR [MΩ]	67.6±4.2	66.7±2.8	**49.1±3.1**	**75.3±4.5*****	89.4±5.0	79.2±4.0
C_m [pF]	27.1±2.3	30.4±2.9	**31.4±2.8**	**21.7±1.7****	22.6±1.8	20.7±1.4
K_{IR} [pA]	59.4±5.0	56.1±6.3	62.2±14.0	63.9±8.3	57.0±12.8	45.8±4.6
K_{IR}/C_m [pA/pF]	2.9±0.3	2.5±0.4	2.4±0.7	3.2±0.4	3.5±0.9	2.7±0.3
K_{DR} [pA]	75.9±18.4	126.8±26.9	166.2±39.1	144.0±31.9	116.7±20.4	74.9±11.8
K_{DR}/C_m [pA/pF]	4.0±0.8	6.3±1.5	7.4±2.3	8.7±3.0	5.8±1.0	3.9±0.6
n	62	55	25	25	61	63

Abbreviations: 4OHT – (Z)-4-hydroxytamoxifen; C_m – membrane capacitance; Dkk1 – Dickkopf 1; dnTCF4 – dominant negative T-cell factor 4; EtOH – ethanol; Ex3 – exon 3; IR – input resistance; K_{DR} – delayed outwardly rectifying K^+ currents; K_{IR} – inwardly rectifying K^+ currents; K_{IR}/C_m, K_{DR}/C_m – current densities; n – number of cells; V_m – membrane potential. Values in bold indicate significant differences between EtOH- and 4OHT-treated cultures; *, $p < 0.05$; **, $p < 0.01$ (unpublished data).

Table 6. Membrane properties of differentiated adult NS/PCs isolated from MCAO mice, and showing a passive current profile.

	dnTCF4		Dkk1		Ex3	
	EtOH	4OHT	EtOH	4OHT	EtOH	4OHT
V_m [mV]	**-84.9±0.7**	**-87.1±0.4****	**-86.0±0.6**	**-89.1±0.3*****	-86.1±0.3	-85.5±0.6
IR [MΩ]	50.1±3.6	47.2±1.9	44.4±3.5	46.3±2.5	45.9±2.1	48.3±2.8
C_m [pF]	40.6±5.0	36.3±2.4	46.6±4.7	36.5±3.5	53.5±9.5	51.4±10.6
K_{IR} [pA]	91.7±10.6	67.6±13.3	109.0±27.0	113.3±14.8	77.9±13.1	70.7±9.0
K_{IR}/C_m [pA/pF]	2.4±0.4	1.9±0.3	2.9±0.6	4.2±0.6	2.0±0.3	2.1±0.3
K_{DR} [pA]	151.1±20.6	133.1±16.8	227.6±48.1	180.4±28.5	218.0±29.4	173.2±26.5
K_{DR}/C_m [pA/pF]	5.9±1.1	4.2±0.5	5.6±1.0	4.6±0.7	5.8±0.7	4.7±0.7
n	25	40	23	32	39	30

Abbreviations: 4OHT – (Z)-4-hydroxytamoxifen; C_m – membrane capacitance; Dkk1 – Dickkopf 1; dnTCF4 – dominant negative T-cell factor 4; EtOH – ethanol; Ex3 – exon 3; IR – input resistance; K_{DR} – delayed outwardly rectifying K^+ currents; K_{IR} – inwardly rectifying K^+ currents; K_{IR}/C_m, K_{DR}/C_m – current densities; n – number of cells; V_m – membrane potential. Values in bold indicate significant differences between EtOH- and 4OHT-treated cultures; *, $p < 0.05$; **, $p < 0.01$ (unpublished data).

Cells with a complex current profile

In cells with a complex current pattern, we observed opposite effects of Wnt signaling inhibition and activation on the values of V_m (Tables 7 and 8). Inhibition of the pathway resulted in hyperpolarization, while Wnt signaling activation led to depolarization of the membrane. Besides the passive membrane properties, Wnt signaling manipulation influenced also the expression of voltage-gated K^+ channels in this cell type. After Wnt signaling activation in CTRL mice, the densities of all examined K^+ currents decreased. This effect of Wnt signaling subsided after the induction of FCI, which is in accordance with our observation that under ischemic conditions, the majority of K^+ currents were upregulated, independently on the Wnt signaling inhibition/activation.

Table 7. Membrane properties of differentiated adult NS/PCs isolated from CTRL mice, and showing a complex current profile.

	dnTCF4		**Dkk1**		**Ex3**	
	EtOH	**4OHT**	**EtOH**	**4OHT**	**EtOH**	**4OHT**
V_m [mV]	**-82.9±1.0**	**-88.6±0.7*** **	-89.0±0.9	-86.9±0.9	**-88.8±0.8**	**-86.5±0.7***
IR [MΩ]	138.2±12.8	153.0±13.8	136.4±9.7	136.3±9.0	**175.6±14.0**	**138.6±7.7***
C_m [pF]	**16.9±1.6**	**12.7±0.8***	14.5±1.1	15.2±1.3	15.7±1.2	16.6±1.1
K_{IR} [pA]	85.9±8.4	85.5±9.2	106.7±9.6	119.4±10.0	**105.4±9.4**	**61.1±5.9*** **
K_{IR}/C_m [pA/pF]	6.1±0.6	7.7±0.9	8.3±0.8	10.7±1.2	**7.9±0.7**	**4.5±0.5*** **
K_{DR} [pA]	489.7±65.6	517.5±64.7	708.2±80.3	881.1±73.3	**545.4±59.9**	**377.4±38.5***
K_{DR}/C_m [pA/pF]	34.9±5.1	52.8±9.0	54.1±6.3	76.0±9.6	**42.1±5.5**	**25.6±2.9****
K_A [pA]	331.9±84.4	200.4±21.3	**507.2±62.3**	**302.4±24.9***	253.9±50.1	143.6±26.6
K_A/C_m [pA/pF]	22.3±4.3	20.8±3.7	**45.4±6.3**	**25.1±2.7***	19.2±4.3	11.4±2.4
n	43	45	39	38	45	58

Abbreviations: 4OHT – (Z)-4-hydroxytamoxifen; C_m – membrane capacitance; Dkk1 – Dickkopf 1; dnTCF4 – dominant negative T-cell factor 4; EtOH – ethanol; Ex3 – exon 3; IR – input resistance; K_A – fast activating and inactivating outwardly rectifying K^+ currents; K_{DR} – delayed outwardly rectifying K^+ currents; K_{IR} – inwardly rectifying K^+ currents; K_{IR}/C_m, K_{DR}/C_m, K_A/C_m – current densities; n – number of cells; V_m – membrane potential. Values in bold indicate significant differences between EtOH- and 4OHT-treated cultures; *, $p < 0.05$; **, $p < 0.01$; ***, $p < 0.001$ (unpublished data).

Table 8. Membrane properties of differentiated adult NS/PCs isolated from MCAO mice, and showing a complex current profile.

	dnTCF4		Dkk1		Ex3	
	EtOH	4OHT	EtOH	4OHT	EtOH	4OHT
V_m [mV]	**-84.7±1.3**	**-88.2±0.7***	**-87.2±0.7**	**-89.4±0.6***	-86.0±0.5	-85.2±1.3
IR [MΩ]	171.9±33.5	120.7±16.3	115.4±26.3	111.8±10.6	93.1±11.4	110.6±11.9
C_m [pF]	21.4±3.5	20.3±3.3	**23.3±2.4**	**15.2±1.2****	34.5±13.8	18.9±2.9
K_{IR} [pA]	98.1±13.2	91.6±11.0	111.0±13.3	135.8±11.6	**83.4±8.8**	**122.1±13.7***
K_{IR}/C_m [pA/pF]	6.1±1.0	6.3±1.2	**6.3±1.4**	**11.7±1.6***	**5.1±0.9**	**9.0±1.4***
K_{DR} [pA]	953.6±115.6	761.0±129.3	578.5±94.8	739.5±95.4	735.1±119.8	643.6±103.2
K_{DR}/C_m [pA/pF]	61.3±9.4	52.4±10.7	32.7±8.0	79.6±16.7	59.4±15.1	54.0±12.0
K_A [pA]	246.7±27.8	404.8±91.1	408.6±93.9	444.6±68.4	421.0±120.0	302.1±123.1
K_A/C_m [pA/pF]	15.9±4.9	27.2±8.7	26.5±9.5	39.0±7.9	38.7±13.5	26.3±11.7
n	15	13	15	34	23	23

Abbreviations: 4OHT – (Z)-4-hydroxytamoxifen; C_m – membrane capacitance; Dkk1 – Dickkopf 1; dnTCF4 – dominant negative T-cell factor 4; EtOH – ethanol; Ex3 – exon 3; IR – input resistance; K_A – fast activating and inactivating outwardly rectifying K^+ currents; K_{DR} – delayed outwardly rectifying K^+ currents; K_{IR} – inwardly rectifying K^+ currents; K_{IR}/C_m, K_{DR}/C_m, K_A/C_m – current densities; n – number of cells; V_m – membrane potential. Values in bold indicate significant differences between EtOH- and 4OHT-treated cultures; *, $p < 0.05$; **, $p < 0.01$; ***, $p < 0.001$ (unpublished data).

Cells with an outwardly rectifying current profile

In cells displaying an outwardly rectifying current pattern, the effect of Wnt signaling inhibition on the V_m was reverse in CTRL and MCAO mice (Tables 9 and 10). In CTRL mice, the membrane was depolarized and conversely, after the induction of FCI, the cells became hyperpolarized, which was observed in all three cell types. The opposite impact of the Wnt signaling pathway on the V_m coincides well with the expression of K^+ channels mediating outward currents. After Wnt signaling inhibition, the current densities of K_{DR} and K_A were decreased or increased only negligibly in CTRL mice while in MCAO mice, their current densities increased significantly. Higher efflux of K^+ ions out of the cell could potentially explain hyperpolarization observed after the induction of FCI in cells with a complex and outwardly rectifying current profile.

Table 9. Membrane properties of differentiated adult NS/PCs isolated from CTRL mice, and showing an outwardly rectifying current profile.

	dnTCF4		Dkk1		Ex3	
	EtOH	4OHT	EtOH	4OHT	EtOH	4OHT
V_m [mV]	**-85.5±1.6**	**-79.4±1.8***	**-86.9±1.3**	**-81.8±1.2****	**-86.2±1.5**	**-77.8±1.8*****
IR [MΩ]	997.1±97.3	887.5±96.0	**959.7±97.2**	**352.4±30.2*****	**1217.6±134.3**	**877.8±91.9***
C_m [pF]	8.4±0.8	9.5±0.6	**9.1±0.5**	**16.1±1.2*****	**9.1±0.6**	**11.1±0.8***
K_{DR} [pA]	**816.5±45.6**	**1024.3±70.0***	**1149.2±65.4**	**1656.5±79.2*****	853.4±45.0	852.9±50.8
K_{DR}/C_m [pA/pF]	112.2±7.1	118.3±9.0	139.6±8.9	150.5±14.1	101.2±4.7	88.5±5.8
K_A [pA]	605.7±53.8	489.7±54.2	**859.7±60.4**	**352.1±36.2*****	**675.3±64.8**	**320.4±35.7*****
K_A/C_m [pA/pF]	84.5±7.6	75.5±12.3	**110.9±9.8**	**40.1±7.2*****	**80.6±7.3**	**44.0±7.1*****
n	47	47	65	57	62	61

Abbreviations: 4OHT – (Z)-4-hydroxytamoxifen; C_m – membrane capacitance; Dkk1 – Dickkopf 1; dnTCF4 – dominant negative T-cell factor 4; EtOH – ethanol; Ex3 – exon 3; IR – input resistance; K_A – fast activating and inactivating outwardly rectifying K^+ currents; K_{DR} – delayed outwardly rectifying K^+ currents; K_{DR}/C_m, K_A/C_m – current densities; n – number of cells; V_m – membrane potential. Values in bold indicate significant differences between EtOH- and 4OHT-treated cultures; *, $p < 0.05$; **, $p < 0.01$; ***, $p < 0.001$ (unpublished data).

Table 10. Membrane properties of differentiated adult NS/PCs isolated from MCAO mice, and showing an outwardly rectifying current profile.

	dnTCF4		Dkk1		Ex3	
	EtOH	4OHT	EtOH	4OHT	EtOH	4OHT
V_m [mV]	**-77.4±2.4**	**-85.7±1.4***	-78.1±2.3	-84.3±2.1	**-80.1±2.5**	**-67.0±3.4****
IR [MΩ]	1112.2±132.8	1028.2±123.1	1166.2±157.2	741.8±132.1	1230.8±228.2	1018.7±156.6
C_m [pF]	8.9±0.4	8.8±0.3	9.0±0.4	7.9±1.3	10.2±1.1	9.1±0.8
K_{DR} [pA]	**880.5±57.6**	**1296.0±156.5****	945.8±56.8	854.6±65.3	960.6±90.6	968.8±87.9
K_{DR}/C_m [pA/pF]	**100.4±5.3**	**149.3±19.5****	109.5±6.7	137.1±17.1	99.3±6.6	114.6±10.9
K_A [pA]	647.0±42.8	826.3±95.9	879.1±82.3	924.1±108.3	785.4±98.2	746.5±152.4
K_A/C_m [pA/pF]	80.8±6.2	95.5±12.1	**103.7±10.1**	**180.3±30.1****	87.5±12.3	94.9±19.4
n	34	19	37	13	18	24

Abbreviations: 4OHT – (Z)-4-hydroxytamoxifen; C_m – membrane capacitance; Dkk1 – Dickkopf 1; dnTCF4 – dominant negative T-cell factor 4; EtOH – ethanol; Ex3 – exon 3; IR – input resistance; K_A – fast activating and inactivating outwardly rectifying K^+ currents; K_{DR} – delayed

outwardly rectifying K^+ currents; K_{DR}/C_m, K_A/C_m – current densities; n – number of cells; V_m – membrane potential. Values in bold indicate significant differences between EtOH- and 4OHT-treated cultures; *, $p < 0.05$; **, $p < 0.01$; ***, $p < 0.001$ (unpublished data).

Additionally, we identified changes in the incidence of neuron-like cells expressing voltage-dependent Na^+ channels (data not shown). Their counts increased both after Wnt signaling activation (from 3 to 11; total numbers in both CTRL and MCAO cultures) and its inhibition in the cell nucleus (from 3 to 9). On the other hand, the attenuation of the Wnt pathway at the membrane receptor level resulted in a smaller number of these cells (from 10 to 7). Interestingly, the same trends were found in *in vitro* cultures derived from CTRL as well as MCAO mice. Finally, the density of Na^+ currents was significantly changed only in non-operated Dkk1 mice. We identified its increase (from 9.8 ± 1.1 pA/pF in EtOH to 19.1 ± 4.3 pA/pF in 4OHT) in cells with an outwardly rectifying current pattern, which could add to depolarization we observed in this cell type.

The electrophysiological analysis gave us an outline of the effect of Wnt signaling on the functional properties of differentiated NS/PCs. Similar to neonatal mice, Wnt manipulation had a minimal impact on the electrophysiological properties of cells with a passive current pattern. Conversely, the most significant changes were identified after FCI in cells with a complex and outwardly rectifying current profile. We observed hyperpolarized cells especially after Wnt signaling inhibition, which can be explained by higher current densities of K_{DR} and K_A. Moreover, we detected only a few cells with voltage-dependent Na^+ channels, corroborating our findings in neonatal cultures. These results imply that Wnt signaling affects the distribution of K^+ and Na^+ channels and thus influences the membrane properties of differentiated cells.

To summarize, the above-described experiments indicate that we were able to influence the output of the canonical Wnt signaling also in NS/PCs derived from adult animals. This was clearly documented in the experiments *in vitro*. When we utilized tissue lysates, the differences between the experimental groups became less significant. Nevertheless, the immunohistochemical analysis in coronal slices provided results that correspond with our findings in neonatal animals. Together, we found that Wnt signaling inhibition promotes gliogenesis and attenuates neurogenesis, while Wnt signaling activation exerts opposite effects. Moreover, the effects of Wnt signaling were enhanced following the induction of FCI. These findings are recapitulated in the following scheme (Figure 35).

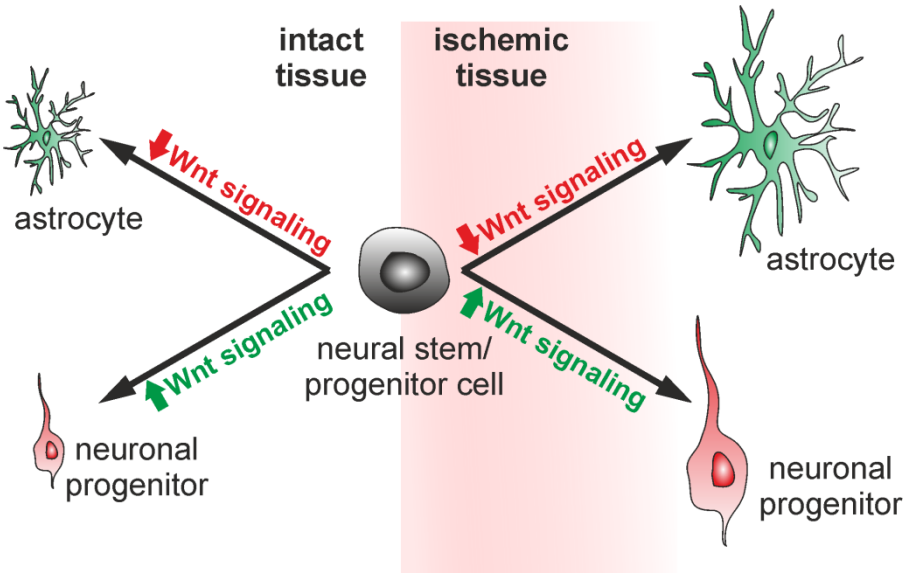

Figure 35. Graphical representation of the changes observed in adult mice. According to our immunohistochemical staining analyses, Wnt signaling inhibition (dnTCF4 or Dkk1) led to the differentiation of NS/PCs to astrocytes, while activation of the pathway (Ex3) promoted neurogenesis. Similar impact of Wnt signaling manipulation after ischemia was confirmed also by the patch-clamp technique. Larger cells represent a greater effect of Wnt signaling after ischemia. Abbreviations: Dkk1 – Dickkopf 1; dnTCF4 – dominant negative T-cell factor 4; Ex3 – exon 3; NS/PCs – neural stem/progenitor cells (unpublished data).

4.3 The differentiation potential of adult NG2 glia

Following the experiments on NS/PCs, we turned our attention to NG2 glial cells, also called polydendrocytes. These cells are considered the most mitotically active glia in the postnatal brain (Dawson et al., 2000), which makes them a promising source of various newly derived cell types in the adult CNS (Kirdajova and Anderova, 2019). Here we analyzed the effect of cellular signaling pathways as well as the impact of FCI on the differentiation potential of these ubiquitous progenitors spread throughout the adult mammalian brain. To achieve this, we employed a transgenic mouse strain in which NG2 cells expressed red fluorescent protein tdTomato, and thus facilitated their 'fate mapping'.

4.3.1 Cell types and their incidence

NG2 cells are restricted to the oligodendrocyte lineage under physiological conditions; nevertheless, ischemic injury turns them into multipotent progenitors. In this study, we assessed the differentiation potential of NG2 cells surrounding the ischemic lesion three, seven, and fourteen days after the induction of FCI by MCAO, and compared it with non-operated controls (Figure 36A). In the CTRL cortex, we identified three distinct Tom-

positive cell populations. One population expressed high levels of *platelet-derived growth factor beta receptor* (*Pdgfrb*), which is characteristic of pericytes. As this cell type does not belong to the oligodendrocyte lineage, it was from now on omitted. Employing the PCA analysis, comparing the expression profiles of cell-type-specific genes, we further identified two more Tom-positive cell types – oligodendrocytes and NG2 cells (Figures 36A-C and 37). Oligodendrocytes (n = 46 cells and 8 mice) were characterized by the expression of *Mbp* and *claudin-11* (*Cldn11*), while NG2 glia (n = 21 cells and 6 mice) expressed *Cspg4* and *platelet-derived growth factor α receptor* (*Pdgfra*; Figure 36B). Surprisingly, *Cnp*, which is a marker of oligodendrocytes, was found in 90.5 ± 6.7% of NG2 glia. Nonetheless, its expression was 60.9 ± 1.2-fold higher in oligodendrocytes (Figure 36C). Besides the cell-type-specific genes, there were several other genes differently expressed in these two Tom-positive populations. Among others, typical astrocytic genes *solute carrier family 1 member 2* (*Slc1a2*) and *solute carrier family 1 member 3* (*Slc1a3*), encoding excitatory amino acid transporter 2 (EAAT2; also known as glutamate transporter 1 (GLT-1) in mice) and excitatory amino acid transporter 1 in humans (EAAT1; also known as glutamate aspartate transporter 1 (GLAST-1) in mice), respectively, were both identified in all NG2 cells. *Slc1a2* was detected in 17.4 ± 4.5% and *Slc1a3* in 35.1 ± 5.6% of oligodendrocytes (Figure 36B). Also the expression of these two genes was higher in NG2 cells (Figure 36C). Another typical astroglial marker, *glutamate-ammonia ligase* (*Glul*), encoding glutamine synthetase (GS), was identified in 96.6 ± 3.4% of oligodendrocytes and 61.9 ± 10.7% of NG2 glia, and its expression was 5.7 ± 1.3-fold higher in the former (Figure 36C). Furthermore, it is known that the canonical Wnt signaling pathway orchestrates the regulation of oligodendrocytic maturation (Guo et al., 2015). For this reason, we analyzed two components of this pathway, *Axin2* and *low density lipoprotein receptor-related protein 5* (*Lrp5*), and found out that the expression of these genes varied in NG2 glia and oligodendrocytes (Figure 36B).

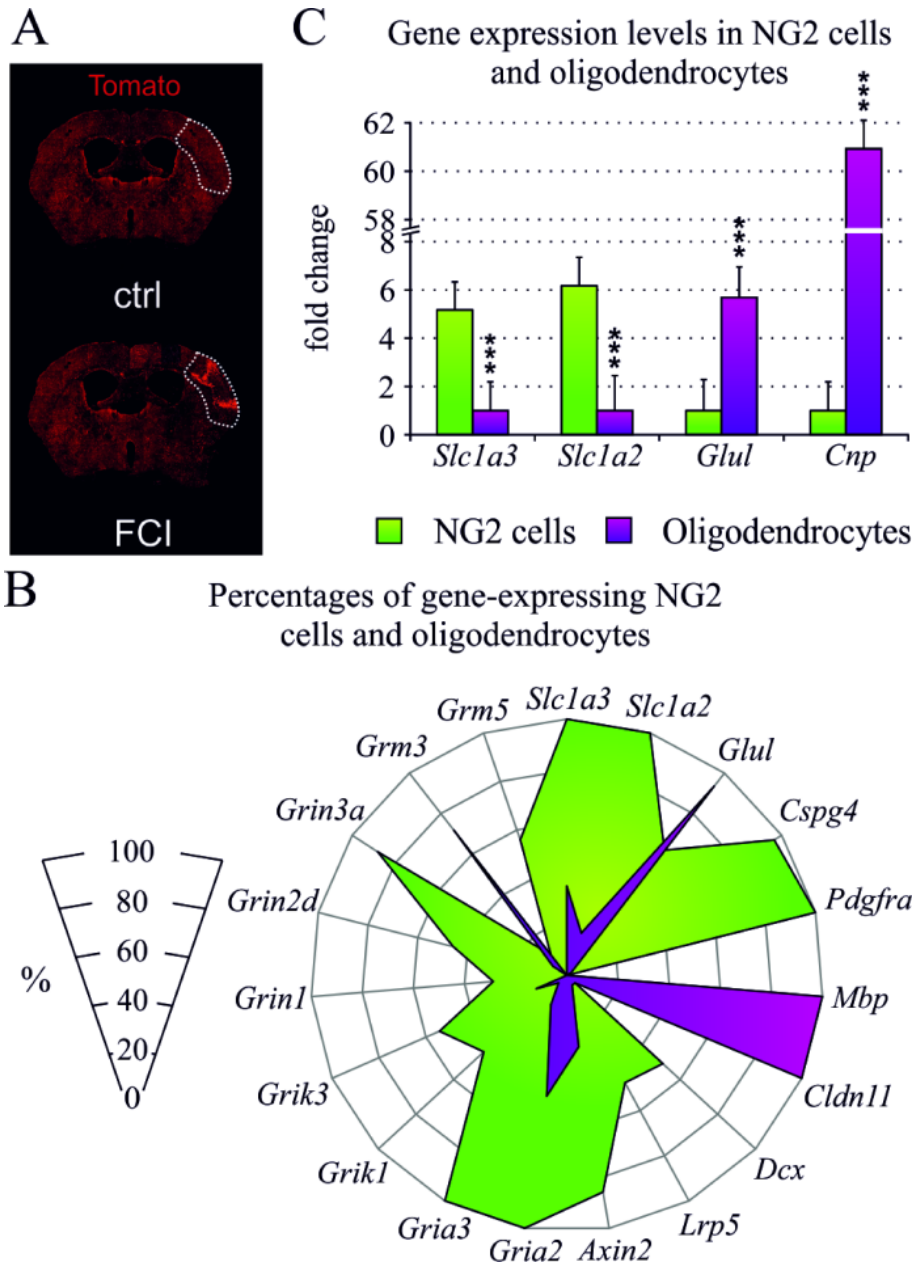

Figure 36. Cortical region of interest and cell types in non-operated mice. (A) Coronal brain slices showing the distribution of Tom-positive cells in the intact, control (CTRL) and ischemic (FCI) brain, and the respective cortical regions (dashed lines) isolated for experiments. **(B, C)** NG2 cells and oligodendrocytes derived from CTRL mice can be distinguished according to the different percentage of cells expressing various genes **(B)** as well as their distinct expression levels **(C)**. All changes in **(B)** are statistically significant; ***, $p < 0.001$. Abbreviations: *Cldn11 – claudin-11*; *Cnp – 2',3'-cyclic-nucleotide 3'-phosphodiesterase*; *Cspg4 – chondroitin sulfate proteoglycan 4*; *Dcx – doublecortin*; FCI – focal cerebral ischemia; *Glul – glutamate-ammonia ligase*; *Gria2/3 – glutamate ionotropic receptor AMPA type subunit 2/3*; *Grik1/3 – glutamate ionotropic receptor kainate type subunit 1/3*; *Grin1/2d/3a – glutamate ionotropic receptor NMDA type subunit 1/2d/3*; *Grm3/5 – glutamate metabotropic receptor 3/5*; *Lrp5 – low density lipoprotein receptor-related protein 5*; *Mbp – myelin basic protein*; *Pdgfra – platelet-derived growth factor alpha receptor*; *Slc1a2 – solute carrier family 1 member 2*; *Slc1a3 – solute carrier family 1 member 3*; Tom – tomato (Valny et al., 2018).

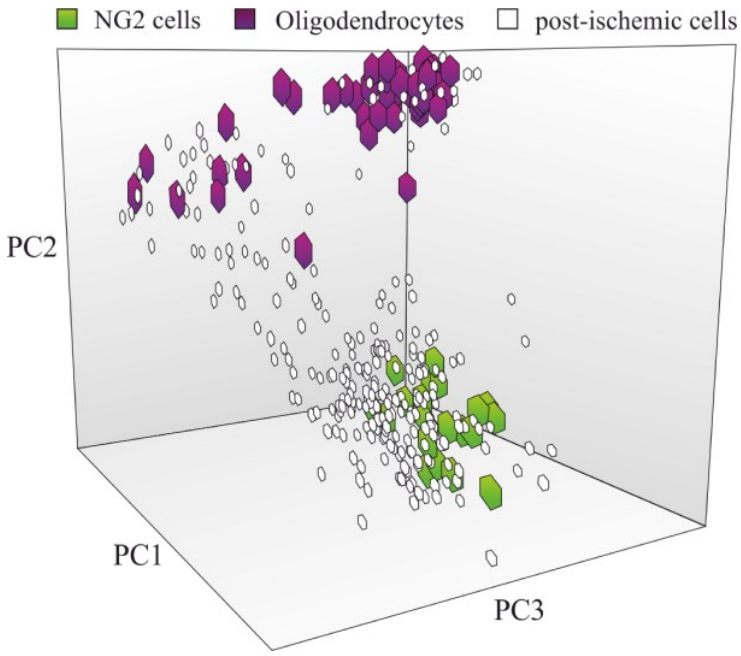

Figure 37. Principal component analysis of cells derived from non-operated mice. Two distinct Tom-positive populations of cells of the oligodendrocytal lineage, separated based on their gene expression profiles, were identified as NG2 glia and oligodendrocytes. Abbreviations: PC – principal component; Tom – tomato (Valny et al., 2018).

Following MCAO, the separation of NG2 glial (n = 199 cells and 8 mice) as well as oligodendroglial (n = 62 cells and 8mice) clusters became less apparent in the PCA analysis (Figure 38). Nevertheless, as the individual populations still expressed the cell-type-specific genes, we were able to distinguish between them. Since the aim of this study was to elucidate the properties of precursor cells, we further dealt only with NG2 glia. After FCI induction, the expression profiles of NG2 cells became more complex and heterogenous and as a consequence, we merged CTRL NG2 cells with those isolated from MCAO mice. Subsequently, we performed SOM analysis, which divided Tom-positive NG2 cells into four distinct subpopulations (Figure 38).

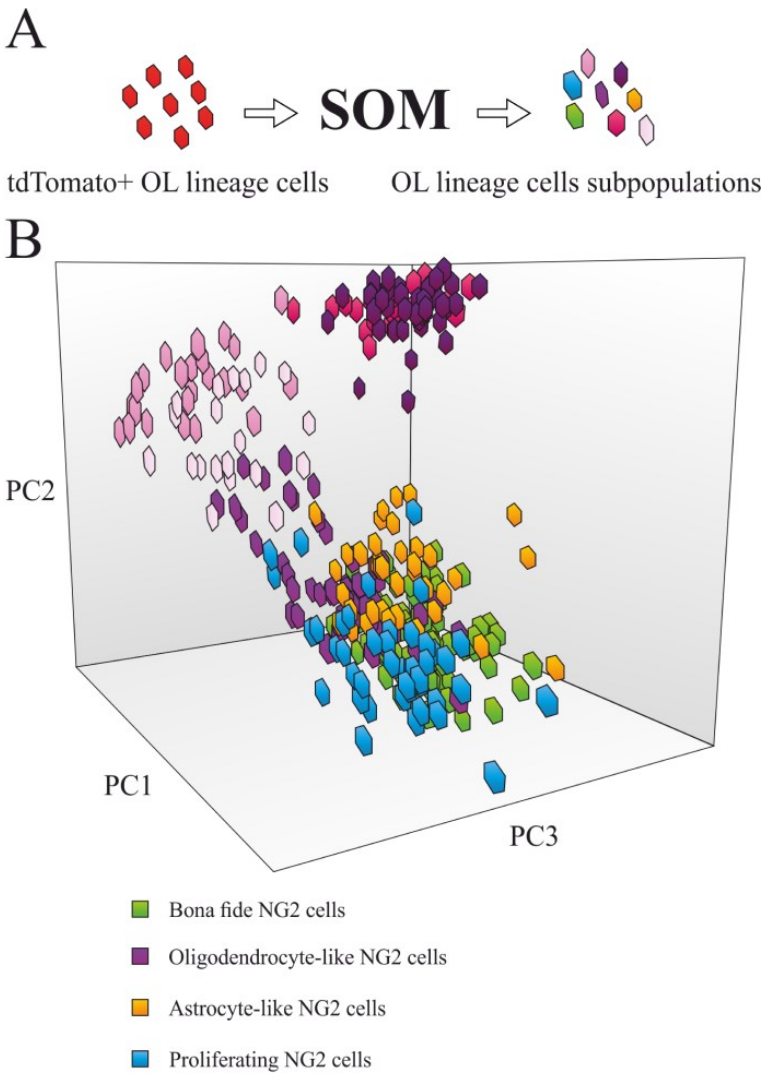

Figure 38. Principal component analysis of cells derived from operated mice. (A) Scheme showing the principle of the SOM analysis. **(B)** Principal component analysis identified four distinct Tom-positive NG2 cells populations, defined by the SOM analysis and separated according to their gene expression profiles. The four violet/pink-ish cell subpopulations in the upper part of the figure represent oligodendrocytic cells, and were not incorporated in this thesis. Abbreviations: OL – oligodendrocyte; PC – principal component; SOM – self-organizing maps; td – tandem dimer; Tom – tomato (adapted from Valny et al. (2018)).

One subpopulation resembled the population of NG2 cells from CTRL mice. These cells were further called *bona fide* NG2 cells (BF-NG2 cells). The other three subpopulations emerged after MCAO (Figure 39). One of them was characterized by a high incidence of cells expressing oligodendroglial markers such as *Mbp* (42.3 ± 9.5%), *Cldn11* (84.6 ± 6.3%), and *transcription factor 7-like 2* (*Tcf7l2*) (94.2 ± 4.9%), encoding the Tcf4 protein, which acts as a Wnt signaling component important for the maturation of oligodendrocytes (Guo et al., 2015). This subpopulation was termed oligodendrocyte-like NG2 glia (OL-NG2 cells; Figure 39A) and also expressed high levels of *Cldn11* and

Cnp, while *Pdgfra* was low when compared to BF-NG2 cells (Figure 39B). Another subpopulation, termed astrocyte-like NG2 glia (A-NG2 cells), predominantly expressed astrocytic genes *Gfap* (43.2 ± 6.0%) and *aquaporin-4* (*Aqp4*; 51.6 ± 9.9%; Figure 39A), while *Gfap* levels were the highest among all subpopulations (Figure 39B). The third "ischemia-induced" subpopulation was composed of cells expressing the marker of proliferation, *Mki67* (84.1 ± 8.3%) and *nestin* (*Nes*; 86.4 ± 8.7%; Figure 39A), a marker of precursor cells in the adult CNS. This subpopulation was named proliferating NG2 glia (P-NG2 cells) and was further characterized by high expression of *Pcna* (Figure 39B). Another typical feature of P-NG2 cells was high expression of *Nes* and *Vim*, while the latter is an intermediate filament commonly found in reactive glia (Figure 39B). Interestingly, the Shh signaling components *Ptch1* and *Smo* were predominantly expressed in the P-NG2 cells subpopulation (81.8 ± 10.3% for *Ptch1*; 40.9 ± 4.0% for *Smo*; Figure 39A).

According to our observations, the incidence of the NG2 glia subpopulations was distributed differently in the course of ischemia (Figure 39C). The highest incidence of P- and A-NG2 cells was detected three days after MCAO (31.5 ± 8.8% for P-NG2 cells; 26.0 ± 3.9% for A-NG2 cells), while OL-NG2 cells predominated seven days after MCAO (34.4 ± 4.1%). At fourteen days after MCAO, the cell distribution started to resemble that observed in CTRL. Additionally, TAM administration on the second day after FCI induction resulted in a significant increase in the incidence of P-NG2 cells three days after MCAO, while the numbers of A-NG2 cells were entirely diminished (Figure 39C).

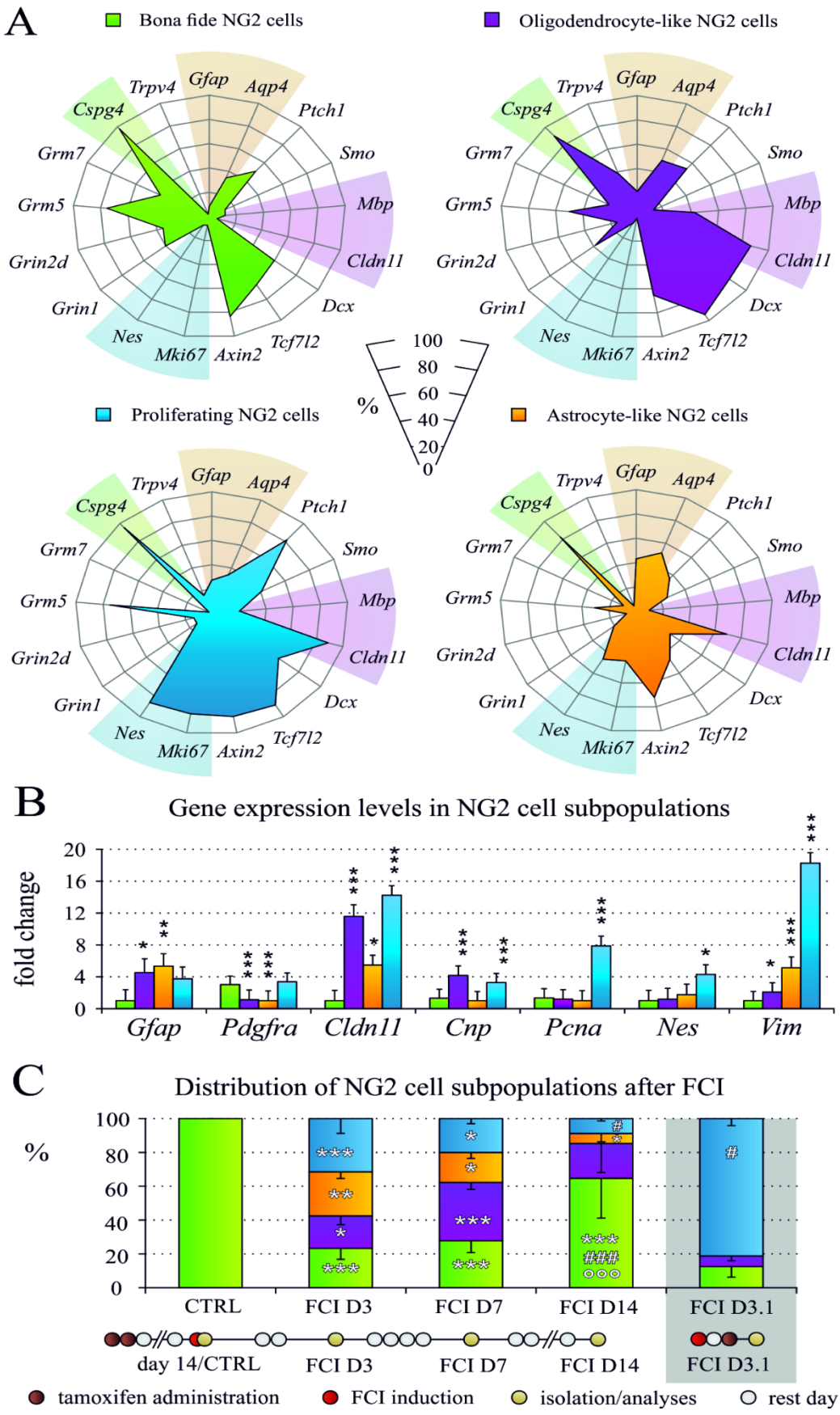

Figure 39. Distinct cell types in operated mice. (A, B) Together four distinct subpopulations of Tom-positive NG2 cells derived from MCAO mice were identified according to the different

percentage of cells expressing various genes **(A)** and their distinct expression levels **(B)**. Background colors in **(A)** highlight genes that represent markers of individual subpopulations. **(C)** In the progression of ischemia, the incidence of individual subpopulations changed. Gray background indicates tamoxifen administration after the onset of FCI. Scheme of tamoxifen administration is shown under the graph. Significance in **(B)** was calculated relative to the "Bona fide NG2 cells" subpopulation, while in **(C)**, asterisks show significance compared to controls ("CTRL"), hashtags show significance compared to "FCI D3", and circles show significance relative to "FCI D7"; $^{*/\#/\circ}$, $p < 0.05$; $^{**/\#\#/\circ\circ}$, $p < 0.01$; $^{***/\#\#\#/\circ\circ\circ}$, $p < 0.001$. Abbreviations: *Aqp4 – aquaporin-4*; *Cldn11 – claudin-11*; *Cnp – 2',3'-cyclic-nucleotide 3'-phosphodiesterase*; *Cspg4 – chondroitin sulfate proteoglycan 4*; D3/7/14 – day 3/7/14; *Dcx – doublecortin*; FCI – focal cerebral ischemia; *Gfap – glial fibrillary acidic protein*; *Grin1/2d – glutamate ionotropic receptor NMDA type subunit 1/2d*; *Grm5/7 – glutamate metabotropic receptor 5/7*; *Mbp – myelin basic protein*; MCAO – middle cerebral artery occlusion; *Mki67* – marker of proliferation; *Nes – nestin*; *Pcna – proliferating cell nuclear antigen*; *Pdgfra – platelet-derived growth factor alpha receptor*; *Ptch1 – patched 1*; *Smo – smoothened*; *Tcf7l2 – transcription factor 7-like 2*; Tom – tomato; *Trpv4 – transient receptor potential cation channel subfamily V member 4*; *Vim – vimentin* (adapted from Valny et al. (2018)).

To second our RT-qPCR data with an analysis at the protein level, we performed immunohistochemical stainings against markers of reactive astrocytes (GFAP), proliferating cells (Ki67), and oligodendrocytes (CC1). We found out that GFAP was expressed in 19.7 ± 3.5% of Tom-positive cells. Additionally, 10.6 ± 0.9% of Tom-positive cells was Ki67-positive and 9.8 ± 0.8% was CC1-positive (Figure 40A-C). Moreover, polydendrocytes are capable of symmetric as well as asymmetric division. To investigate how reactive astrocytes were generated from NG2 cells, we performed EdU staining (Figure 41). We identified 73.1 ± 4.9% of GFAP- and Tom-positive cells as EdU-positive, suggesting that the rest differentiated without preceding cell division. Nevertheless, we were able to identify also EdU- and Tom-positive recently divided daughter cells, with GFAP-positive either only one cell (Figure 41A) or both cells (Figure 41B).

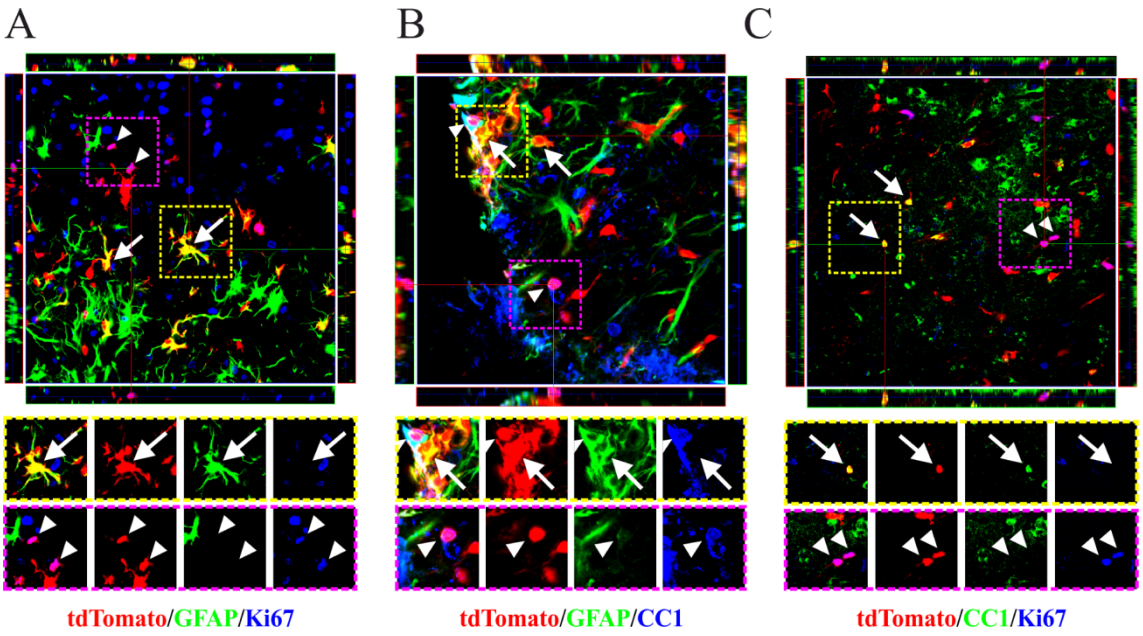

Figure 40. Immunohistochemical staining in operated mice. (A, B, C) Representative images showing the heterogeneity of NG2 glia close to the ischemic lesion seven days after MCAO. **(A)** Tom-positive NG2 glia express astroglial marker GFAP and the marker of proliferating cells, Ki67. **(B)** Tom-positive NG2 cells express GFAP together with CC1, a marker of oligodendrocytes. **(C)** Tomato-positive NG2 glia express CC1 and Ki67. Arrows signify the co-localization of green and red signals, while arrowheads show the co-localization of red and blue signals. Abbreviations: CC1 – APC clone CC1; GFAP – glial fibrillary acidic protein; Ki67 – marker of proliferation; MCAO – middle cerebral artery occlusion; td – tandem dimer; Tom – tomato (Valny et al., 2018).

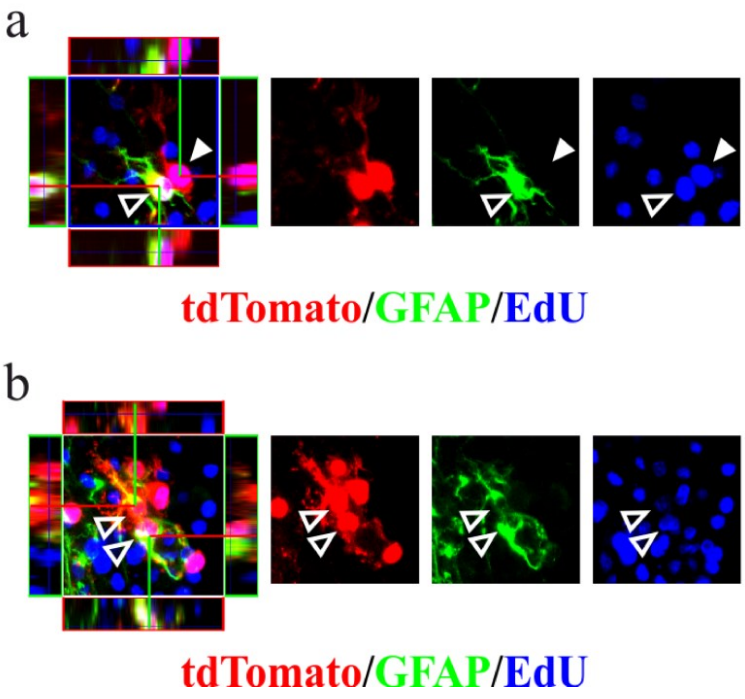

Figure 41. Immunohistochemical staining of NG2-derived reactive astrocytes in operated mice. (A, B) Representative images show asymmetric **(A)** or symmetric **(B)** division of Tom-positive dividing NG2 glia close to the ischemic lesion seven days after MCAO. Filled

arrowheads point at GFAP-negative cells, while empty arrowheads show GFAP-positive cells. Abbreviations: EdU – 5-ethynyl-2´-deoxyuridine; GFAP – glial fibrillary acidic protein; MCAO – middle cerebral artery occlusion; td – tandem dimer; Tom – tomato (adapted from Valny et al. (2018)).

Our results show that NG2 glia under physiological conditions give rise to oligodendrocytes. During this process, they down-regulate the expression of Wnt pathway components such as *Axin2* and *Lrp5* (Figure 36B). Nevertheless, FCI induces the multipotent differentiation potential of polydendrocytes, as they are able to differentiate to OL-, A-, or P-NG2 cells, with their specific expression of Wnt signaling components and cell-type-specific genes, while the expression of Shh-associated genes was highest in the P-NG2 cells subpopulation. Differentiation to oligodendrocytes, reactive astrocytes, or proliferating cells was documented also at the protein level. Finally, we proved that NG2-derived GFAP-positive reactive astrocytes (A-NG2 cells) can be generated symmetrically as well as asymmetrically.

4.3.2 Reactive astrocytes and Shh signaling

Previously, we confirmed that NG2 cells are able to differentiate to reactive astrocytes characterized by high expression of *Gfap*. This subpopulation of NG2 cells appears after FCI induction and harbors certain mRNA levels of Wnt and Shh signaling components. In this study, we concentrated on the effect of the Shh signaling pathway on the differentiation potential of NG2 glia, with a particular focus on reactive astrocytes.

Here, we researched NG2 cells under physiological as well as ischemic conditions, while the role of Shh inhibition/activation was assessed at the mRNA, protein, and functional levels, both *in vitro* and *in vivo*. First, we inspected whether Shh signaling is responsible for differentiation of Tom-positive NG2 cells, derived from CTRL mice, *in vitro*. Seven days after the onset of differentiation, the vast majority of analyzed cells (68.6 ± 6.4%) expressed NG2 proteoglycan, a marker typical of NG2 cells (Figure 42A, B). Approximately one third (34.5 ± 8.7%) of Tom-positive cells expressed MOSP, which categorized them into the oligodendroglial cell type. Additionally, 6.3 ± 2.4% of cells was positive to the astrocytic marker GFAP (Figure 42A, E). NG2-positive cells isolated four days after MCAO and cultured for another seven days constituted only 30.9 ± 3.0% of all Tom-positive cells (Figure 42A, C). Nevertheless, a strong impact of FCI resulted also in an increase in numbers of GFAP-positive cells (22.6 ± 3.4%) when compared to CTRLs (Figure 42A, F). To evaluate the effect of Shh signaling on the differentiation potential of

NG2 cells, we added the Shh blocker Cyc to differentiation medium and found out that it led to the higher number of NG2-expressing cells (87.6 ± 2.5%), while the counts of GFAP-positive cells decreased (3.6 ± 1.5%; Figure 42A,). Cultivation with the activator Shh increased the numbers of GFAP-positive cells (21.5 ± 6.4%) but in contrast to ischemic cells, it did not lower the proportion of NG2-positive precursors. Adding Cyc abolished the effect of Shh. We also assessed the effect of the potent Shh signaling activator SAG, which reproduced the phenotype observed after Shh treatment. However, we detected even more GFAP-positive cells (52.4 ± 7.7%; Figure 42A, D, and G). Interestingly, we did not observe any significant changes in the expression of oligodendrocytic markers under various *in vitro* conditions (data not shown), which suggests that activated Shh pathway promotes the differentiation of NG2 cells towards the astrocytic phenotype, while mimicking the impact of FCI.

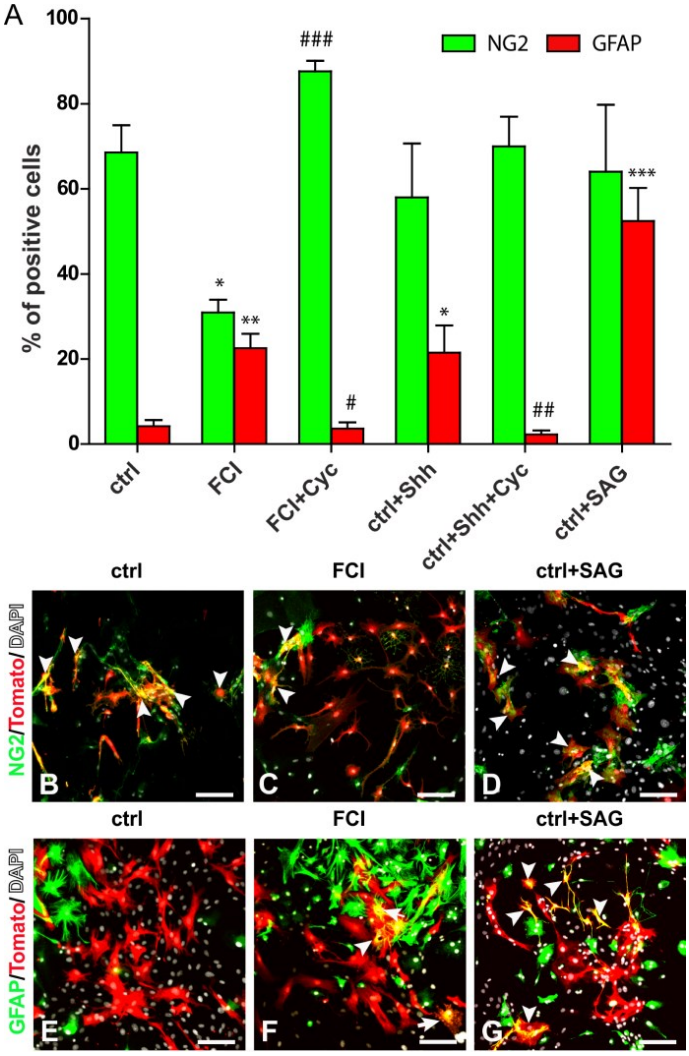

Figure 42. Ischemia and Shh signaling change the differentiation potential of Tom-positive cells *in vitro*. (A) Quantification of NG2 proteoglycan (NG2) and glial fibrillary acidic protein

(GFAP) expression in Tom-positive cells derived from CTRL and MCAO (FCI) mice. The signaling pathway was either inhibited (Cyc) or activated (Shh, SAG). **(B-G)** Representative immunofluorescence images of NG2 proteoglycan and GFAP in Tom-positive cells. The data are represented as means ± standard error of the mean (S.E.M.) and asterisks indicate significant differences when compared to CTRLs, while hashtags indicate differences when compared to the FCI groups. Scale bars = 50 μm. Abbreviations: CTRL – control, non-operated; Cyc – cyclopamine; DAPI – 4′,6-diamidino-2-phenylindole; FCI – focal cerebral ischemia; MCAO – middle cerebral artery occlusion; SAG – Smo agonist; Shh – Sonic hedgehog; Tom – tomato (Honsa et al., 2016).

Employing the electrophysiological analysis, we identified five distinct Tom-positive populations (Figure 43) with their characteristic membrane properties (Table 11). The prevalent cell type (42.7 ± 5.5%; Figure 43D) showed a complex current pattern, and these NG2 cells were mainly NG2- and PDGFαR-positive (Figure 43A). The GFAP-positive cells displaying a non-decaying passive current profile (22.0 ± 4.1%; Figure 43D) were considered astrocytes under control conditions (Figure 43B). The third most common subpopulation of Tom-positive cells (18.7 ± 5.0%; Figure 43D) showed a decaying passive current profile, and these oligodendrocytes were CNP- or MOSP-positive (Figure 43C). The other two remaining cell types represented a minority of Tom-positive cells. Whereas the PDGFβR-positive subpopulation of pericytes was detected also in our previous experiments with NG2 cells, DCX-positive neuroblasts/neuron-like cells formed only ~3% of all Tom-positive cells.

The incidence of these identified subpopulations was influenced by ischemia as well as Shh signaling manipulation (Figure 43D). The incidence of astrocytes after FCI increased to 74.1 ± 5.4%, while only 14.9 ± 3.9% of NG2 cells was detected. This confirms the previous immunocytochemical analysis (Figure 42A). Furthermore, the Cyc blocker elevated the percentage of NG2 cells in ischemic cultures, while the number of astrocytes dropped. The presence of Shh and SAG activators resulted in increased incidence of astrocytes (43.2 ± 7.8% for Shh and 66.7 ± 12.2% for SAG), whereas Cyc treatment abrogated this effect and even decreased the number of cells with a non-decaying passive current pattern. Thus, we demonstrated that changes in the cell incidence caused by FCI or/and Shh signaling manipulation, and confirmed at the protein level, are also translated into the functional level.

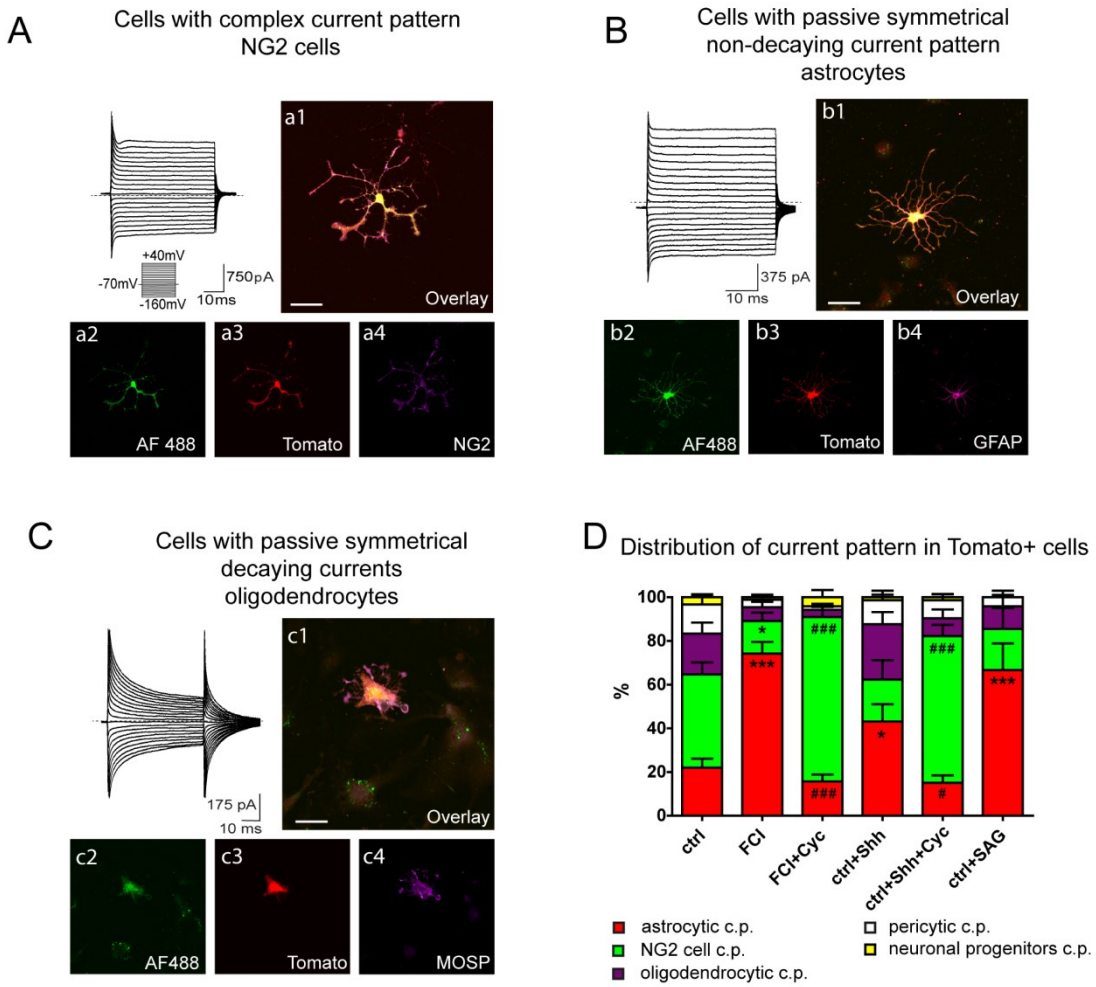

Figure 43. Alterations in the incidence of distinct Tom-positive cell types after ischemia and Shh signaling manipulation *in vitro*. (A) Polydendrocytes (NG2 cells) displayed a complex current pattern and were positive to NG2 proteoglycan **(A1-4)**. **(B)** Astrocytes showed a non-decaying passive current profile, while they were glial fibrillary acidic protein (GFAP)-positive **(B1-4)**. **(C)** Oligodendrocytes were characterized by their decaying passive current profiles, while showing myelin/oligodendrocyte-specific protein (MOSP) positivity **(C1-4)**. **(D)** Graph shows the incidence of Tom-positive cells based on their current patterns. The cells were isolated from CTRL as well as MCAO (FCI) animals, and Shh signaling was either activated (Shh, SAG) or inhibited (Cyc). The data are represented as means ± standard error of the mean (S.E.M.) and asterisks indicate significant differences when compared to CTRLs, while hashtags indicate differences when compared to the FCI groups. Scale bars = 50 µm. Abbreviations: AF488 – Alexa Fluor 488 hydrazide; c.p. – current pattern; CTRL – control, non-operated; Cyc – cyclopamine; FCI – focal cerebral ischemia; MCAO – middle cerebral artery occlusion; SAG – Smo agonist; Shh – Sonic hedgehog; Tom – tomato (Honsa et al., 2016).

Table 11. Membrane properties of Tom-positive cells isolated from CTRL mice.

	NG2 cells	astrocytes	oligodendrocytes	pericytes	neuroblasts
V_m [mV]	-78.0±2.2	-83.1±1.8	**-41.7±3.9***	**-50.0±6.2****	-82.3±1.5
IR [MΩ]	124.6±11.3	85.9±7.3	694.1±196.4	**2329.0±746.9***	654.8±247.8
C_m [pF]	23.8±2.6	21.2±3.8	32.6±4.2	17.7±2.5	14.2±1.7
K_{IR}/C_m [pA/pF]	7.7±0.7	**4.1±0.8***	**3.4±1.0****	**2.3±1.5****	2.4±1.3
K_{DR}/C_m [pA/pF]	19.8±2.3	**1.9±0.8*****	**6.0±1.6*****	**2.1±0.9*****	**97.6±11.4*****
K_A/C_m [pA/pF]	19.1±2.3	**0.1±0.1*****	**0.2±0.2*****	**0.0±0.0*****	**40.2±6.3*****
Na/C_m [pA/pF]	4.9±1.4	**0.0±0.0***	0.4±0.4	0.0±0.0	**21.3±9.7*****
n	56	35	28	16	6
incidence [%]	42.7±5.5	22.0±4.1	18.7±5.0	13.3±3.8	3.3±1.3

Abbreviations: C_m – membrane capacitance; CTRL – control, non-operated; IR – input resistance; K_A – fast activating and inactivating outwardly rectifying K^+ currents; K_{DR} – delayed outwardly rectifying K^+ currents; K_{IR} – inwardly rectifying K^+ currents; K_{IR}/C_m, K_{DR}/C_m, K_A/C_m, Na/C_m – current densities; n – number of cells; Na – Na^+ current; Tom – tomato; V_m – membrane potential. Values in bold indicate significant differences when compared to NG2 cells; *, $p < 0.05$; **, $p < 0.01$; ***, $p < 0.001$ (adapted from Honsa et al. (2016)).

To complement our data with the evaluation of mRNA expression *in vivo*, we employed the single-cell RT-qPCR analysis. We compared the gene expression of several genes in cells isolated from CTRL mice as well as from mice three, seven, and fourteen days after MCAO (FCI D3/7/14; Figure 44A). First, we excluded the aforementioned *Pdgfrb*-positive pericytes from our analyses. Then, we observed increased numbers of Tom-positive cells expressing *Ki67* three and seven days after MCAO (Figure 44B). We also detected higher numbers of cells expressing *Gfap*, a marker of astrocytes and reactive astrocytes, after the induction of FCI, while the expression of *Dcx* was more abundant in the later phases of ischemia. Moreover, mRNA of the Shh signaling receptor *Smo* was found in Tom-positive cells mainly on the third day and roughly copied the gene expression of *Ki67* and *Gfap* during the progression of ischemic injury. This analysis showed that Shh signaling has a role in post-ischemic differentiation of NG2 cells.

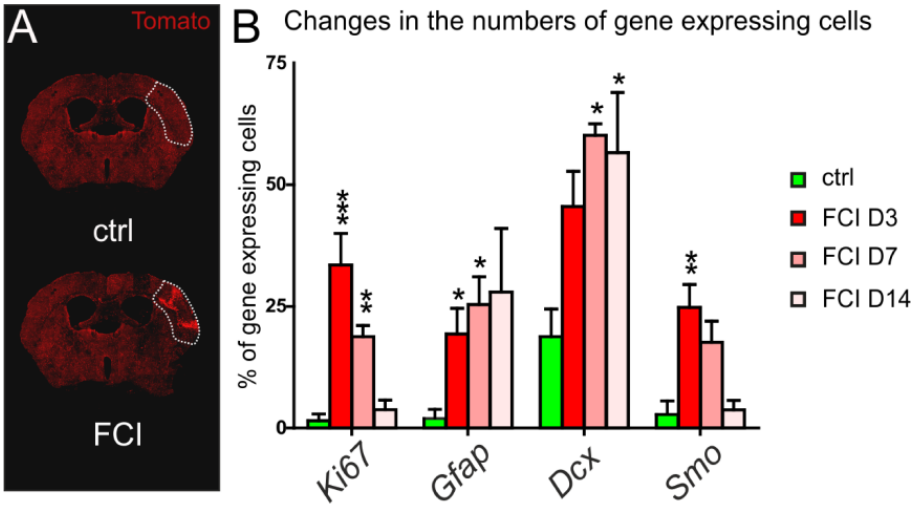

Figure 44. Gene expression in Tom-positive cells after ischemia. (A) Coronal brain slices showing the distribution of Tom-positive cells in the intact, control (CTRL) and ischemic (FCI) brain, and the respective cortical regions (dashed lines) isolated for the experiments. **(B)** Percentage of Tom-positive cells in CTRL mice as well as in mice three, seven, and fourteen days after MCAO (FCI D3/7/14) expressing *Ki67*, *Gfap*, *Dcx*, and *Smo* genes. We analyzed 65 CTRL cells, 95 FCI D3 cells, 133 FCI D7 cells, and 54 FCI D14 cells. Data represent means ± standard error of the mean (S.E.M.) and asterisks indicate significant differences when compared to CTRLs; *, $p < 0.05$; **, $p < 0.01$; ***, $p < 0.001$. Abbreviations: *Dcx* – doublecortin; FCI – focal cerebral ischemia; *Gfap* – glial fibrillary acidic protein; *Ki67* – marker of proliferation; MCAO – middle cerebral artery occlusion; *Smo* – smoothened; Tom – tomato (Honsa et al., 2016).

As our previous data suggest, Shh shifts the differentiation potential of NG2 cells after FCI towards the phenotype of reactive astrocytes. We inhibited Shh signaling by i.p. injections of Cyc after FCI, and compared the gene expression of several genes with the Cyc-untreated counterparts seven days after MCAO (Figure 45). Inhibition of the pathway led to a decrease in the counts of cells expressing astrocytic genes *Gfap*, *10-formyltetrahydrofolate dehydrogenase* (*Aldh1l1*), and *Vim* (Figure 45A), while it stimulated the expression of *Cspg4* and *Pdgfra* (Figure 45B). Additionally, a significant decrease in the incidence of *Dcx*-expressing cells was observed after inhibition of the pathway (from 60.1 ± 2.4% to 35.0 ± 7.0%). Manipulation of the pathway did not alter the expression of *Ki67*, which may imply that Shh did not influence proliferation of Tom-positive cells. Moreover, it is worth pointing out that Shh signaling inhibition suppressed the expression of genes associated with reactive astrocytes.

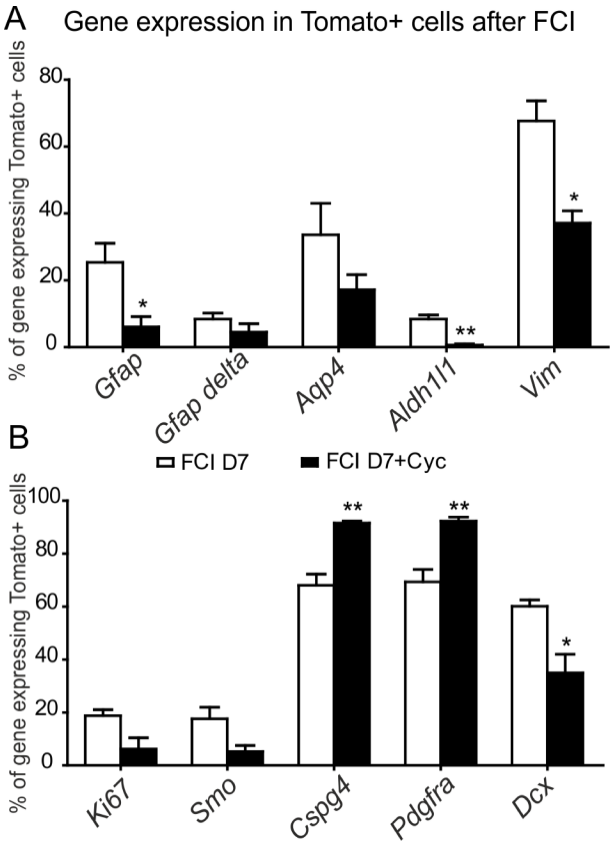

Figure 45. Differentiation of Tom-positive cells is influenced by Shh signaling. (A) Proportion of Tom-positive cells expressing genes specific for astrocytes (*Gfap*, *Gfap delta*, *Aqp4*, *Aldh1l1*, *Vim*) seven days after focal cerebral ischemia (FCI D7) in non-treated and cyclopamine (Cyc)-treated mice. **(B)** Expression of several other genes was either unchanged (*Ki67*, *Smo*) or altered (*Cspg4*, *Pdgfra*, *Dcx*). We analyzed 133 non-treated FCI D7 cells and 65 Cyc-treated cells. Data represent means ± standard error of the mean (S.E.M.) and asterisks indicate significant changes when compared to FCI D7 cells; *, $p < 0.05$; **, $p < 0.01$. Abbreviations: *Aldh1l1* – 10-formyltetrahydrofolate dehydrogenase; *Aqp4* – aquaporin-4; *Cspg4* – chondroitin sulfate proteoglycan 4; *Dcx* – doublecortin; *Gfap* – glial fibrillary acidic protein; *Ki67* – marker of proliferation; *Pdgfra* – platelet-derived growth factor alpha receptor; *Smo* – smoothened; Tom – tomato; *Vim* – vimentin (Honsa et al., 2016).

Finally, we analyzed the effect of Shh signaling inhibition/activation after MCAO utilizing immunohistochemical staining against GFAP and DCX (Figure 46). This analysis was supplemented with the BrdU assay that detects proliferating cells. In untreated mice, with non-manipulated Shh signaling, 32.0 ± 2.6% of Tom-positive cells was also GFAP-positive (Figure 46A, B). It is worth mentioning that these cells were identified mainly in the penumbra, close to the ischemic core. Inhibition by Cyc resulted in decreased numbers of GFAP-positive cells (16.0 ± 1.4%), while SAG had the opposite effect (49.1 ± 2.7%). Furthermore, also the incidence of DCX-positive cells (Figure 46C, D) was lowered after Shh signaling inhibition. To eliminate the possibility that distinct

counts of GFAP-positive cells after Shh pathway manipulation were caused by altered proliferation of Tom-positive cells, we assessed BrdU incorporation in proliferating cells after different treatments (Figure 46E, F). We observed that 34.8 ± 2.3% of Tom-positive cells was BrdU-positive seven days after MCAO, and that this number was not markedly altered after Shh signaling manipulation. Altogether, this may signify that Shh signaling influences the differentiation potential of Tom-positive cells following FCI, and that the activated Shh pathway directly promotes differentiation of NG2 cells to reactive astrocytes (Figure 47).

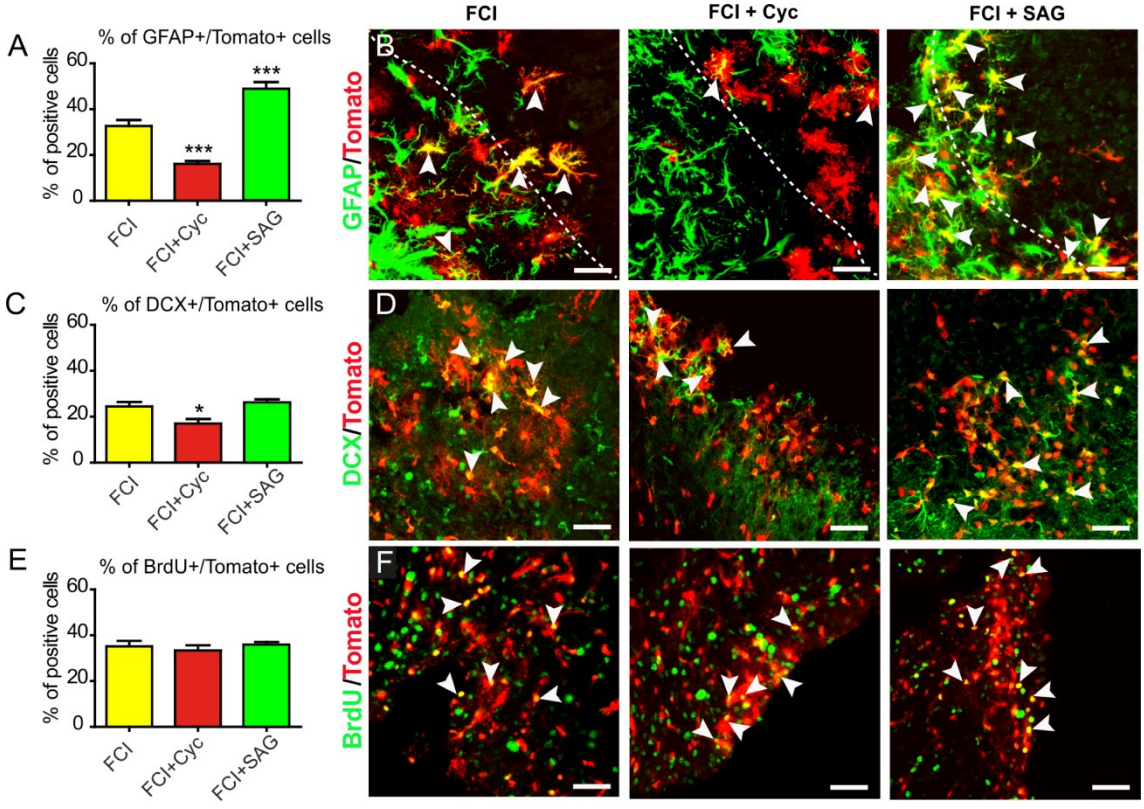

Figure 46. Shh signaling manipulation changes the differentaition potential of Tom-positive cells after ischemia. We employed immunohistochemical staining in mice with non-manipulated (FCI), inhibited (Cyc), or activated (SAG) Shh signaling seven days after focal cerebral ischemia (FCI). **(A, B)** Graph and representative images show the proportion of Tom-positive cells that are also GFAP-positive. Dashed curves mark the border between the ischemic core and the glial scar. **(C, D)** Graph and representative images show the proportion of Tom-positive cells that also express doublecortin (DCX). **(E, F)** Graph and representative images show unchanged numbers of dividing (BrdU) Tom-positive cells. Scale bars = 50 µm. Data represent means ± standard error of the mean (S.E.M.) and asterisks indicate significant alterations when compared to FCI treatment; *, $p < 0.05$; ***, $p < 0.001$. Abbreviations: BrdU – 5-bromo-2'-deoxyuridine; Cyc – cyclopamine; DCX – doublecortin; GFAP – glial fibrillary acidic protein; SAG – Smo agonist; Shh – Sonic hedgehog; Tom – tomato (Honsa et al., 2016).

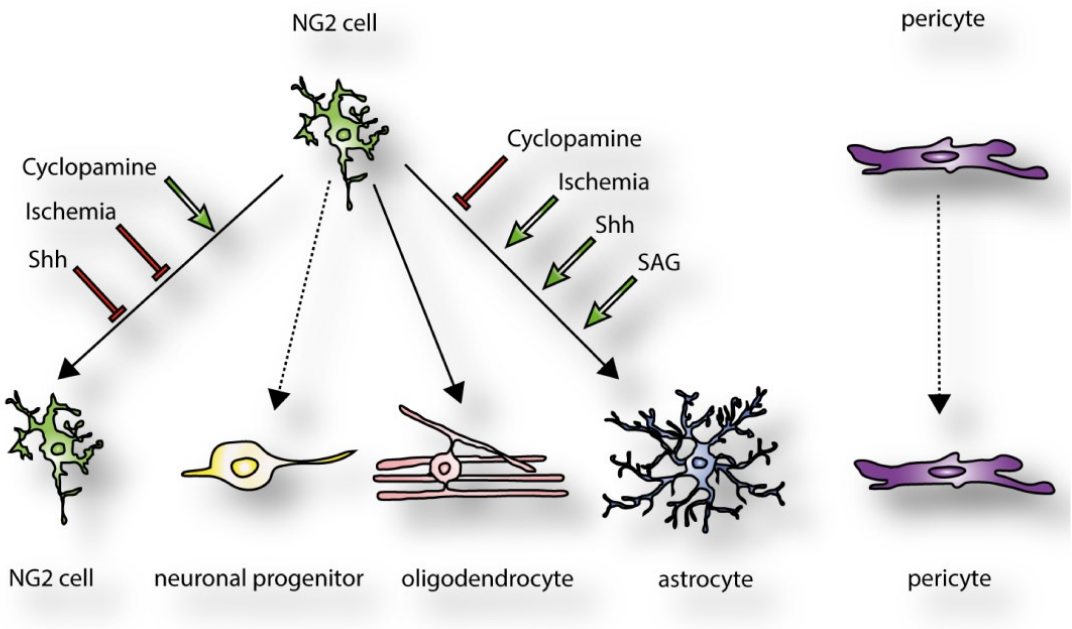

Figure 47. Graphical representation of observed and possible differentiation scenarios of NG2 cells. Polydendrocytes (NG2 glia) can proliferate and give rise to more NG2 cells, or they can differentiate to other cell types. They generate oligodendrocytes mainly under physiological conditions, astrocytes during development or after severe CNS injuries (reactive astrocytes), and neuroblasts, probably only in *in vitro* conditions. The differentiation potential of NG2 cells is regulated by Shh signaling and ischemia. Ischemic injury or Shh signaling activation (SAG, Shh) both promote differentiation to astrocytes, while Shh signaling inhibition (cyclopamine) rises the counts of NG2 glial cells. Pericytes do not belong to the oligodendroglial lineage and preferentially give rise to the same cell type. Abbreviations: CNS – central nervous system; SAG – Smo agonist; Shh – Sonic hedgehog (Honsa et al., 2016).

5 DISCUSSION

Although the role of canonical Wnt and Shh signalings in neural development has been a main subject of countless studies, relatively little is known about their functions in postnatal neurogenesis and gliogenesis. The lack of information may stem from the fact that severe dysregulations of these pathways result in embryonic lethality (van Amerongen and Berns, 2006; Kietzman et al., 2014). In this study, we employed transgenic mouse strains that allowed TAM-induced, conditional inhibition or activation of Wnt signaling, thus circumventing the issue of prenatal CNS malformations that cause mortality. Employing neonatal as well as adult transgenic mouse strains together with the series of aforementioned laboratory approaches, we demonstrated that, in our hands, Wnt/β-catenin signaling has an impact on the differentiation potential of NS/PCs. Moreover, we also showed that Wnt signaling is also active in NG2 cells, as we identified components of the pathway in this cell type of high differentiation potential, while NG2 differentiation to astrocytes after FCI is regulated by Shh.

5.1 Wnt signaling manipulation in neonatal cell cultures

In the first part of our research work, we found out that the expression of Wnt signaling blocker Dkk1 resulted in decreased amounts of β-catenin, while the stabilization of the pathway, accompanied by higher quantities of β-catenin, was detected in Ex3 cells producing a stable, truncated variant of the protein. Wnt/β-catenin signaling activation enhanced the expression of the neuronal marker β III tubulin and decreased the incidence of GFAP-positive cells displaying passive time- and voltage-independent K^+ currents. On the contrary, Wnt pathway suppression led to a marginal increase in the incidence of GFAP-positive cells, while the number of DCX/MAP2-positive cells expressing outwardly rectifying K^+ currents decreased significantly. Furthermore, Wnt signaling activation increased the counts of cells showing outwardly rectifying K^+ currents together with inwardly rectifying Na^+ currents, and also influenced the ability of cells to transport Ca^{2+} after the application of glutamate and ATP.

We employed three different strains of genetically manipulated mice, enabling tamoxifen-inducible Cre-mediated DNA recombination (Figure 12). They facilitated inhibition of Wnt signaling either at the nuclear or membrane receptor level or, alternatively, activation of the Wnt pathway via the production of a stable form of β-catenin protein. Wnt pathway manipulation at various points of the signaling relay gave

us a better insight into the possible molecular mechanisms underlying NS/PCs differentiation in the neonatal mouse brain. In contrast to our study, other authors opted for different approaches. For example, Hirsch et al. (2007) added recombinant Wnt3a ligand to differentiation medium and Prajerova et al. (2010b) used NS/PCs that were transduced with Wnt7a. It is worth mentioning that this ligand was one of the highly expressed ligands in our *in vitro* cultures together with Wnt5a and Wnt7b (Figure 19). Additionally, Meyers et al. (2012) employed pharmacological and heat-shock-inducible genetic manipulation of the Wnt signaling pathway. However, none of the studies listed above combined all the approaches and methods utilized in the present study, where we carried out immunofluorescence analyses as well as functional studies (patch-clamp technique, Ca^{2+} imaging) on NS/PCs derived from the neonatal mouse brain. All this allowed us to perform a comprehensive analysis of effects caused by either activation or inhibition of the Wnt signaling pathway at different subcellular levels. Nonetheless, we obtained similar results as the above-mentioned authors. Inhibition of the pathway in the nucleus (dnTCF4 mice) did not affect the levels of β-catenin expression. This accords well with the fact that this alteration in the pathway occurs downstream of the β-catenin destruction complex, so that it should not influence the expression of β-catenin directly (Figures 20 and 21). This was not the case in Dkk1 and Ex3 mice, where the alterations occurred at the membrane and in the protein itself, respectively. Next, we assessed the expression of putative Wnt signaling target genes, namely *Axin 2*, *Sp5* and *Troy* (Figure 22). These genes should be correlated positively with Wnt/β-catenin signaling as shown previously (Buttitta et al., 2003; Fujimura et al., 2007; Jho et al., 2002). In our hands, Wnt signaling hyper-activation led to a markedly higher expression of all analyzed genes, which goes along with the findings of Fafilek et al. (2013), Fujimura et al. (2007) and Hirsch et al. (2007). These groups found that after Wnt stimulation, stem cells express higher levels of inhibitory components of the Wnt pathway. Examples of such components are the aforementioned genes – *Axin 2*, *Sp5* and *Troy*. Surprisingly, the expression of *Axin 2* was not altered after Wnt signaling inhibition. This inconsistency might be due to overall low expression of *Axin 2* (C_t values ~32) in our dnTCF4 and Dkk1 cultures, which might imply that in these two models, the Wnt signaling pathway is prevented from activation, rather than being inhibited after its activation, while Wnt signaling is still able to affect the cell fate. On the other hand, after Wnt signaling activation, the expression of *Axin 2* was much higher (C_t values ~27), and thus the protein was able to act as a negative feedback loop that controls Wnt signaling activity (Lustig et

al., 2002). Additionally, we analyzed mRNA levels of Wnt ligands and found out that *Wnt4*, *Wnt5a*, *Wnt5b*, *Wnt7a*, *Wnt7b*, *Wnt9a*, and *Wnt10b* are present in all control *in vitro* cultures (Figure 19), while these signals are typical of both canonical and non-canonical Wnt pathways. This correlates, to some extent, with the data from Hirsch et al. (2007), as they found *Wnt3*, *Wnt4*, *Wnt5a*, *Wnt7a*, *Wnt7b* and *Wnt11* genes to be expressed in NS/PCs. For example, non-canonical Wnt5a enhances neurogenesis and improves functional integration of newly derived neurons *in vivo* (Parish et al., 2008). Similar functions are also exercised by Wnt7a, since this Wnt ligand stimulates NS/PCs proliferation and promotes neuronal differentiation and maturation (Qu et al., 2013). Interestingly, over-expression of Wnt7b impairs neuronal differentiation of neural progenitors, and thus antagonizes the effect of Wnt5a and Wnt7a ligands (Papachristou et al., 2014). However, other functions may also be performed by these ligands according to the developmental stages of experimental animals, as presented by Hirabayashi et al. (2004) and reviewed by Inestrosa and Varela-Nallar (2015). Moreover, it could be fairly challenging to determine the function of a Wnt ligand, as the very same ligand is able to activate both β-catenin-dependent and non-canonical pathways (Nalesso et al., 2011).

Next, we showed that hyper-activated Wnt signaling increases the abundance of neuronal marker β III tubulin and decreases the expression of GFAP (Figure 25). This suggests a tendency towards neurogenesis after Wnt signaling activation. Hirsch et al. (2007) demonstrated similar effects of Wnt signaling on the expression of β III tubulin, although the numbers of GFAP-positive cells remained unchanged. This discrepancy might be explained by differences in Wnt pathway activation between our and their study. We took advantage of employing transgenic mouse models and activated the pathway in NS/PCs using the "general" intracellular signal mediator β-catenin, whereas Hirsch et al. (2007) applied specifically only Wnt3a ligand to their differentiation media.

Furthermore, we observed that Wnt signaling causes higher incidence of DCX/MAP2-positive cells that display branched processes (this can be partially seen in Figure 25A), indicating a more advanced developmental stage. These branched and overlayed processes could be responsible for the fact that we were not able to identify significant changes in the levels of DCX and MAP2 (Figure 24). Our observations are in concordance with previously published data from the *in vitro* experiments by Kunke et al. (2009). These authors transduced mouse NS/PCs with constructs producing Wnt7a or Dkk1 and showed that those molecules influenced cell fate during differentiation. Expression of Wnt7a, which activates Wnt signaling, led to an increase in the incidence

of MAP2-positive cells, while the numbers of GFAP-positive cells decreased. In contrast, Dkk1, i.e. inhibiting Wnt signaling, significantly increased gliogenesis at the expense of neurogenesis. In the above mentioned study, the authors incubated single cells derived from trypsinized neurospheres for only four days. In the present study, we employed the same approach but analyzed differentiated cells after eight days of *in vitro* differentiation. Therefore, our results complement those of Kunke et al. (2009) and show that after Wnt signaling inhibition or activation, differentiated cells preserve similar characteristics for a longer period of time. Mardones et al. (2016) showed that Wnt signaling inhibition by retrovirus-mediated RNAi, causing knockdown of Frizzled-1 receptor, though in the adult hippocampus, resulted in a decrease in the percentage of cells expressing DCX and concomitantly, in increased differentiation to astrocytes. Independently of the Wnt signaling inhibition or activation, the incidence of PDGFαR-positive precursors showing a complex current pattern was increased. This phenotype might be attributed to the fact that any intervention in the homeostasis of the CNS (either artificial, non-physiological Wnt signaling manipulation or ischemia) can "activate" precursor cells and alter the expression of cell-type-specific proteins or ion channels. In summary, from our results (Figures 24 and 25) and previously published studies it is evident that Wnt signaling plays a crucial role in the control of the differentiation potential of neuronal progenitors.

Relatively recently, it has been shown that Wnt signaling activation affects the electrophysiological properties of differentiated neural precursors (Prajerova et al., 2010b). Activated Wnt signaling caused a higher incidence of cells expressing outwardly rectifying K^+ currents together with TTX-sensitive inwardly rectifying Na^+ currents and generating action potentials. This neuron-like current pattern with outward currents also prevailed in our experiments (Figure 26). In our work, we further disclosed that MAP2-positive cells displayed large K_A and K_{DR} current amplitudes (Table 4), which agrees with previous studies in neonatal NS/PCs transduced with Wnt7a (Prajerova et al., 2010b). Concurrently, in differentiated NS/PCs upon Wnt signaling inhibition, we found that the response of MAP2/DCX-positive cells to glutamate application decreased (Figure 27A). These data based on calcium imaging analyses support the presence of glutamate receptors on neural progenitors. As suggested by Deisseroth et al. (2004), glutamate receptors mediate excitation-induced neurogenesis by inhibiting the expression of the glial transcription factor *hairy and enhancer of split-1* (*Hes1*) and *inhibitor of DNA binding 2* (*Id2*), and by promoting expression of the pro-neuronal transcription factor *neuronal differentiation* (*NeuroD*). Using retrovirus-mediated gene knock-out in mice,

Tashiro et al. (2006) showed that the survival of maturing neurons is competitively regulated by their own N-methyl-D-aspartate (NMDA) receptors, which was observed during a short period after neuronal birth. Following this, we found that inhibition of the Wnt pathway led to increased numbers of cells responding to the ATP application (Figure 27A) but nevertheless, elevated Wnt/β-catenin signaling resulted in a lower average response amplitude (Figure 27B). This is in contrast with the observations that ATP upregulates the expression of neuronal markers, such as neuron-specific class III β-tubulin (Tuj1), neuronal nuclei (NeuN) and β-catenin expression, and thus promotes neuronal differentiation of stem cells (Tu et al., 2014). This discrepancy might be related to the use of different cells. Whereas we utilized NS/PCs, Tu et al. (2014) employed mesenchymal stem cells in their study.

In summary, Wnt signaling regulates neurogenesis, as its hyper-activation drives neonatal NS/PCs differentiation to the DCX/MAP2-positive cells that express outwardly rectifying K^+ currents and inwardly rectifying Na^+ currents. Importantly, our results indicate that the manipulation of Wnt/β-catenin signaling in NS/PCs might provide novel approaches for the treatment of neurological disorders. For instance, studies of progenitor cells in the olfactory epithelium performed in neonatal as well as adult mice suggested a key role of Wnt signaling in progenitor cells proliferation and neuroregeneration after epithelial lesion (Chen et al., 2014). Moreover, a connection between Alzheimer's disease and Wnt signaling pathway impairments has also been suggested (Inestrosa and Varela-Nallar, 2015; Inestrosa et al., 2002).

5.2 Effect of Wnt pathway on adult NS/PCs

Having assessed the effect of Wnt signaling on the differentiation potential of NS/PCs isolated from adult non-operated mice as well as from those that had undergone MCAO, we observed alterations in the expression of various cell-type-specific markers. Wnt signaling inhibition by Dkk1 caused lower immunopositivity of NS/PCs cultures for β-catenin, while higher immunoreactivity was identified after the hyper-activation of the pathway. The expression of several Wnt target genes was also affected by our TAM-induced animal model. However, these changes were not translated into any alterations in the incidence of distinct cell types in CTRL mice, based on electrophysiological measurements. Interestingly, a neonatal-like pattern of the shifts in the incidence was recovered after the induction of ischemia. Our immunohistochemical analysis revealed

similar effects of Wnt signaling on the expression of PCNA, GFAP, and DCX in CTRL and MCAO mice. Nonetheless, the expression of all markers was upregulated three days after the induction of FCI, which represents earlier phases of ischemia, while in later phases, the expression of cell-type specific proteins may be different. Wnt signaling manipulation also affected passive electrophysiological properties (V_m, IR, C_m) of all cell types found in our *in vitro* cultures, while it had no effect on the expression of voltage-dependent K^+ channels in cells with a passive current profile.

In our experiments on NS/PCs derived from the adult SVZ, we employed the same three mouse strains as in the study on neonatal mice (Figure 12) so that we could take advantage of these convenient means of either Wnt/β-catenin pathway activation or inhibition at two different subcellular levels. This TAM-induced and Cre-mediated system, together with the high reproducibility of well-defined *in vitro* conditions, was probably the strong point of our research. Here, we assessed CTRL mice as well as MCAO mice. Nevertheless, there were a few main differences in utilizing neonatal and adult NS/PCs. Some of them were only minor matters for consideration, while the other ones represented setbacks in our experiments.

A variety of factors may influence the differentiation potential of NS/PCs as well as the outcome of FCI in the adult mouse. Among others, the differences in gender, age, region of the brain, or even the circadian system are probably the most important players in these processes (Vancamp et al., 2019; Lembach et al., 2018). A lot of publications have emerged in the last years particularly on the topic of sex-specific differences impeding the interpretation of experiments. These publications declare that high amount of estrogen in females acts as an endogenous neuroprotectant after the induction of cerebral ischemia, which was confirmed in clinical observations as well as in experimental stroke (Hurn and Macrae, 2000). Since the comparison between males and females was not the aim of this study, we had to choose whether we would work only on female mice or only on male mice and because a stronger impact of ischemia is usually seen in males, we decided to employ male animals. The use of female mice would otherwise contradict our effort to induce focal ischemic injury in the brain. In our experiments on neonatal mice, we did not distinguish between male and female pups because it is not easy to determine the gender in neonatal mice (Wolterink-Donselaar et al., 2009) and, above all, in newborns, estrogen levels are relatively low as well as the quantities of estradiol, the most potent and prevalent estrogen, are similar in males and females (Konkle and McCarthy, 2011). Nevertheless, once the pups are weaned, which is

around postnatal day 21 in mice, establishing the gender can be easily carried out (Wolterink-Donselaar et al., 2009). Taken together, to avoid any gender-, age-, region-of-the-brain-, or circadian-system-related disturbances in our experiments, we used only male mice, with a strictly defined time window when we sacrificed them, and only one experimenter isolated all the SVZs at the specific time of the day.

Another difference between neonatal and adult mice was that in the former, we isolated a presumptive SVZ region (a part of the frontal lobe) while in the latter, we cut out a specified region of the brain – the SVZ (Figure 17). There is a slim chance that this could lead to lower yields of differentiated cells for our further experiments, a phenomenon that was not improved even by a longer incubation of highly proliferative NS/PCs in proliferation medium. A more probable explanation of the lower numbers of cells derived from adult mice would be the fact that adult NS/PCs are normally found in a quiescent state (Urbán and Guillemot, 2014). Bone morphogenetic protein (BMP), which was identified in non-dividing cells of the adult hippocampus, is responsible for this behavior of precursor cells. Active BMP signaling reversibly diminished the proliferation of NS/PCs, while its inactivation enhanced proliferation only transiently, with a subsequent reduction in the numbers of precursors (Mira et al., 2010). However, once activated, young and old NS/PCs exhibit similar proliferation and differentiation capacity (Kalamakis et al., 2019). Activated NS/PCs are characterized by the expression of epidermal growth factor receptor (EGFR; Codega et al., 2014). Since EGF is required for increased proliferation of SVZ-derived cells (O'Keeffe et al., 2009) and, at the same time, NS/PCs can interconvert between the quiescent and activated state (Codega et al., 2014; Lugert et al., 2010), we increased the concentration of EGF in proliferation media by 50% (from 20 ng/ml in neonatal cultures to 30 ng/ml in adult cultures) in an attempt to enhance the yield of cells. Nevertheless, to initiate differentiation of expanded NS/PCs, we had to withdraw this mitogenic agent from differentiation medium (Johe et al., 1996). Unfortunately, much fewer cells were retrieved from neurospheres after two weeks of *in vitro* proliferation (~500,000 cells from an adult mouse versus several millions of cells from a single neonatal mouse). Together with a worse survival of adult cells, this resulted in insufficient material for our experiments. As a consequence, only electrophysiological measurements and immunocytochemical staining against β-catenin were performed *in vitro*. After those, we switched from cell cultures to the utilization of brain tissue in our next experiments, specifically Western blotting, RT-qPCR analysis, and immunohistochemical staining. The use of tissue specimens from the SVZ on the one

hand guaranteed the enrichment in NS/PCs but on the other hand, it could result in a sort of dilution of NS/PCs by other cell types in the brain tissue. As a result, this might also interfere with the composition of the niche, with a subsequent impact on the differentiation potential of NS/PCs. This is in contrast with our *in vitro* experiments, where only cells derived from NS/PCs were present in a well-defined environment of culture media, while they spent 8-9 days in differentiation medium. In tissue specimens, cells had only 3 days to differentiate after i.p. TAM injections or after MCAO. However, this amount of time should be sufficient for their differentiation (Honsa et al., 2013; Zhao et al., 2009), which was, after all, shown also in our study (Figure 34). The fact that the microenvironment around NS/PCs in the tissue specimens was not thoroughly defined might be considered a weakness of our study. Nevertheless, as we had controls for each mouse strain and for each treatment, this should not have a big impact on the assessment of the effect of Wnt signaling on differentiation of neural precursors in our mouse models.

Our results from immunocytochemical staining against β-catenin in adult CTRL cell cultures (Figure 29) resembled those obtained in young animals (Figure 20), showing elevated expression of the protein after Wnt signaling activation and decreased expression of β-catenin only after inhibition by Dkk1. Nevertheless, the results from adult mice were less significant, which could be partially attributed to the transition from neonatal to adult NS/PCs niche, with possible changes in the responsiveness to intrinsic or extrinsic stimuli (Urbán and Guillemot, 2014; Morrison and Spradling, 2008). The exact moment when the switch from embryonic to adult neurogenesis occurs is elusive but it has been suggested that it is between the first and the third postnatal week in the rodent dentate gyrus (Pleasure et al., 2000).

In the rest of our experiments, except for the electrophysiological analysis, we assessed the impact of the Wnt pathway in CTRL as well as MCAO mice. The differentiated NS/PCs were evaluated three days after MCAO. This time period represents earlier phases of ischemia and differentiation of precursor cells probably has different outcome in the later phases. Additionally, we utilized tissue specimens of the SVZ, as explained and discussed earlier in this chapter. Here, it is worth mentioning that in our *in vitro* cultures, bFGF was present, which was not the case in the directly dissected, non-cultured tissue specimens. It was reported that this growth factor increases the activity of the Wnt/β-catenin pathway and, which is more important, overexpression of β-catenin in the presence of bFGF promotes the proliferative state of NS/PCs, while in

its absence, neuronal differentiation is enhanced (Israsena et al., 2004). This could be at the root of the discrepancies detected between *in vitro* and *in situ* experiments.

The Western blotting analysis of β-catenin protein in differentiated adult NS/PCs (Figure 30) only partly corresponded with immunocytochemical staining of the protein. This inconsistency might be caused by the presence of other cell types in the tissue and the finding that Wnt/b-catenin responses can be cell-type-specific (Wallmen et al., 2012). The expression of Wnt target genes was similarly influenced by Wnt signaling in both CTRL and MCAO mice (Figure 31) but we detected higher mRNA levels of the studied targets after ischemia. This observation coincided well with our immunohistochemical analysis, where we found that after FCI, all analyzed proteins were upregulated (Figure 34). Otherwise, the changes in the expression of the Wnt target genes corresponded with those identified in neonatal mice (Figure 22), with few exceptions. In neonatal mice, least responsive strain appeared to be Dkk1, while in adult mice, it was Ex3. This could be a result of an overall reduction in the activity of Wnt signaling, which increases with age and may compensate the hyper-activation of the pathway by Ex3. It was found that with age, various components of the pathway are downregulated, while levels of Wnt antagonists Dkk1 and secreted frizzled-related proteins (sFRPs) as well as niche-derived inflammatory signals are increased. The combination of these processes might induce quiescence of NS/PCs and at least partly interfere with the mouse model (Kalamakis et al., 2019; Kase et al., 2019; Seib et al., 2013). The expression pattern of one target gene, *Sp5*, was distinct from the others (Figure 31). In CTRL mice, it was always overexpressed after Wnt signaling manipulation, while its expression dropped after MCAO. This target gene is positively regulated by Wnt signaling and acts as a transcriptional repressor of another protein from the same family, Sp1 (Fujimura et al., 2007), while the latter is a transcription factor that probably plays a role in protecting cells against oxidative stress following brain injury (https://www.uniprot.org/uniprot/P08047#function). We deem that after ischemic injury, Sp5 is downregulated, which releases Sp1 from its inhibition. Subsequently, Sp1 can perform its function in the tissue affected by ischemia and add to its recovery.

Our primary cultures consisted of the same three cell types that were identified within neonatal cell cultures. These cell types comprised GFAP-positive astrocytes, DCX/MAP2-positive neuron-like cells, and PDGFαR-positive precursors, all with their specific electrophysiological properties (Figure 23). The incidence of these cell types after Wnt signaling manipulation was not changed in intact (CTRL) mice. Nonetheless,

the effect of Wnt signaling manipulation observed in neonatal cultures was partially recovered in MCAO mice, especially in the Dkk1 strain (Figure 32). The reason why we did not detect any changes in the incidence in CTRL cultures might be the continuous, age-related depletion of the NS/PCs pool (Encinas et al., 2011). Another feature of the adult mammalian brain is that quiescent NS/PCs prevail (Codega et al., 2014), and while Wnt inhibition (dnTCF4 and Dkk1) adds to this BMP- and Notch-induced quiescence, its activation in Ex3 mice may only ineffectively go against this state of NS/PCs (Urbán and Guillemot, 2014). Moreover, majority of cells differentiated from NS/PCs undergo apoptosis and are rapidly phagocytized by resident microglia in the niche (Sierra et al., 2010). Interestingly, subpopulations of microglia have distinct effects on the differentiation potential of NS/PCs, as one subpopulation promotes astrogliogenesis, while the other supports neurogenesis, while both inhibit NS/PCs proliferation (Vay et al., 2018). On the other hand, we detected alterations in the incidence of distinct cell types among differentiated cells that were isolated from MCAO animals. This corresponds with our observations from Western blotting experiments, where the majority of identified changes in the expression of cell-type-specific proteins occurred after ischemia (Figure 33). As we mentioned, Notch signaling as well as its transcriptional target Shh perform the same function as BMP in the CTRL CNS. However, they are upregulated after MCAO and both increase cell proliferation in the adult SVZ and may be thus involved in ischemia-induced neurogenesis (Wang et al., 2009). Another study corroborated the previous one with the finding that CNS injury induces proliferation of NS/PCs, while over-expression of Notch1 and nestin was observed. Although CNS injury is known to activate primary astrogliosis, their results suggested that NS/PCs preferentially gave rise to gamma-aminobutyric acid (GABA)ergic neurons (Anderson et al., 2020). This might be resolved by the observation that transplantation of NS/PCs early after hypoxia–ischemia leads to greater differentiation into astrocytes, whereas transplantation at later time points leads to preferential differentiation into neurons (Rosenblum et al., 2012).

The Western blotting experiments on the expression of cell-type-specific proteins in differentiated adult NS/PCs from tissue specimens were mostly inconclusive (Figure 33). For this reason, we performed an exhaustive immunohistochemical analysis of coronal slices with the SVZ region (Figure 34). This approach revealed overall increased immunoreactivity after FCI. This ischemia-triggered upregulation of cell-type-specific proteins was observed also in our experiments analyzing *Cspg4*$^{+}$ precursors, where a steep rise in the expression of GFAP and PCNA was detected three as well as seven days

after MCAO (data not shown). Also Shruster et al. (2012) showed that stroke potently stimulates cell proliferation in the neurogenic niches and that newly generated cells migrate to the injured striatum and cortex, while Wnt signaling promotes the survival of differentiated cells. Furthermore, in the present work we documented that Wnt signaling inhibition results in the abundance of GFAP in the SVZ, while, conversely, Wnt pathway hyper-activation leads to overexpression of PCNA and DCX in CTRL mice. This finding corresponds well with the data obtained from neonatal animals, where Wnt signaling activation promoted neurogenesis at the expense of gliogenesis (Figures 24 and 25). The neurogenic effect of the Wnt pathway was seconded also by others (Kase et al., 2019; Mastrodonato et al., 2018).

Wnt signaling in adult NS/PCs influenced also their membrane properties, while its manipulation resulted in complex changes in their passive membrane properties as well as in the expression of K^+ channels. We identified three distinct cell types and characterized their expression of voltage-dependent K^+ channels, which were manifested as distinct combinations of K^+ currents, and their different cell densities. Our data accord with other authors that also measured electrophysiological properties of these cell types. For example, we identified DCX/MAP2-positive neuron-like cells that showed highest K_A and K_{DR} current densities (Tables 9 and 10) which were comparable with previous studies from our laboratory (Prajerova et al., 2010b). Moreover, we characterized GFAP-positive astrocytes with only very low densities of K^+ currents (Tables 5 and 6), and PDGFαR-positive precursors that were defined by moderate values of K_A, K_{DR}, and K_{IR}, with sporadic expression of voltage-gated Na^+ channels (Tables 7 and 8). Similar membrane properties were observed and discussed also by others (Walz, 2000). Additionally, we identified significant changes in the density of Na^+ currents of neuron-like cells only in CTRL mice. The inability to detect any significant changes in the cultures derived from MCAO mice could be caused by overall decreased expression of voltage-dependent Na^+ channels after ischemia (Yao et al., 2002). However, another group identified exactly opposite effects of ischemia on ion channels expression (Hernandez-Encarnacion et al., 2017). Regardless of the downregulation or upregulation, the effect of ischemic injury could overwhelm the effect of Wnt signaling in our model.

All in all, canonical Wnt signaling has a specific impact also on the differentiation potential of NS/PCs in adult mice. Nevertheless, our data suggest that it takes effect to a greater extent in cells affected by ischemia. As in some of our experiments we were not able to distinguish NS/PCs from other cell types in the SVZ and the surrounding nervous

tissue, this study would probably deserve a deeper molecular analysis of intra- and extracellular processes specifically in this cell type. For example, utilizing the state-of-the-art approaches such as RNA sequencing (RNA-Seq) could afford another view on the brain cells affected by Wnt signaling manipulation or by ischemia. Another strategy could be employing single-cell RT-qPCR analysis on FACS-sorted cells isolated from the SVZ. However, it is arduous to find a set of high-quality, working fluorescent antibodies against NS/PCs. This issue could be overcome by a method, in which a researcher pulls the cells after patch-clamp measurement out of the tissue for further single-cell RT-qPCR analysis. However, this method would be challenging and time-consuming since our study comprised many experimental groups of cells. This is the reason why the method of our choice was to use tissue specimens.

It seems that, at least in our hands, ageing takes its toll on the regenerative potential of NS/PCs since in adult mice, the differentiation potential of these cells was reduced to that extent that we were not able to identify any changes in the cell incidence caused by Wnt signaling manipulation. In our experiments, we analyzed the effect of ischemia only as a catalyst, modulator of Wnt-signaling-dependent alterations. As it can be seen in the immunohistochemical stainings of the SVZ (Figure 34), the expression of all studied proteins was elevated after MCAO. For this reason, we assessed the effect of Wnt signaling in CTRL mice and, in a similar way, the effect of Wnt signaling in MCAO mice, while keeping the controls for all the experimental groups.

Researchers as well as clinicians have high hopes for postnatal endogenous NS/PCs, or for induced pluripotent stem cells (iPSC), to be utilized in regenerative medicine after decline in numbers of neural cells caused by ischemia, traumatic injury, or neurodegenerative diseases. Hopefully, our findings add to the knowledge of the processes that are necessary for the proper guidance of stem cells to the desired cell types.

5.3 Differentiation potential of NG2 glia

In the experiments on NG2 cells, we employed the fate-mapping analysis, tracking the fluorescence of Tom-positive polydendrocytes and their progeny. Here we utilized the single-cell RT-qPCR analysis, supplemented with immunohistochemical staining and electrophysiological recordings, to assess the influence of cellular signaling pathways as well as ischemia on the differentiation potential of NG2 glia. To induce ischemia, we used the MCAO model in 3-month-old mice. This model of FCI in rodents is well

established and highly reproducible, as it was reported that in ~80% of animals, the cerebral cortex is affected (Ginsberg, 2003). Nevertheless, our own experience says that the infarct lesion in the cortical region occurs more frequently, in more than 90% of cases (data not shown). To evaluate the impact of the progression of ischemic injury, we collected tissue after three, seven, and fourteen days upon its induction. The tissue was isolated from the cortex surrounding the ischemic lesion, the site where the penumbra occurs.

At the beginning, we looked into the NG2 cells differentiation under physiological conditions and detected three Tom-positive populations – pericytes, oligodendrocytes, and NG2 glia. Pericytes were identified because of their relatively high expression of NG2 proteoglycan (Smyth et al., 2018). In later phases of brain injury, these cells are essential for tissue scarring, blood–brain barrier (BBB) repair, and angiogenesis in the CNS. However, as they do not belong to the oligodendroglial lineage, they were excluded from further analyses. This was possible due to their expression of *Pdgfrb* (Roth et al., 2019; Zehendner et al., 2015). The presence of the other two populations clearly confirmed that NG2 cells are oligodendrocyte precursor cells (Figures 36 and 37), which has already been shown (Butt et al., 2019; Chen et al., 2018). Besides the markers typical of individual cell types, we assessed also several other genes. Among others, we detected higher expression of astroglial *Slc1a2* and *Slc1a3* in NG2 cells and, conversely, higher levels of *Glul* in oligodendrocytes. Similar expression patterns were also observed by others (Marques et al., 2016; Zhang et al., 2014b; Liu et al., 2013). The presence of glutamate transporters was found to support oligodendrocyte maturation (Martinez-Lozada et al., 2014), while GS in myelinating cells may regulate cell differentiation and promote myelination (Saitoh and Araki, 2010). Furthermore, we identified components of the canonical Wnt signaling pathway in Tom-positive cells. *Axin2* was expressed predominantly by NG2 cells, while no levels of *Lrp5* were identified in oligodendrocytes. This corresponds well with the finding that Wnt signaling regulates the differentiation of OPCs to oligodendrocytes, as well as their subsequent maturation (Guo et al., 2015). It was suggested that the Wnt pathway inhibits the development of oligodendrocytes in the spinal cord, as it prevents OPCs from differentiation to immature oligodendrocytes (Shimizu et al., 2005). Another study showed that active Wnt signaling inhibits the differentiation of OPCs and delays oligodendrocyte development *in vivo*, while it does not interfere with OPCs proliferation (Feigenson et al., 2009). On the contrary, inhibition

of Wnt signaling by dnLRP6 co-receptor resulted in hypomyelination in another *in vivo* study; however, this study was conducted in zebrafish embryos (Tawk et al., 2011).

Brain ischemia triggered the expanded differentiation potential of NG2 cells. After MCAO, we identified together four distinct Tom-positive cell subpopulations – BF-, OL-, A-, and P-NG2 cells (Figures 38 and 39), while the heterogeneity of NG2 cells after FCI was supported by the immunohistochemical analysis (Figure 40). The BF-NG2 cells subpopulation resembled NG2 cells identified in CTRL mice, while OL-NG2 cells expressed oligodendrocyte-commited genes. Moreover, mRNA of *Tcf7l2* gene, encoding the Wnt-associated transcription factor Tcf4, was identified in all cells of this subpopulation. This finding is quite surprising and unexpected as we mentioned earlier that Wnt signaling probably hinders the differentiation of OPCs to oligodendrocytes (Shimizu et al., 2005). As a consequence, its components should not be present in OL-NG2 cells, at least not in all cells. Nevertheless, this discrepancy can be also found in the literature, showing that it is still not well established whether *Tcf7l2* is more highly expressed in NG2 cells or in differentiated oligodendrocytes during distinct developmental stages. For example, one work showed that *Tcf7l2* is expressed in OPCs, but not in mature oligodendrocytes (Fancy et al., 2009), while another publication from the same group revealed the presence of this transcription factor in a subpopulation of oligodendrocytes (Fancy et al., 2011). These incompatible results might lead to a hypothesis that Tcf4 has also another role in oligodendroglial lineage cells. This idea can be supported by the fact that its role in the Wnt signaling relay can adapt another protein called B cell lymphoma 9 (BCL9), which is highly expressed in tumors (Takada et al., 2012). Moreover, the impact of FCI may be another explanation of the the ubiquitous expression of *Tcf7l2* in OL-NG2 cells. This opinion is based on the findings that OPCs transplanted after MCAO promoted neurological recovery via increased β-catenin expression (Wang et al., 2020) and that *Tcf4* was not detected in normal adult white matter, but it was found after artificially induced demyelination in the mouse CNS (Fancy et al., 2009).

The subpopulation defined by high expression of *Mki67*, *Nes*, *Vim*, and *Pcna* was formed by P-NG2 cells. This cell type typically arises after FCI (Honsa et al., 2012; Anderova et al., 2011), which was probably also the case in our experiments on NS/PCs in MCAO mice (Figures 32 and 34). It is worth mentioning that a large proportion of these cells expressed *Ptch1* and *Smo*. Overall spread expression of these genes in the subpopulation may result from the need to rapidly replace lost oligodendrocytes after

ischemic injury, since the Shh pathway was identified as an essential factor for oligodendrocyte lineage development (Shimizu et al., 2005).

The A-NG2 cells subpopulation was characterized by the highest levels of *Gfap* mRNA, while this gene was here expressed also by the highest proportion of cells among all Tom-positive subpopulations. Such expression pattern is a hallmark of reactive astrocytes (Hara et al., 2017), confirming thus that NG2 cells are able to differentiate to reactive astrocytes after a CNS insult (Honsa et al., 2012; Zhao et al., 2009). Nevertheless, their differentiation to GFAP-positive cells strongly depends on the nature of the injury and the ontogenetic stage (Dimou and Gallo, 2015). Additionally, we examined whether NG2 glia give rise to GFAP-positive cells by symmetric or asymmetric division, and found out that both processes occur in the ischemic CNS. This result is concomitant with the findings of Boda et al. (2015), who furthermore revealed that both intrinsic and extrinsic factors influence the heterogeneity of daughter cells.

The distribution of the four Tom-positive NG2-glia-derived subpopulations was unequal at different time points after MCAO (Figure 39C). Three days after FCI, P- and A-NG2 cells reached their maximal incidence, while OL-NG2 cells were most abundant later, seven days after FCI. The BF-NG2 cells subpopulation became prevalent two weeks after MCAO. Tamoxifen administration just after the induction of FCI resulted in dominant P-NG2 cells three days after MCAO, while no A-NG2 cells were detected. Such a steep rise in the counts of P-NG2 cells in the early phases of ischemia was observed also by Honsa et al. (2012), and could signify the need for subsequent prompt glial scarring by A-NG2 cells to prevent ischemia-associated detrimental factors from entering the spared penumbral regions. The transition from P-NG2 cells to their A-NG2 counterparts may be regulated by Shh. This hypothesis stems from our observation that the expression of Shh components was found predominantly in P-NG2 cells, and from the work of others, localizing this pathway specifically to astrocytes under physiological as well as pathophysiological conditions (Ugbode et al., 2017).

For this reason, we utilized the very same transgenic mouse strain in the following *in vitro* and *in vivo* experiments, where we analyzed the effect of Shh signaling on the differentiation potential of Tom-positive NG2 glia after FCI. We observed increased numbers of reactive astrocytes after Shh signaling activation, while its inhibition resulted in the reverse effect.

Previously, it was reported that following severe brain injury, Shh has a key role in the signaling among reactive glia and is probably responsible for their multipotency

(Sirko et al., 2013). Interestingly, this ligand is under physiological conditions released by neurons and maintains the non-reactive phenotypes of astrocytes (Garcia et al., 2010). Nevertheless, following injury to the cerebral cortex, it is reactive astrocytes what produces Shh, while astrocytic Shh probably promotes NG2 proliferation and the transition into, and maintenance of, the reactive status (Amankulor et al., 2009). To investigate the effect of Shh signaling in more detail, we first analyzed NG2 cells under physiological conditions *in vitro*. We observed that the majority of Tom-positive cells were NG2-positive (Figure 42A, B), while we also identified a relatively large population of oligodendrocytes and a small proportion of GFAP-positive cells (Figure 42A, E). After ischemia, the number of NG2 cells decreased, while the counts of GFAP-positive cells increased (Figure 42A, C, F). In the spinal cord, the effect of injury was similar, as enhanced proliferation of precursor cells was accompanied with higher incidence of GFAP-positive cells. Only a very few astrocytes in the cultures from uninjured animals were observed, while increased numbers of GFAP-positive cells were identified after spinal cord injury as well as after longer *in vitro* cultivation (Yoo and Wrathall, 2007). The Shh blocker Cyc increased the numbers of NG2 cells and, at the same time, the counts of astrocytes decreased (Figure 42A,). Conversely, the activator Shh enhanced differentiation to GFAP-positive cells; however, the proportion of NG2 cells remained the same, unlike after ischemia, which could indicate a more complex role of ischemic injury, perhaps due to some factors present at the site of injury. This could be manifested by the treatment of OPCs with neuroinflammatory interferon γ, which led to downregulation of PDGFαR and to the simultaneous increased generation of GFAP-positive astrocytes from NG2 cells (Tanner et al., 2011). The blocker Cyc suppressed the effect of Shh. The activator SAG had a similar effect on the differentiation as Shh (Figure 42A, D, and G).

Next, we detected five Tom-positive subpopulations in our CTRL cultures. These populations were distinguished by their specific membrane properties (Table 11) and markers (Figure 43). We detected NG2 cells, astrocytes, oligodendrocytes, pericytes, and neuroblasts (or immature neurons). Their incidence was affected by ischemia and Shh signaling manipulation, while it copied the trends from our immunochemical analyses.

The analysis of mRNA levels in Tom-positive cells revealed higher expression of *Ki67*, *Gfap*, *Dcx*, and *Smo* after FCI, mainly three and seven days after its induction (Figure 44B). These results might again signify that ischemia has its role in proliferation and differentiation of NG2 cells. Increased proliferation of NG2 cells after FCI was observed also in our previous experiments (Figure 39), where we also indicated, based on

elevated levels of *Gfap*, that this cell type may serve as a source for reactive astrocytes (Figures 39 and 41), while others reported a shortened cell cycle in NG2 cells also after stab wound injury (Simon et al., 2011). Moreover, the increase in *Smo* expression can indicate a role of Shh signaling in the process of polydendrocyte-to-reactive-astrocyte transition. Higher *Smo* expression was confirmed also after cortical stab wound injury (Sirko et al., 2013). Next, we assessed the effect of Shh signaling on polydendrocytes *in vivo*. Our belief that Shh influences differentiation of polydendrocytes preferentially to reactive astrocytes was nourished also in these experiments, while its role in proliferation of NG2 glia was rejected (Figures 45 and 46). The application of SAG to the injured cortex resulted in higher counts of astrocytes also in another study (Sirko et al., 2013). Moreover, Shh signaling was identified as a factor responsible for proliferation of NS/PCs and DCX-positive cells; nevertheless, its effect on NG2 cells after traumatic brain injury was null (Mierzwa et al., 2014). This was supported by our BrdU assay that revealed no Shh-signaling-induced cell proliferation in ischemic tissue (Figure 46E, F). Finally, in our studies on NG2 cells, we failed to identify mature neuronal cells. This is in agreement with some other studies (Kang et al., 2010), while there is also evidence of development to neurons (Geha et al., 2010). This may indicate that NG2 cells are void of the ability to generate this cell type, or that a synergic effect of more factors that normally do not coincide *in vivo* is required to promote the neurogenic potential of NG2 cells (Heinrich et al., 2014).

Taken together, we documented that the generation of reactive astrocytes from NG2 cells is regulated by Shh signaling. Since reactive astrocytes form the glial scar, Shh may shape its composition and thus have a beneficial impact on the extent of ischemic injury as well as on the resulting consequences.

6 CONCLUSIONS

In the present work, we assessed the differentiation potential of NS/PCs and NG2 glia. To follow the fate of these precursor cells under various conditions, we employed transgenic mice and took advantage of several laboratory methods that helped us identify changes at the mRNA, protein, or functional level.

First, we analyzed the impact of Wnt signaling manipulation on differentiation of NS/PCs derived from neonatal mice. Since Wnt signaling was manipulated in each of the mouse strains slightly differently and evaluating its effect at several points of the signaling relay would give us a better insight into the possible molecular mechanisms underlying NS/PCs differentiation, we could not exclude any of them from further experiments (Hypothesis 1, Aim 1). Furthermore, our results showed that canonical Wnt signaling affects the fate of neonatal NS/PCs, as it influenced the incidence of distinct cell types differentiated from NS/PCs, as well as their electrophysiological properties. We concluded that Wnt signaling in neonatal mice promotes neurogenesis at the expense of gliogenesis (Hypothesis 1, Aim 2).

Next, we assessed NS/PCs isolated from the adult mouse brain and found out that under physiological conditions, the Wnt/β-catenin pathway influences differentiation of these cells to a lesser extent as we failed to detect any changes in the cell incidence. Nevertheless, we observed alterations in the expression of cell-type-specific proteins (Hypothesis 1, Aim 2). On the other hand, the effect of Wnt signaling was stronger after the induction of FCI. The alterations in the incidence of distinct cell types resembled the changes we identified in neonatal mice, while the effect of the Wnt pathway was particularly evident in Dkk1 mice. Our immunohistochemical analysis revealed overall higher expression of cell-type-specific markers after MCAO, together with the abundance of proliferating and neuron-like precursors after Wnt signaling hyper-activation (Hypothesis 2, Aim 3).

Finally, we evaluated the differentiation potential of NG2 glia and confirmed that under physiological conditions, they give rise predominantly to oligodendrocytes, and that this transition is probably inhibited by Wnt signaling. However, after the induction of ischemia, NG2 cells started to proliferate and acquired a multipotent phenotype. As a result, they differentiated mainly to astrocytes and oligodendrocytes. Moreover, we found that the generation of reactive astrocytes from NG2 glia is regulated by Shh signaling (Hypothesis 3, Aim 4).

Taken together, cellular signaling pathways have a substantial impact on the fate of neural precursor cells in the postnatal mouse brain. In healthy tissue, they exert their functions in proliferation and differentiation. Additionally, ischemic injury also affects the differentiation potential of NS/PCs and NG2 cells, as it induces their multipotency. All these findings might be helpful in developing new strategies for therapy of the diseased CNS.

7 REFERENCES

Adachi K, Mirzadeh Z, Sakaguchi M, Yamashita T, Nikolcheva T, Gotoh Y, Peltz G, Gong L, Kawase T, Alvarez-Buylla A, Okano H, Sawamoto K. (2007) Beta-catenin signaling promotes proliferation of progenitor cells in the adult mouse subventricular zone. Stem Cells. 2007 Nov;25(11):2827-36. Epub 2007 Aug 2.

Aguirre AA, Chittajallu R, Belachew S, Gallo V. (2004) NG2-expressing cells in the subventricular zone are type C-like cells and contribute to interneuron generation in the postnatal hippocampus. J Cell Biol. 2004 May 24;165(4):575-89.

Aguirre A and Gallo V. (2004) Postnatal neurogenesis and gliogenesis in the olfactory bulb from NG2-expressing progenitors of the subventricular zone. J Neurosci. 2004 Nov 17;24(46):10530-41.

Altman J and Das GD. (1965) Autoradiographic and histological evidence of postnatal hippocampal neurogenesis in rats. J Comp Neurol. 1965 Jun;124(3):319-35.

Alvarez AR, Godoy JA, Mullendorff K, Olivares GH, Bronfman M, Inestrosa NC. (2004) Wnt-3a overcomes beta-amyloid toxicity in rat hippocampal neurons. Exp Cell Res. 2004 Jul 1;297(1):186-96.

Amankulor NM, Hambardzumyan D, Pyonteck SM, Becher OJ, Joyce JA, Holland EC. (2009) Sonic hedgehog pathway activation is induced by acute brain injury and regulated by injury-related inflammation. J Neurosci. 2009 Aug 19;29(33):10299-308. doi: 10.1523/JNEUROSCI.2500-09.2009.

Anderová M, Kubinová S, Jelitai M, Neprasová H, Glogarová K, Prajerová I, Urdzíková L, Chvátal A, Syková E. (2006) Transplantation of embryonic neuroectodermal progenitor cells into the site of a photochemical lesion: immunohistochemical and electrophysiological analysis. J Neurobiol. 2006 Sep 1;66(10):1084-100.

Anderova M, Vorisek I, Pivonkova H, Benesova J, Vargova L, Cicanic M, Chvatal A, Sykova E. (2011) Cell death/proliferation and alterations in glial morphology contribute to changes in diffusivity in the rat hippocampus after hypoxia-ischemia. J Cereb Blood Flow Metab. 2011 Mar;31(3):894-907. doi: 10.1038/jcbfm.2010.168. Epub 2010 Sep 29.

Anderson J, Patel M, Forenzo D, Ai X, Cai C, Wade Q, Risman R, Cai L. (2020) A novel mouse model for the study of endogenous neural stem and progenitor cells after traumatic brain injury. Exp Neurol. 2020 Mar;325:113119. doi: 10.1016/j.expneurol.2019.113119. Epub 2019 Nov 18.

Androutsellis-Theotokis A, Leker RR, Soldner F, Hoeppner DJ, Ravin R, Poser SW, Rueger MA, Bae SK, Kittappa R, McKay RD. (2006) Notch signalling regulates stem cell numbers in vitro and in vivo. Nature. 2006 Aug 17;442(7104):823-6. Epub 2006 Jun 25.

Baron JC. (2001) Perfusion thresholds in human cerebral ischemia: historical perspective and therapeutic implications. Cerebrovasc Dis. 2001;11 Suppl 1:2-8.

Belachew S, Chittajallu R, Aguirre AA, Yuan X, Kirby M, Anderson S, Gallo V. (2003) Postnatal NG2 proteoglycan-expressing progenitor cells are intrinsically multipotent and generate functional neurons. J Cell Biol. 2003 Apr 14;161(1):169-86. Epub 2003 Apr 7.

Belov Kirdajova D, Kriska J, Tureckova J, Anderova M. (2020) Ischemia-triggered glutamate excitotoxicity from the perspective of glial cells. Front Cell Neurosci. 2020 Mar 19;14(51):1-27. doi: 10.3389/fncel.2020.00051.

Bergles DE, Roberts JD, Somogyi P, Jahr CE. (2000) Glutamatergic synapses on oligodendrocyte precursor cells in the hippocampus. Nature. 2000 May 11;405(6783):187-91.

Bergmann O, Liebl J, Bernard S, Alkass K, Yeung MS, Steier P, Kutschera W, Johnson L, Landén M, Druid H, Spalding KL, Frisén J. (2012) The age of olfactory bulb neurons in humans. Neuron. 2012 May 24;74(4):634-9. doi: 10.1016/j.neuron.2012.03.030.

Bizen N, Inoue T, Shimizu T, Tabu K, Kagawa T, Taga T. (2014) A growth-promoting signaling component cyclin D1 in neural stem cells has antiastrogliogenic function to execute self-renewal. Stem Cells. 2014 Jun;32(6):1602-15. doi: 10.1002/stem.1613.

Boda E, Di Maria S, Rosa P, Taylor V, Abbracchio MP, Buffo A. (2015) Early phenotypic asymmetry of sister oligodendrocyte progenitor cells after mitosis and its modulation by aging and extrinsic factors. Glia. 2015 Feb;63(2):271-86. doi: 10.1002/glia.22750. Epub 2014 Sep 12.

Boehme AK, Esenwa C1, Elkind MS. (2017) Stroke Risk Factors, Genetics, and Prevention. Circ Res. 2017 Feb 3;120(3):472-495. doi: 10.1161/CIRCRESAHA.116.308398.

Bonfanti E, Gelosa P, Fumagalli M, Dimou L, Viganò F, Tremoli E, Cimino M, Sironi L, Abbracchio MP. (2017) The role of oligodendrocyte precursor cells expressing the GPR17 receptor in brain remodeling after stroke. Cell Death Dis. 2017 Jun 8;8(6):e2871. doi: 10.1038/cddis.2017.256.

Bonnert TP, Bilsland JG, Guest PC, Heavens R, McLaren D, Dale C, Thakur M, McAllister G, Munoz-Sanjuan I. (2006) Molecular characterization of adult mouse subventricular zone progenitor cells during the onset of differentiation. Eur J Neurosci. 2006 Aug;24(3):661-75.

Borday C, Parain K, Thi Tran H, Vleminckx K, Perron M, Monsoro-Burq AH. (2018) An atlas of Wnt activity during embryogenesis in Xenopus tropicalis. PLoS One. 2018 Apr 19;13(4):e0193606. doi: 10.1371/journal.pone.0193606. eCollection 2018.

Boshans LL, Factor DC, Singh V, Liu J, Zhao C, Mandoiu I, Lu QR, Casaccia P, Tesar PJ, Nishiyama A. (2019) The Chromatin Environment Around Interneuron Genes in Oligodendrocyte Precursor Cells and Their Potential for Interneuron Reprograming. Front Neurosci. 2019 Aug 8;13:829. doi: 10.3389/fnins.2019.00829. eCollection 2019.

Bowman AN, van Amerongen R, Palmer TD, Nusse R. (2013) Lineage tracing with Axin2 reveals distinct developmental and adult populations of Wnt/β-catenin-responsive neural stem

cells. Proc Natl Acad Sci U S A. 2013 Apr 30;110(18):7324-9. doi: 10.1073/pnas.1305411110. Epub 2013 Apr 15.

Brault V, Moore R, Kutsch S, Ishibashi M, Rowitch DH, McMahon AP, Sommer L, Boussadia O, Kemler R. (2001) Inactivation of the beta-catenin gene by Wnt1-Cre-mediated deletion results in dramatic brain malformation and failure of craniofacial development. Development. 2001 Apr;128(8):1253-64.

Brown DL, Feskanich D, Sánchez BN, Rexrode KM, Schernhammer ES, Lisabeth LD. (2009) Rotating night shift work and the risk of ischemic stroke. Am J Epidemiol. 2009 Jun 1;169(11):1370-7. doi: 10.1093/aje/kwp056. Epub 2009 Apr 8.

Bu J, Banki A, Wu Q, Nishiyama A. (2004) Increased NG2(+) glial cell proliferation and oligodendrocyte generation in the hypomyelinating mutant shiverer. Glia. 2004 Oct;48(1):51-63.

Butt AM, Papanikolaou M, Rivera A. (2019) Physiology of Oligodendroglia. Adv Exp Med Biol. 2019;1175:117-128. doi: 10.1007/978-981-13-9913-8_5.

Butti E, Bacigaluppi M, Chaabane L, Ruffini F, Brambilla E, Berera G, Montonati C, Quattrini A, Martino G. (2019) Neural Stem Cells of the Subventricular Zone Contribute to Neuroprotection of the Corpus Callosum after Cuprizone-Induced Demyelination. J Neurosci. 2019 Jul 10;39(28):5481-5492. doi: 10.1523/JNEUROSCI.0227-18.2019. Epub 2019 May 28.

Buttitta L, Tanaka TS, Chen AE, Ko MS, Fan CM. (2003) Microarray analysis of somitogenesis reveals novel targets of different WNT signaling pathways in the somitic mesoderm. Dev Biol. 2003 Jun 1;258(1):91-104.

Callejo A, Quijada L, Guerrero I. (2007) Detecting tagged Hedgehog with intracellular and extracellular immunocytochemistry for functional analysis. Methods Mol Biol. 2007;397:91-103.

Caltana L, Merelli A, Lazarowski A, Brusco A. (2009) Neuronal and glial alterations due to focal cortical hypoxia induced by direct cobalt chloride (CoCl2) brain injection. Neurotox Res. 2009 May;15(4):348-58. doi: 10.1007/s12640-009-9038-9. Epub 2009 Mar 20.

Calver AR, Hall AC, Yu WP, Walsh FS, Heath JK, Betsholtz C, Richardson WD. (1998) Oligodendrocyte population dynamics and the role of PDGF in vivo. Neuron. 1998 May;20(5):869-82.

Carballo GB, Honorato JR, de Lopes GPF, Spohr TCLSE. (2018) A highlight on Sonic hedgehog pathway. Cell Commun Signal. 2018 Mar 20;16(1):11. doi: 10.1186/s12964-018-0220-7.

Chen JK, Taipale J, Cooper MK, Beachy PA. (2002) Inhibition of Hedgehog signaling by direct binding of cyclopamine to Smoothened. Genes Dev. 2002 Nov 1;16(21):2743-8.

Chen M, Tian S, Yang X, Lane AP, Reed RR, Liu H. (2014) Wnt-responsive Lgr5$^+$ globose basal cells function as multipotent olfactory epithelium progenitor cells. J Neurosci. 2014 Jun 11;34(24):8268-76. doi: 10.1523/JNEUROSCI.0240-14.2014.

Chen TJ, Kula B, Nagy B, Barzan R, Gall A, Ehrlich I, Kukley M. (2018) In Vivo Regulation of Oligodendrocyte Precursor Cell Proliferation and Differentiation by the AMPA-Receptor Subunit GluA2. Cell Rep. 2018 Oct 23;25(4):852-861.e7. doi: 10.1016/j.celrep.2018.09.066.

Chen Z, Venkatesan AM, Dehnhardt CM, Dos Santos O, Delos Santos E, Ayral-Kaloustian S, Chen L, Geng Y, Arndt KT, Lucas J, Chaudhary I, Mansour TS. (2009) 2,4-Diamino-quinazolines as inhibitors of beta-catenin/Tcf-4 pathway: Potential treatment for colorectal cancer. Bioorg Med Chem Lett. 2009 Sep 1;19(17):4980-3. doi: 10.1016/j.bmcl.2009.07.070. Epub 2009 Jul 17.

Chenn A and Walsh CA. (2002) Regulation of cerebral cortical size by control of cell cycle exit in neural precursors. Science. 2002 Jul 19;297(5580):365-9.

Chittajallu R, Aguirre A, Gallo V. (2004) NG2-positive cells in the mouse white and grey matter display distinct physiological properties. J Physiol. 2004 Nov 15;561(Pt 1):109-22. Epub 2004 Sep 9.

Chodelkova O, Masek J, Korinek V, Kozmik Z, Machon O. (2018) Tcf7L2 is essential for neurogenesis in the developing mouse neocortex. Neural Dev. 2018 May 11;13(1):8. doi: 10.1186/s13064-018-0107-8.

Clevers H, Loh KM, Nusse R. (2014) Stem cell signaling. An integral program for tissue renewal and regeneration: Wnt signaling and stem cell control. Science. 2014 Oct 3;346(6205):1248012. doi: 10.1126/science.1248012. Epub 2014 Oct 2.

Codega P, Silva-Vargas V, Paul A, Maldonado-Soto AR, Deleo AM, Pastrana E, Doetsch F. (2014) Prospective identification and purification of quiescent adult neural stem cells from their in vivo niche. Neuron. 2014 May 7;82(3):545-59. doi: 10.1016/j.neuron.2014.02.039.

Coletti AM, Singh D, Kumar S, Shafin TN, Briody PJ, Babbitt BF, Pan D, Norton ES, Brown EC, Kahle KT, Del Bigio MR, Conover JC. (2018) Characterization of the ventricular-subventricular stem cell niche during human brain development. Development. 2018 Oct 26;145(20). pii: dev170100. doi: 10.1242/dev.170100.

Cui XP, Xing Y, Chen JM, Dong SW, Ying DJ, Yew DT. (2011) Wnt/beta-catenin is involved in the proliferation of hippocampal neural stem cells induced by hypoxia. Ir J Med Sci. 2011 Jun;180(2):387-93. doi: 10.1007/s11845-010-0566-3. Epub 2010 Sep 2.

Dawson MR, Levine JM, Reynolds R. (2000) NG2-expressing cells in the central nervous system: are they oligodendroglial progenitors? J Neurosci Res. 2000 Sep 1;61(5):471-9.

Dawson MR, Polito A, Levine JM, Reynolds R. (2003) NG2-expressing glial progenitor cells: an abundant and widespread population of cycling cells in the adult rat CNS. Mol Cell Neurosci. 2003 Oct;24(2):476-88.

Deisseroth K, Singla S, Toda H, Monje M, Palmer TD, Malenka RC. (2004) Excitation-neurogenesis coupling in adult neural stem/progenitor cells. Neuron. 2004 May 27;42(4):535-52.

Dimou L and Gallo V. (2015) NG2-glia and their functions in the central nervous system. Glia. 2015 Aug;63(8):1429-51. doi: 10.1002/glia.22859. Epub 2015 May 24.

Doetsch F. (2003) The glial identity of neural stem cells. Nat Neurosci. 2003 Nov;6(11):1127-34. Epub 2003 Oct 28.

Doetsch F, Caillé I, Lim DA, García-Verdugo JM, Alvarez-Buylla A. (1999) Subventricular zone astrocytes are neural stem cells in the adult mammalian brain. Cell. 1999 Jun 11;97(6):703-16.

Doubravska L, Krausova M, Gradl D, Vojtechova M, Tumova L, Lukas J, Valenta T, Pospichalova V, Fafilek B, Plachy J, Sebesta O, Korinek V. (2011) Fatty acid modification of Wnt1 and Wnt3a at serine is prerequisite for lipidation at cysteine and is essential for Wnt signalling. Cell Signal. 2011 May;23(5):837-48. doi: 10.1016/j.cellsig.2011.01.007. Epub 2011 Jan 16.

Doyle KP, Simon RP, Stenzel-Poore MP. (2008) Mechanisms of ischemic brain damage. Neuropharmacology. 2008 Sep;55(3):310-8. doi: 10.1016/j.neuropharm.2008.01.005. Epub 2008 Jan 25.

Du XY, Zhu XD, Dong G, Lu J, Wang Y, Zeng L, Zhao TY, Ye HH, Li RS, Bai JY, Chen ZW. (2011) Characteristics of circle of Willis variations in the mongolian gerbil and a newly established ischemia-prone gerbil group. ILAR J. 2011;52(1):E1-7.

Encinas JM, Michurina TV, Peunova N, Park JH, Tordo J, Peterson DA, Fishell G, Koulakov A, Enikolopov G. (2011) Division-coupled astrocytic differentiation and age-related depletion of neural stem cells in the adult hippocampus. Cell Stem Cell. 2011 May 6;8(5):566-79. doi: 10.1016/j.stem.2011.03.010.

Ernst A, Alkass K, Bernard S, Salehpour M, Perl S, Tisdale J, Possnert G, Druid H, Frisén J. (2014) Neurogenesis in the striatum of the adult human brain. Cell. 2014 Feb 27;156(5):1072-83. doi: 10.1016/j.cell.2014.01.044. Epub 2014 Feb 20.

Etherton MR, Wu O, Cougo P, Giese AK, Cloonan L, Fitzpatrick KM, Kanakis AS, Boulouis G, Karadeli HH, Lauer A, Rosand J, Furie KL, Rost NS. (2017) Structural Integrity of Normal Appearing White Matter and Sex-Specific Outcomes After Acute Ischemic Stroke. Stroke. 2017 Dec;48(12):3387-3389. doi: 10.1161/STROKEAHA.117.019258. Epub 2017 Nov 10.

Fafilek B, Krausova M, Vojtechova M, Pospichalova V, Tumova L, Sloncova E, Huranova M, Stancikova J, Hlavata A, Svec J, Sedlacek R, Luksan O, Oliverius M, Voska L, Jirsa M, Paces J, Kolar M, Krivjanska M, Klimesova K, Tlaskalova-Hogenova H, Korinek V. (2013) Troy, a tumor necrosis factor receptor family member, interacts with lgr5 to inhibit wnt signaling in intestinal stem cells. Gastroenterology. 2013 Feb;144(2):381-91. doi: 10.1053/j.gastro.2012.10.048. Epub 2012 Nov 7.

Fancy SP, Baranzini SE, Zhao C, Yuk DI, Irvine KA, Kaing S, Sanai N, Franklin RJ, Rowitch DH. (2009) Dysregulation of the Wnt pathway inhibits timely myelination and remyelination in the mammalian CNS. Genes Dev. 2009 Jul 1;23(13):1571-85. doi: 10.1101/gad.1806309. Epub 2009 Jun 10.

Fancy SP, Harrington EP, Yuen TJ, Silbereis JC, Zhao C, Baranzini SE, Bruce CC, Otero JJ, Huang EJ, Nusse R, Franklin RJ, Rowitch DH. (2011) Axin2 as regulatory and therapeutic target in newborn brain injury and remyelination. Nat Neurosci. 2011 Jun 26;14(8):1009-16. doi: 10.1038/nn.2855.

Feigenson K, Reid M, See J, Crenshaw EB 3rd, Grinspan JB. (2009) Wnt signaling is sufficient to perturb oligodendrocyte maturation. Mol Cell Neurosci. 2009 Nov;42(3):255-65. doi: 10.1016/j.mcn.2009.07.010. Epub 2009 Jul 18.

Fujimura N, Vacik T, Machon O, Vlcek C, Scalabrin S, Speth M, Diep D, Krauss S, Kozmik Z. (2007) Wnt-mediated down-regulation of Sp1 target genes by a transcriptional repressor Sp5. J Biol Chem. 2007 Jan 12;282(2):1225-37. Epub 2006 Nov 6.

Furutachi S, Matsumoto A, Nakayama KI, Gotoh Y. (2013) p57 controls adult neural stem cell quiescence and modulates the pace of lifelong neurogenesis. EMBO J. 2013 Apr 3;32(7):970-81. doi: 10.1038/emboj.2013.50. Epub 2013 Mar 12.

Gage FH, Coates PW, Palmer TD, Kuhn HG, Fisher LJ, Suhonen JO, Peterson DA, Suhr ST, Ray J. (1995) Survival and differentiation of adult neuronal progenitor cells transplanted to the adult brain. Proc Natl Acad Sci U S A. 1995 Dec 5;92(25):11879-83.

Garcia AD, Petrova R, Eng L, Joyner AL. (2010) Sonic hedgehog regulates discrete populations of astrocytes in the adult mouse forebrain. J Neurosci. 2010 Oct 13;30(41):13597-608. doi: 10.1523/JNEUROSCI.0830-10.2010.

Geha S, Pallud J, Junier MP, Devaux B, Leonard N, Chassoux F, Chneiweiss H, Daumas-Duport C, Varlet P. (2010) NG2+/Olig2+ cells are the major cycle-related cell population of the adult human normal brain. Brain Pathol. 2010 Mar;20(2):399-411. doi: 10.1111/j.1750-3639.2009.00295.x. Epub 2009 May 22.

Gil-Perotín S, Duran-Moreno M, Cebrián-Silla A, Ramírez M, García-Belda P, García-Verdugo JM. (2013) Adult neural stem cells from the subventricular zone: a review of the neurosphere assay. Anat Rec (Hoboken). 2013 Sep;296(9):1435-52. doi: 10.1002/ar.22746. Epub 2013 Jul 31.

Ginsberg MD. (2003) Adventures in the pathophysiology of brain ischemia: penumbra, gene expression, neuroprotection: the 2002 Thomas Willis Lecture. Stroke. 2003 Jan;34(1):214-23.

Glinka A, Wu W, Delius H, Monaghan AP, Blumenstock C, Niehrs C. (1998) Dickkopf-1 is a member of a new family of secreted proteins and functions in head induction. Nature. 1998 Jan 22;391(6665):357-62.

Groves N, O'Keeffe I, Lee W, Toft A, Blackmore D, Bandhavkar S, Coulson EJ, Bartlett PF, Jhaveri DJ. (2019) Blockade of TrkB but not $p75^{NTR}$ activates a subpopulation of quiescent neural precursor cells and enhances neurogenesis in the adult mouse hippocampus. Dev Neurobiol. 2019 Sep;79(9-10):868-879. doi: 10.1002/dneu.22729. Epub 2020 Jan 14.

Guo F, Lang J, Sohn J, Hammond E, Chang M, Pleasure D. (2015) Canonical Wnt signaling in the oligodendroglial lineage--puzzles remain. Glia. 2015 Oct;63(10):1671-93. doi: 10.1002/glia.22813. Epub 2015 Mar 18.

Hamada F, Tomoyasu Y, Takatsu Y, Nakamura M, Nagai S, Suzuki A, Fujita F, Shibuya H, Toyoshima K, Ueno N, Akiyama T. (1999) Negative regulation of Wingless signaling by D-axin, a Drosophila homolog of axin. Science. 1999 Mar 12;283(5408):1739-42.

Hara M, Kobayakawa K, Ohkawa Y, Kumamaru H, Yokota K, Saito T, Kijima K, Yoshizaki S, Harimaya K, Nakashima Y, Okada S. (2017) Interaction of reactive astrocytes with type I collagen induces astrocytic scar formation through the integrin-N-cadherin pathway after spinal cord injury. Nat Med. 2017 Jul;23(7):818-828. doi: 10.1038/nm.4354. Epub 2017 Jun 19.

Harada N, Tamai Y, Ishikawa T, Sauer B, Takaku K, Oshima M, Taketo MM. (1999) Intestinal polyposis in mice with a dominant stable mutation of the beta-catenin gene. EMBO J. 1999 Nov 1;18(21):5931-42.

Harukuni I and Bhardwaj A. (2006) Mechanisms of brain injury after global cerebral ischemia. Neurol Clin. 2006 Feb;24(1):1-21.

Haubensak W, Attardo A, Denk W, Huttner WB. (2004) Neurons arise in the basal neuroepithelium of the early mammalian telencephalon: a major site of neurogenesis. Proc Natl Acad Sci U S A. 2004 Mar 2;101(9):3196-201. Epub 2004 Feb 12.

Heinrich C, Bergami M, Gascón S, Lepier A, Viganò F, Dimou L, Sutor B, Berninger B, Götz M. (2014) Sox2-mediated conversion of NG2 glia into induced neurons in the injured adult cerebral cortex. Stem Cell Reports. 2014 Dec 9;3(6):1000-14. doi: 10.1016/j.stemcr.2014.10.007. Epub 2014 Nov 20.

Heiss WD, Sobesky J, Hesselmann V. (2004) Identifying thresholds for penumbra and irreversible tissue damage. Stroke. 2004 Nov;35(11 Suppl 1):2671-4. Epub 2004 Sep 30.

Hernandez-Encarnacion L, Sharma P, Simon R, Zhou A. (2017) Condition-specific transcriptional regulation of neuronal ion channel genes in brain ischemia. Int J Physiol Pathophysiol Pharmacol. 2017 Dec 25;9(6):192-201. eCollection 2017.

Hinzman JM, DiNapoli VA, Mahoney EJ, Gerhardt GA, Hartings JA. (2015) Spreading depolarizations mediate excitotoxicity in the development of acute cortical lesions. Exp Neurol. 2015 May;267:243-53. doi: 10.1016/j.expneurol.2015.03.014. Epub 2015 Mar 24.

Hirabayashi Y, Itoh Y, Tabata H, Nakajima K, Akiyama T, Masuyama N, Gotoh Y. (2004) The Wnt/beta-catenin pathway directs neuronal differentiation of cortical neural precursor cells. Development. 2004 Jun;131(12):2791-801. Epub 2004 May 13.

Hirsch C, Campano LM, Wöhrle S, Hecht A. (2007) Canonical Wnt signaling transiently stimulates proliferation and enhances neurogenesis in neonatal neural progenitor cultures. Exp Cell Res. 2007 Feb 1;313(3):572-87. Epub 2006 Nov 10.

Ho KS and Scott MP. (2002) Sonic hedgehog in the nervous system: functions, modifications and mechanisms. Curr Opin Neurobiol. 2002 Feb;12(1):57-63.

Honsa P, Pivonkova H, Anderova M. (2013) Focal cerebral ischemia induces the neurogenic potential of mouse Dach1-expressing cells in the dorsal part of the lateral ventricles. Neuroscience. 2013 Jun 14;240:39-53. doi: 10.1016/j.neuroscience.2013.02.048. Epub 2013 Mar 1.

Honsa P, Pivonkova H, Dzamba D, Filipova M, Anderova M. (2012) Polydendrocytes display large lineage plasticity following focal cerebral ischemia. PLoS One. 2012;7(5):e36816. doi: 10.1371/journal.pone.0036816. Epub 2012 May 10.

Honsa P, Valny M, Kriska J, Matuskova H, Harantova L, Kirdajova D, Valihrach L, Androvic P, Kubista M, Anderova M. (2016) Generation of reactive astrocytes from NG2 cells is regulated by sonic hedgehog. Glia. 2016 Sep;64(9):1518-31. doi: 10.1002/glia.23019. Epub 2016 Jun 24.

Hurn PD and Macrae IM. (2000) Estrogen as a neuroprotectant in stroke. J Cereb Blood Flow Metab. 2000 Apr;20(4):631-52.

Husson B, Hertz-Pannier L, Adamsbaum C, Renaud C, Presles E, Dinomais M, Kossorotoff M, Landrieu P, Chabrier S. (2016) MR angiography findings in infants with neonatal arterial ischemic stroke in the middle cerebral artery territory: A prospective study using circle of Willis MR angiography. Eur J Radiol. 2016 Jul;85(7):1329-35. doi: 10.1016/j.ejrad.2016.05.002. Epub 2016 May 6.

Ihrie RA and Alvarez-Buylla A. (2008) Cells in the astroglial lineage are neural stem cells. Cell Tissue Res. 2008 Jan;331(1):179-91. Epub 2007 Sep 5.

Ihrie RA, Shah JK, Harwell CC, Levine JH, Guinto CD, Lezameta M, Kriegstein AR, Alvarez-Buylla A. (2011) Persistent sonic hedgehog signaling in adult brain determines neural stem cell positional identity. Neuron. 2011 Jul 28;71(2):250-62. doi: 10.1016/j.neuron.2011.05.018.

Inestrosa N, De Ferrari GV, Garrido JL, Alvarez A, Olivares GH, Barría MI, Bronfman M, Chacón MA. (2002) Wnt signaling involvement in beta-amyloid-dependent neurodegeneration. Neurochem Int. 2002 Nov;41(5):341-4.

Inestrosa NC and Varela-Nallar L. (2015) Wnt signalling in neuronal differentiation and development. Cell Tissue Res. 2015 Jan;359(1):215-23. doi: 10.1007/s00441-014-1996-4. Epub 2014 Sep 19.

Israsena N, Hu M, Fu W, Kan L, Kessler JA. (2004) The presence of FGF2 signaling determines whether beta-catenin exerts effects on proliferation or neuronal differentiation of neural stem cells. Dev Biol. 2004 Apr 1;268(1):220-31.

Jacobs S, Lie DC, DeCicco KL, Shi Y, DeLuca LM, Gage FH, Evans RM. (2006) Retinoic acid is required early during adult neurogenesis in the dentate gyrus. Proc Natl Acad Sci U S A. 2006 Mar 7;103(10):3902-7. Epub 2006 Feb 27.

Janeckova L, Fafilek B, Krausova M, Horazna M, Vojtechova M, Alberich-Jorda M, Sloncova E, Galuskova K, Sedlacek R, Anderova M, Korinek V. (2016) Wnt Signaling Inhibition Deprives Small Intestinal Stem Cells of Clonogenic Capacity. Genesis. 2016 Mar;54(3):101-14. doi: 10.1002/dvg.22922. Epub 2016 Feb 16.

Jho EH, Zhang T, Domon C, Joo CK, Freund JN, Costantini F. (2002) Wnt/beta-catenin/Tcf signaling induces the transcription of Axin2, a negative regulator of the signaling pathway. Mol Cell Biol. 2002 Feb;22(4):1172-83.

Jiang MQ, Zhao YY, Cao W, Wei ZZ, Gu X, Wei L, Yu SP. (2017) Long-term survival and regeneration of neuronal and vasculature cells inside the core region after ischemic stroke in adult mice. Brain Pathol. 2017 Jul;27(4):480-498. doi: 10.1111/bpa.12425. Epub 2016 Nov 4.

Johe KK, Hazel TG, Muller T, Dugich-Djordjevic MM, McKay RD. (1996) Single factors direct the differentiation of stem cells from the fetal and adult central nervous system. Genes Dev. 1996 Dec 15;10(24):3129-40.

Jung S, Wiest R, Gralla J, McKinley R, Mattle H, Liebeskind D. (2017) Relevance of the cerebral collateral circulation in ischaemic stroke: time is brain, but collaterals set the pace. Swiss Med Wkly. 2017 Dec 11;147:w14538. doi: 10.4414/smw.2017.14538. eCollection 2017.

Kalamakis G, Brüne D, Ravichandran S, Bolz J, Fan W, Ziebell F, Stiehl T, Catalá-Martinez F, Kupke J, Zhao S, Llorens-Bobadilla E, Bauer K, Limpert S, Berger B, Christen U, Schmezer P, Mallm JP, Berninger B, Anders S, Del Sol A, Marciniak-Czochra A, Martin-Villalba A. (2019) Quiescence Modulates Stem Cell Maintenance and Regenerative Capacity in the Aging Brain. Cell. 2019 Mar 7;176(6):1407-1419.e14. doi: 10.1016/j.cell.2019.01.040. Epub 2019 Feb 28.

Kalani MY, Cheshier SH, Cord BJ, Bababeygy SR, Vogel H, Weissman IL, Palmer TD, Nusse R. (2008) Wnt-mediated self-renewal of neural stem/progenitor cells. Proc Natl Acad Sci U S A. 2008 Nov 4;105(44):16970-5. doi: 10.1073/pnas.0808616105. Epub 2008 Oct 28.

Kang SH, Fukaya M, Yang JK, Rothstein JD, Bergles DE. (2010) NG2+ CNS glial progenitors remain committed to the oligodendrocyte lineage in postnatal life and following neurodegeneration. Neuron. 2010 Nov 18;68(4):668-81. doi: 10.1016/j.neuron.2010.09.009.

Kase Y, Otsu K, Shimazaki T, Okano H. (2019) Involvement of p38 in Age-Related Decline in Adult Neurogenesis via Modulation of Wnt Signaling. Stem Cell Reports. 2019 Jun 11;12(6):1313-1328. doi: 10.1016/j.stemcr.2019.04.010. Epub 2019 May 9.

Kietzman HW, Everson JL, Sulik KK, Lipinski RJ. (2014) The teratogenic effects of prenatal ethanol exposure are exacerbated by Sonic Hedgehog or GLI2 haploinsufficiency in the mouse. PLoS One. 2014 Feb 19;9(2):e89448. doi: 10.1371/journal.pone.0089448. eCollection 2014.

Kirdajova D and Anderova M. (2019) NG2 cells and their neurogenic potential. Curr Opin Pharmacol. 2019 Dec 23;50:53-60. doi: 10.1016/j.coph.2019.11.005. [Epub ahead of print]

Kokaia Z, Thored P, Arvidsson A, Lindvall O. (2006) Regulation of stroke-induced neurogenesis in adult brain--recent scientific progress. Cereb Cortex. 2006 Jul;16 Suppl 1:i162-7.

Komada M, Saitsu H, Kinboshi M, Miura T, Shiota K, Ishibashi M. (2008) Hedgehog signaling is involved in development of the neocortex. Development. 2008 Aug;135(16):2717-27. doi: 10.1242/dev.015891. Epub 2008 Jul 9.

Komitova M, Perfilieva E, Mattsson B, Eriksson PS, Johansson BB. (2006) Enriched environment after focal cortical ischemia enhances the generation of astroglia and NG2 positive polydendrocytes in adult rat neocortex. Exp Neurol. 2006 May;199(1):113-21. Epub 2006 Jan 20.

Komitova M, Serwanski DR, Lu QR, Nishiyama A. (2011) NG2 cells are not a major source of reactive astrocytes after neocortical stab wound injury. Glia. 2011 May;59(5):800-9. doi: 10.1002/glia.21152. Epub 2011 Feb 23.

Komitova M, Zhu X, Serwanski DR, Nishiyama A. (2009) NG2 cells are distinct from neurogenic cells in the postnatal mouse subventricular zone. J Comp Neurol. 2009 Feb 10;512(5):702-16. doi: 10.1002/cne.21917.

Konkle AT and McCarthy MM. (2011) Developmental time course of estradiol, testosterone, and dihydrotestosterone levels in discrete regions of male and female rat brain. Endocrinology. 2011 Jan;152(1):223-35. doi: 10.1210/en.2010-0607. Epub 2010 Nov 10.

Korinek V, Barker N, Moerer P, van Donselaar E, Huls G, Peters PJ, Clevers H. (1998) Depletion of epithelial stem-cell compartments in the small intestine of mice lacking Tcf-4. Nat Genet. 1998 Aug;19(4):379-83.

Kriska J, Honsa P, Dzamba D, Butenko O, Kolenicova D, Janeckova L, Nahacka Z, Andera L, Kozmik Z, Taketo MM, Korinek V, Anderova M. (2016) Manipulating Wnt signaling at different subcellular levels affects the fate of neonatal neural stem/progenitor cells. Brain Res. 2016 Nov 15;1651:73-87. doi: 10.1016/j.brainres.2016.09.026. Epub 2016 Sep 19.

Kunke D, Bryja V, Mygland L, Arenas E, Krauss S. (2009) Inhibition of canonical Wnt signaling promotes gliogenesis in P0-NSCs. Biochem Biophys Res Commun. 2009 Sep 4;386(4):628-33. doi: 10.1016/j.bbrc.2009.06.084. Epub 2009 Jun 21.

Lai K, Kaspar BK, Gage FH, Schaffer DV. (2003) Sonic hedgehog regulates adult neural progenitor proliferation in vitro and in vivo. Nat Neurosci. 2003 Jan;6(1):21-7.

Lamus F, Martín C, Carnicero E, Moro JA, Fernández JMF, Mano A, Gato Á, Alonso MI. (2020) FGF2/EGF contributes to brain neuroepithelial precursor proliferation and neurogenesis in rat embryos: the involvement of embryonic cerebrospinal fluid. Dev Dyn. 2020 Jan;249(1):141-153. doi: 10.1002/dvdy.135. Epub 2019 Dec 9.

Lee C, Hu J, Ralls S, Kitamura T, Loh YP, Yang Y, Mukouyama YS, Ahn S. (2012) The molecular profiles of neural stem cell niche in the adult subventricular zone. PLoS One. 2012;7(11):e50501. doi: 10.1371/journal.pone.0050501. Epub 2012 Nov 29.

Lembach A, Stahr A, Ali AAH, Ingenwerth M, von Gall C. (2018) Sex-Dependent Effects of Bmal1-Deficiency on Mouse Cerebral Cortex Infarction in Response to Photothrombotic Stroke. Int J Mol Sci. 2018 Oct 11;19(10). pii: E3124. doi: 10.3390/ijms19103124.

Lepourcelet M, Chen YN, France DS, Wang H, Crews P, Petersen F, Bruseo C, Wood AW, Shivdasani RA. (2004) Small-molecule antagonists of the oncogenic Tcf/beta-catenin protein complex. Cancer Cell. 2004 Jan;5(1):91-102.

Lewis C and Krieg PA. (2014) Reagents for developmental regulation of Hedgehog signaling. Methods. 2014 Apr 1;66(3):390-7. doi: 10.1016/j.ymeth.2013.08.022. Epub 2013 Aug 24.

Lie DC, Colamarino SA, Song HJ, Désiré L, Mira H, Consiglio A, Lein ES, Jessberger S, Lansford H, Dearie AR, Gage FH. (2005) Wnt signalling regulates adult hippocampal neurogenesis. Nature. 2005 Oct 27;437(7063):1370-5.

Lim X and Nusse R. (2013) Wnt signaling in skin development, homeostasis, and disease. Cold Spring Harb Perspect Biol. 2013 Feb 1;5(2). pii: a008029. doi: 10.1101/cshperspect.a008029.

Lin SC and Bergles DE. (2002) Physiological characteristics of NG2-expressing glial cells. J Neurocytol. 2002 Jul-Aug;31(6-7):537-49.

Liu C, Wu W, Zhang B, Xiang J, Zou J. (2013) Temporospatial expression and cellular localization of glutamine synthetase following traumatic spinal cord injury in adult rats. Mol Med Rep. 2013 May;7(5):1431-6. doi: 10.3892/mmr.2013.1383. Epub 2013 Mar 20.

Lu W, Yamamoto V, Ortega B, Baltimore D. (2004) Mammalian Ryk is a Wnt coreceptor required for stimulation of neurite outgrowth. Cell. 2004 Oct 1;119(1):97-108.

Lugert S, Basak O, Knuckles P, Haussler U, Fabel K, Götz M, Haas CA, Kempermann G, Taylor V, Giachino C. (2010) Quiescent and active hippocampal neural stem cells with distinct morphologies respond selectively to physiological and pathological stimuli and aging. Cell Stem Cell. 2010 May 7;6(5):445-56. doi: 10.1016/j.stem.2010.03.017.

Lui JH, Hansen DV, Kriegstein AR. (2001) Development and evolution of the human neocortex. Cell. 2011 Jul 8;146(1):18-36. doi: 10.1016/j.cell.2011.06.030.

Lukas J, Mazna P, Valenta T, Doubravska L, Pospichalova V, Vojtechova M, Fafilek B, Ivanek R, Plachy J, Novak J, Korinek V. (2009) Dazap2 modulates transcription driven by the Wnt effector TCF-4. Nucleic Acids Res. 2009 May;37(9):3007-20. doi: 10.1093/nar/gkp179. Epub 2009 Mar 20.

Lustig B, Jerchow B, Sachs M, Weiler S, Pietsch T, Karsten U, van de Wetering M, Clevers H, Schlag PM, Birchmeier W, Behrens J. (2002) Negative feedback loop of Wnt signaling through upregulation of conductin/axin2 in colorectal and liver tumors. Mol Cell Biol. 2002 Feb;22(4):1184-93.

Machon O, van den Bout CJ, Backman M, Røsok Ø, Caubit X, Fromm SH, Geronimo B, Krauss S. (2002) Forebrain-specific promoter/enhancer D6 derived from the mouse Dach1 gene controls expression in neural stem cells. Neuroscience. 2002;112(4):951-66.

Malatesta P, Appolloni I, Calzolari F. (2008) Radial glia and neural stem cells. Cell Tissue Res. 2008 Jan;331(1):165-78. Epub 2007 Sep 11.

Mardones MD, Andaur GA, Varas-Godoy M, Henriquez JF, Salech F, Behrens MI, Couve A, Inestrosa NC, Varela-Nallar L. (2016) Frizzled-1 receptor regulates adult hippocampal neurogenesis. Mol Brain. 2016 Mar 15;9:29. doi: 10.1186/s13041-016-0209-3.

Marinaro C, Pannese M, Weinandy F, Sessa A, Bergamaschi A, Taketo MM, Broccoli V, Comi G, Götz M, Martino G, Muzio L. (2012) Wnt signaling has opposing roles in the developing and the adult brain that are modulated by Hipk1. Cereb Cortex. 2012 Oct;22(10):2415-27. doi: 10.1093/cercor/bhr320. Epub 2011 Nov 17.

Marini C, Totaro R, Carolei A. (1999) Long-term prognosis of cerebral ischemia in young adults. National Research Council Study Group on Stroke in the Young. Stroke. 1999 Nov;30(11):2320-5.

Marques S, Zeisel A, Codeluppi S, van Bruggen D, Mendanha Falcão A, Xiao L, Li H, Häring M, Hochgerner H, Romanov RA, Gyllborg D, Muñoz Manchado A, La Manno G, Lönnerberg P, Floriddia EM, Rezayee F, Ernfors P, Arenas E, Hjerling-Leffler J, Harkany T, Richardson WD, Linnarsson S, Castelo-Branco G. (2016) Oligodendrocyte heterogeneity in the mouse juvenile and adult central nervous system. Science. 2016 Jun 10;352(6291):1326-1329. doi: 10.1126/science.aaf6463.

Martinez-Lozada Z, Waggener CT, Kim K, Zou S, Knapp PE, Hayashi Y, Ortega A, Fuss B. (2014) Activation of sodium-dependent glutamate transporters regulates the morphological aspects of oligodendrocyte maturation via signaling through calcium/calmodulin-dependent kinase IIβ's actin-binding/-stabilizing domain. Glia. 2014 Sep;62(9):1543-1558. doi: 10.1002/glia.22699. Epub 2014 May 28.

Mastrodonato A, Barbati SA, Leone L, Colussi C, Gironi K, Rinaudo M, Piacentini R, Denny CA, Grassi C. (2018) Olfactory memory is enhanced in mice exposed to extremely low-frequency electromagnetic fields via Wnt/β-catenin dependent modulation of subventricular zone neurogenesis. Sci Rep. 2018 Jan 10;8(1):262. doi: 10.1038/s41598-017-18676-1.

Matsumoto M, Hatakeyama T, Morimoto K, Yanagihara T. (1990) Cerebral blood flow and neuronal damage during progressive cerebral ischemia in gerbils. Stroke. 1990 Oct;21(10):1470-7.

Merkle FT, Fuentealba LC, Sanders TA, Magno L, Kessaris N, Alvarez-Buylla A. (2014) Adult neural stem cells in distinct microdomains generate previously unknown interneuron types. Nat Neurosci. 2014 Feb;17(2):207-14. doi: 10.1038/nn.3610. Epub 2013 Dec 22.

Meyers JR, Hu L, Moses A, Kaboli K, Papandrea A, Raymond PA. (2012) β-catenin/Wnt signaling controls progenitor fate in the developing and regenerating zebrafish retina. Neural Dev. 2012 Aug 24;7:30. doi: 10.1186/1749-8104-7-30.

Mierzwa AJ, Sullivan GM, Beer LA, Ahn S, Armstrong RC. (2014) Comparison of cortical and white matter traumatic brain injury models reveals differential effects in the subventricular zone and divergent Sonic hedgehog signaling pathways in neuroblasts and oligodendrocyte progenitors. ASN Neuro. 2014 Sep 23;6(5). pii: 1759091414551782. doi: 10.1177/1759091414551782. Print 2014.

Mikels AJ and Nusse R. (2006) Purified Wnt5a protein activates or inhibits beta-catenin-TCF signaling depending on receptor context. PLoS Biol. 2006 Apr;4(4):e115. Epub 2006 Apr 4.

Miller FD and Gauthier AS. (2007) Timing is everything: making neurons versus glia in the developing cortex. Neuron. 2007 May 3;54(3):357-69.

Mira H, Andreu Z, Suh H, Lie DC, Jessberger S, Consiglio A, San Emeterio J, Hortigüela R, Marqués-Torrejón MA, Nakashima K, Colak D, Götz M, Fariñas I, Gage FH. (2010) Signaling through BMPR-IA regulates quiescence and long-term activity of neural stem cells in the adult hippocampus. Cell Stem Cell. 2010 Jul 2;7(1):78-89. doi: 10.1016/j.stem.2010.04.016.

Molenaar M, van de Wetering M, Oosterwegel M, Peterson-Maduro J, Godsave S, Korinek V, Roose J, Destrée O, Clevers H. (1996) XTcf-3 transcription factor mediates beta-catenin-induced axis formation in Xenopus embryos. Cell. 1996 Aug 9;86(3):391-9.

Morrison SJ and Spradling AC. (2008) Stem cells and niches: mechanisms that promote stem cell maintenance throughout life. Cell. 2008 Feb 22;132(4):598-611. doi: 10.1016/j.cell.2008.01.038.

Mosimann C, Hausmann G, Basler K. (2009) Beta-catenin hits chromatin: regulation of Wnt target gene activation. Nat Rev Mol Cell Biol. 2009 Apr;10(4):276-86. doi: 10.1038/nrm2654.

Nadarajan V, Perry RJ, Johnson J, Werring DJ. (2014) Transient ischaemic attacks: mimics and chameleons. Pract Neurol. 2014 Feb;14(1):23-31. doi: 10.1136/practneurol-2013-000782.

Nakano M, Tamura Y, Yamato M, Kume S, Eguchi A, Takata K, Watanabe Y, Kataoka Y. (2017) NG2 glial cells regulate neuroimmunological responses to maintain neuronal function and survival. Sci Rep. 2017 Feb 14;7:42041. doi: 10.1038/srep42041.

Nalesso G, Sherwood J, Bertrand J, Pap T, Ramachandran M, De Bari C, Pitzalis C, Dell'accio F. (2011) WNT-3A modulates articular chondrocyte phenotype by activating both canonical and noncanonical pathways. J Cell Biol. 2011 May 2;193(3):551-64. doi: 10.1083/jcb.201011051.

Namba T, Mochizuki H, Onodera M, Mizuno Y, Namiki H, Seki T. (2005) The fate of neural progenitor cells expressing astrocytic and radial glial markers in the postnatal rat dentate gyrus. Eur J Neurosci. 2005 Oct;22(8):1928-41.

Nelson WJ and Nusse R. (2004) Convergence of Wnt, beta-catenin, and cadherin pathways. Science. 2004 Mar 5;303(5663):1483-7.

Neprasova H, Anderova M, Petrik D, Vargova L, Kubinova S, Chvatal A, Sykova E. (2007) High extracellular K(+) evokes changes in voltage-dependent K(+) and Na (+) currents and volume regulation in astrocytes. Pflugers Arch. 2007 Mar;453(6):839-49. Epub 2006 Oct 10.

Nishiyama A, Komitova M, Suzuki R, Zhu X. (2009) Polydendrocytes (NG2 cells): multifunctional cells with lineage plasticity. Nat Rev Neurosci. 2009 Jan;10(1):9-22. doi: 10.1038/nrn2495.

Noctor SC, Martínez-Cerdeño V, Ivic L, Kriegstein AR. (2004) Cortical neurons arise in symmetric and asymmetric division zones and migrate through specific phases. Nat Neurosci. 2004 Feb;7(2):136-44. Epub 2004 Jan 4.

Nusse R. (2008) Wnt signaling and stem cell control. Cell Res. 2008 May;18(5):523-7. doi: 10.1038/cr.2008.47.

O'Keeffe GC, Tyers P, Aarsland D, Dalley JW, Barker RA, Caldwell MA. (2009) Dopamine-induced proliferation of adult neural precursor cells in the mammalian subventricular zone is mediated through EGF. Proc Natl Acad Sci U S A. 2009 May 26;106(21):8754-9. doi: 10.1073/pnas.0803955106. Epub 2009 May 11.

Oliveira-Ferreira AI, Major S, Przesdzing I, Kang EJ, Dreier JP. (2019) Spreading depolarizations in the rat endothelin-1 model of focal cerebellar ischemia. J Cereb Blood Flow Metab. 2019 Jul 7:271678X19861604. doi: 10.1177/0271678X19861604. [Epub ahead of print]

Pai R, Tarnawski AS, Tran T. (2004) Deoxycholic acid activates beta-catenin signaling pathway and increases colon cell cancer growth and invasiveness. Mol Biol Cell. 2004 May;15(5):2156-63. Epub 2004 Mar 5.

Palma V, Lim DA, Dahmane N, Sánchez P, Brionne TC, Herzberg CD, Gitton Y, Carleton A, Alvarez-Buylla A, Ruiz i Altaba A. (2005) Sonic hedgehog controls stem cell behavior in the postnatal and adult brain. Development. 2005 Jan;132(2):335-44. Epub 2004 Dec 16.

Papachristou P, Dyberg C, Lindqvist M, Horn Z, Ringstedt T. (2014) Transgenic increase of Wnt7b in neural progenitor cells decreases expression of T-domain transcription factors and impairs neuronal differentiation. Brain Res. 2014 Aug 12;1576:27-34. doi: 10.1016/j.brainres.2014.06.015. Epub 2014 Jun 19.

Parish CL, Castelo-Branco G, Rawal N, Tonnesen J, Sorensen AT, Salto C, Kokaia M, Lindvall O, Arenas E. (2008) Wnt5a-treated midbrain neural stem cells improve dopamine cell replacement therapy in parkinsonian mice. J Clin Invest. 2008 Jan;118(1):149-60.

Pekny M, Wilhelmsson U, Pekna M. (2014) The dual role of astrocyte activation and reactive gliosis. Neurosci Lett. 2014 Apr 17;565:30-8. doi: 10.1016/j.neulet.2013.12.071. Epub 2014 Jan 7.

Pivonkova H, Benesova J, Butenko O, Chvatal A, Anderova M. (2010) Impact of global cerebral ischemia on K+ channel expression and membrane properties of glial cells in the rat

hippocampus. Neurochem Int. 2010 Dec;57(7):783-94. doi: 10.1016/j.neuint.2010.08.016. Epub 2010 Sep 15.

Pleasure SJ, Collins AE, Lowenstein DH. (2000) Unique expression patterns of cell fate molecules delineate sequential stages of dentate gyrus development. J Neurosci. 2000 Aug 15;20(16):6095-105.

Prajerova I, Honsa P, Chvatal A, Anderova M. (2010a) Neural stem/progenitor cells derived from the embryonic dorsal telencephalon of D6/GFP mice differentiate primarily into neurons after transplantation into a cortical lesion. Cell Mol Neurobiol. 2010 Mar;30(2):199-218. doi: 10.1007/s10571-009-9443-x. Epub 2009 Aug 26.

Prajerova I, Honsa P, Chvatal A, Anderova M. (2010b) Distinct effects of sonic hedgehog and Wnt-7a on differentiation of neonatal neural stem/progenitor cells in vitro. Neuroscience. 2010 Dec 15;171(3):693-711. doi: 10.1016/j.neuroscience.2010.09.023. Epub 2010 Sep 21.

Puig B, Brenna S, Magnus T. (2018) Molecular Communication of a Dying Neuron in Stroke. Int J Mol Sci. 2018 Sep 19;19(9). pii: E2834. doi: 10.3390/ijms19092834.

Qu Q, Sun G, Murai K, Ye P, Li W, Asuelime G, Cheung YT, Shi Y. (2013) Wnt7a regulates multiple steps of neurogenesis. Mol Cell Biol. 2013 Jul;33(13):2551-9. doi: 10.1128/MCB.00325-13. Epub 2013 Apr 29.

Rajsic S, Gothe H, Borba HH, Sroczynski G, Vujicic J, Toell T, Siebert U. (2019) Economic burden of stroke: a systematic review on post-stroke care. Eur J Health Econ. 2019 Feb;20(1):107-134. doi: 10.1007/s10198-018-0984-0. Epub 2018 Jun 16.

Rakic P. (1995) A small step for the cell, a giant leap for mankind: a hypothesis of neocortical expansion during evolution. Trends Neurosci. 1995 Sep;18(9):383-8.

Rama R and García JC. (2016) “Excitotoxicity and Oxidative Stress in Acute Stroke” in Ischemic Stroke – Updates. London: IntechOpen Limited, 2016. 17-42. doi: 10.5772/64991.

Ramasamy S, Narayanan G, Sankaran S, Yu YH, Ahmed S. (2013) Neural stem cell survival factors. Arch Biochem Biophys. 2013 Jun;534(1-2):71-87. doi: 10.1016/j.abb.2013.02.004. Epub 2013 Mar 5.

Rash BG and Grove EA. (2011) Shh and Gli3 regulate formation of the telencephalic-diencephalic junction and suppress an isthmus-like signaling source in the forebrain. Dev Biol. 2011 Nov 15;359(2):242-50. doi: 10.1016/j.ydbio.2011.08.026. Epub 2011 Sep 7.

Ravanelli AM, Kearns CA, Powers RK, Wang Y, Hines JH, Donaldson MJ, Appel B. (2018) Sequential specification of oligodendrocyte lineage cells by distinct levels of Hedgehog and Notch signaling. Dev Biol. 2018 Dec 15;444(2):93-106. doi: 10.1016/j.ydbio.2018.10.004. Epub 2018 Oct 19.

Reeves MJ, Bushnell CD, Howard G, Gargano JW, Duncan PW, Lynch G, Khatiwoda A, Lisabeth L. (2008) Sex differences in stroke: epidemiology, clinical presentation, medical care,

and outcomes. Lancet Neurol. 2008 Oct;7(10):915-26. doi: 10.1016/S1474-4422(08)70193-5. Epub 2008 Aug 21.

Rivers LE, Young KM, Rizzi M, Jamen F, Psachoulia K, Wade A, Kessaris N, Richardson WD. (2008) PDGFRA/NG2 glia generate myelinating oligodendrocytes and piriform projection neurons in adult mice. Nat Neurosci. 2008 Dec;11(12):1392-401. doi: 10.1038/nn.2220. Epub 2008 Oct 8.

Rosenblum S, Wang N, Smith TN, Pendharkar AV, Chua JY, Birk H, Guzman R. (2012) Timing of intra-arterial neural stem cell transplantation after hypoxia-ischemia influences cell engraftment, survival, and differentiation. Stroke. 2012 Jun;43(6):1624-31. doi: 10.1161/STROKEAHA.111.637884. Epub 2012 Apr 24.

Rossi DJ, Brady JD, Mohr C. (2007) Astrocyte metabolism and signaling during brain ischemia. Nat Neurosci. 2007 Nov;10(11):1377-86.

Roth M, Gaceb A, Enström A, Padel T, Genové G, Özen I, Paul G. (2019) Regulator of G-protein signaling 5 regulates the shift from perivascular to parenchymal pericytes in the chronic phase after stroke. FASEB J. 2019 Aug;33(8):8990-8998. doi: 10.1096/fj.201900153R. Epub 2019 May 2.

Ruzicka J, Machova-Urdzikova L, Gillick J, Amemori T, Romanyuk N, Karova K, Zaviskova K, Dubisova J, Kubinova S, Murali R, Sykova E, Jhanwar-Uniyal M, Jendelova P. (2017) A Comparative Study of Three Different Types of Stem Cells for Treatment of Rat Spinal Cord Injury. Cell Transplant. 2017 Apr 13;26(4):585-603. doi: 10.3727/096368916X693671. Epub 2016 Nov 2.

Saitoh F and Araki T. (2010) Proteasomal degradation of glutamine synthetase regulates schwann cell differentiation. J Neurosci. 2010 Jan 27;30(4):1204-12. doi: 10.1523/JNEUROSCI.3591-09.2010.

Seib DR, Corsini NS, Ellwanger K, Plaas C, Mateos A, Pitzer C, Niehrs C, Celikel T, Martin-Villalba A. (2013) Loss of Dickkopf-1 restores neurogenesis in old age and counteracts cognitive decline. Cell Stem Cell. 2013 Feb 7;12(2):204-14. doi: 10.1016/j.stem.2012.11.010.

Serwanski DR, Jukkola P, Nishiyama A. (2017) Heterogeneity of astrocyte and NG2 cell insertion at the node of ranvier. J Comp Neurol. 2017 Feb 15;525(3):535-552. doi: 10.1002/cne.24083. Epub 2016 Aug 18.

Seshadri S, Beiser A, Kelly-Hayes M, Kase CS, Au R, Kannel WB, Wolf PA. (2006) The lifetime risk of stroke: estimates from the Framingham Study. Stroke. 2006 Feb;37(2):345-50. Epub 2006 Jan 5.

Shimizu T, Kagawa T, Wada T, Muroyama Y, Takada S, Ikenaka K. (2005) Wnt signaling controls the timing of oligodendrocyte development in the spinal cord. Dev Biol. 2005 Jun 15;282(2):397-410.

Shruster A, Ben-Zur T, Melamed E, Offen D. (2012) Wnt signaling enhances neurogenesis and improves neurological function after focal ischemic injury. PLoS One. 2012;7(7):e40843. doi: 10.1371/journal.pone.0040843. Epub 2012 Jul 17.

Sierra A, Encinas JM, Deudero JJ, Chancey JH, Enikolopov G, Overstreet-Wadiche LS, Tsirka SE, Maletic-Savatic M. (2010) Microglia shape adult hippocampal neurogenesis through apoptosis-coupled phagocytosis. Cell Stem Cell. 2010 Oct 8;7(4):483-95. doi: 10.1016/j.stem.2010.08.014.

Simon C, Götz M, Dimou L. (2011) Progenitors in the adult cerebral cortex: cell cycle properties and regulation by physiological stimuli and injury. Glia. 2011 Jun;59(6):869-81. doi: 10.1002/glia.21156. Epub 2011 Mar 28.

Sirko S, Behrendt G, Johansson PA, Tripathi P, Costa M, Bek S, Heinrich C, Tiedt S, Colak D, Dichgans M, Fischer IR, Plesnila N, Staufenbiel M, Haass C, Snapyan M, Saghatelyan A, Tsai LH, Fischer A, Grobe K, Dimou L, Götz M. (2013) Reactive glia in the injured brain acquire stem cell properties in response to sonic hedgehog. [corrected]. Cell Stem Cell. 2013 Apr 4;12(4):426-39. doi: 10.1016/j.stem.2013.01.019.

Smyth LCD, Rustenhoven J, Scotter EL, Schweder P, Faull RLM, Park TIH, Dragunow M5. (2018) Markers for human brain pericytes and smooth muscle cells. J Chem Neuroanat. 2018 Oct;92:48-60. doi: 10.1016/j.jchemneu.2018.06.001. Epub 2018 Jun 7.

Sorrells SF, Paredes MF, Cebrian-Silla A, Sandoval K, Qi D, Kelley KW, James D, Mayer S, Chang J, Auguste KI, Chang EF, Gutierrez AJ, Kriegstein AR, Mathern GW, Oldham MC, Huang EJ, Garcia-Verdugo JM, Yang Z, Alvarez-Buylla A. (2018) Human hippocampal neurogenesis drops sharply in children to undetectable levels in adults. Nature. 2018 Mar 15;555(7696):377-381. doi: 10.1038/nature25975. Epub 2018 Mar 7.

Spassky N, Goujet-Zalc C, Parmantier E, Olivier C, Martinez S, Ivanova A, Ikenaka K, Macklin W, Cerruti I, Zalc B, Thomas JL. (1998) Multiple restricted origin of oligodendrocytes. J Neurosci. 1998 Oct 15;18(20):8331-43.

Stallcup WB. (1981) The NG2 antigen, a putative lineage marker: immunofluorescent localization in primary cultures of rat brain. Dev Biol. 1981 Apr 15;83(1):154-65.

Takada K, Zhu D, Bird GH, Sukhdeo K, Zhao JJ, Mani M, Lemieux M, Carrasco DE, Ryan J, Horst D, Fulciniti M, Munshi NC, Xu W, Kung AL, Shivdasani RA, Walensky LD, Carrasco DR. (2012) Targeted disruption of the BCL9/β-catenin complex inhibits oncogenic Wnt signaling. Sci Transl Med. 2012 Aug 22;4(148):148ra117. doi: 10.1126/scitranslmed.3003808.

Tanaka K, Nogawa S, Ito D, Suzuki S, Dembo T, Kosakai A, Fukuuchi Y. (2001) Activation of NG2-positive oligodendrocyte progenitor cells during post-ischemic reperfusion in the rat brain. Neuroreport. 2001 Jul 20;12(10):2169-74.

Tannenberg RK, Scott HL, Westphalen RI, Dodd PR. (2004) The identification and characterization of excitotoxic nerve-endings in Alzheimer disease. Curr Alzheimer Res. 2004 Feb;1(1):11-25.

Tanner DC, Cherry JD, Mayer-Pröschel M. (2011) Oligodendrocyte progenitors reversibly exit the cell cycle and give rise to astrocytes in response to interferon-γ. J Neurosci. 2011 Apr 20;31(16):6235-46. doi: 10.1523/JNEUROSCI.5905-10.2011.

Tashiro A, Sandler VM, Toni N, Zhao C, Gage FH. (2006) NMDA-receptor-mediated, cell-specific integration of new neurons in adult dentate gyrus. Nature. 2006 Aug 24;442(7105):929-33. Epub 2006 Aug 13.

Tawk M, Makoukji J, Belle M, Fonte C, Trousson A, Hawkins T, Li H, Ghandour S, Schumacher M, Massaad C. (2011) Wnt/beta-catenin signaling is an essential and direct driver of myelin gene expression and myelinogenesis. J Neurosci. 2011 Mar 9;31(10):3729-42. doi: 10.1523/JNEUROSCI.4270-10.2011.

ten Berge D, Brugmann SA, Helms JA, Nusse R. (2008) Wnt and FGF signals interact to coordinate growth with cell fate specification during limb development. Development. 2008 Oct;135(19):3247-57. doi: 10.1242/dev.023176.

Tsoa RW, Coskun V, Ho CK, de Vellis J, Sun YE. (2014) Spatiotemporally different origins of NG2 progenitors produce cortical interneurons versus glia in the mammalian forebrain. Proc Natl Acad Sci U S A. 2014 May 20;111(20):7444-9. doi: 10.1073/pnas.1400422111. Epub 2014 May 5.

Tu J, Yang F, Wan J, Liu Y, Zhang J, Wu B, Liu Y, Zeng S, Wang L. (2014) Light-controlled astrocytes promote human mesenchymal stem cells toward neuronal differentiation and improve the neurological deficit in stroke rats. Glia. 2014 Jan;62(1):106-21. doi: 10.1002/glia.22590. Epub 2013 Nov 6.

Ugbode CI, Smith I, Whalley BJ, Hirst WD, Rattray M. (2017) Sonic hedgehog signalling mediates astrocyte crosstalk with neurons to confer neuroprotection. J Neurochem. 2017 Aug;142(3):429-443. doi: 10.1111/jnc.14064. Epub 2017 Jun 20.

Urbán N and Guillemot F. (2014) Neurogenesis in the embryonic and adult brain: same regulators, different roles. Front Cell Neurosci. 2014 Nov 27;8:396. doi: 10.3389/fncel.2014.00396. eCollection 2014.

Valny M, Honsa P, Kriska J, Anderova M. (2017) Multipotency and therapeutic potential of NG2 cells. Biochem Pharmacol. 2017 Oct 1;141:42-55. doi: 10.1016/j.bcp.2017.05.008. Epub 2017 May 15.

Valny M, Honsa P, Waloschkova E, Matuskova H, Kriska J, Kirdajova D, Androvic P, Valihrach L, Kubista M, Anderova M. (2018) A single-cell analysis reveals multiple roles of oligodendroglial lineage cells during post-ischemic regeneration. Glia. 2018 May;66(5):1068-1081. doi: 10.1002/glia.23301. Epub 2018 Feb 2.

van Amerongen R. (2012) Alternative Wnt pathways and receptors. Cold Spring Harb Perspect Biol. 2012 Oct 1;4(10). pii: a007914. doi: 10.1101/cshperspect.a007914.

van Amerongen R and Berns A. (2006) Knockout mouse models to study Wnt signal transduction. Trends Genet. 2006 Dec;22(12):678-89. Epub 2006 Oct 11.

Vancamp P, Gothié JD, Luongo C, Sébillot A, Le Blay K, Butruille L, Pagnin M, Richardson SJ, Demeneix BA, Remaud S. (2019) Gender-specific effects of transthyretin on neural stem cell fate in the subventricular zone of the adult mouse. Sci Rep. 2019 Dec 23;9(1):19689. doi: 10.1038/s41598-019-56156-w.

VanGilder RL, Huber JD, Rosen CL, Barr TL. (2012) The transcriptome of cerebral ischemia. Brain Res Bull. 2012 Jul 1;88(4):313-9. doi: 10.1016/j.brainresbull.2012.02.002. Epub 2012 Feb 21.

Varela-Nallar L, Arredondo SB, Tapia-Rojas C, Hancke J, Inestrosa NC. (2015) Andrographolide Stimulates Neurogenesis in the Adult Hippocampus. Neural Plast. 2015;2015:935403. doi: 10.1155/2015/935403. Epub 2015 Dec 22.

Vay SU, Flitsch LJ, Rabenstein M, Rogall R, Blaschke S, Kleinhaus J, Reinert N, Bach A, Fink GR, Schroeter M, Rueger MA. (2018) The plasticity of primary microglia and their multifaceted effects on endogenous neural stem cells in vitro and in vivo. J Neuroinflammation. 2018 Aug 13;15(1):226. doi: 10.1186/s12974-018-1261-y.

Ventura A, Kirsch DG, McLaughlin ME, Tuveson DA, Grimm J, Lintault L, Newman J, Reczek EE, Weissleder R, Jacks T. (2007) Restoration of p53 function leads to tumour regression in vivo. Nature. 2007 Feb 8;445(7128):661-5. Epub 2007 Jan 24.

Verma M, Wills Z, Chu CT. (2018) Excitatory Dendritic Mitochondrial Calcium Toxicity: Implications for Parkinson's and Other Neurodegenerative Diseases. Front Neurosci. 2018 Aug 2;12:523. doi: 10.3389/fnins.2018.00523. eCollection 2018.

Vrselja Z, Brkic H, Mrdenovic S, Radic R, Curic G. (2014) Function of circle of Willis. J Cereb Blood Flow Metab. 2014 Apr;34(4):578-84. doi: 10.1038/jcbfm.2014.7. Epub 2014 Jan 29.

Vukovic J, Blackmore DG, Jhaveri D, Bartlett PF. (2011) Activation of neural precursors in the adult neurogenic niches. Neurochem Int. 2011 Sep;59(3):341-6. doi: 10.1016/j.neuint.2011.04.003. Epub 2011 May 27.

Wallmen B, Schrempp M, Hecht A. (2012) Intrinsic properties of Tcf1 and Tcf4 splice variants determine cell-type-specific Wnt/β-catenin target gene expression. Nucleic Acids Res. 2012 Oct;40(19):9455-69. doi: 10.1093/nar/gks690. Epub 2012 Aug 2.

Walz W. (2000) Controversy surrounding the existence of discrete functional classes of astrocytes in adult gray matter. Glia. 2000 Aug;31(2):95-103.

Wang L, Geng J, Qu M, Yuan F, Wang Y, Pan J, Li Y, Ma Y, Zhou P, Zhang Z, Yang GY. (2020) Oligodendrocyte precursor cells transplantation protects blood-brain barrier in a mouse model of brain ischemia via Wnt/β-catenin signaling. Cell Death Dis. 2020 Jan 6;11(1):9. doi: 10.1038/s41419-019-2206-9.

Wang X, Mao X, Xie L, Greenberg DA, Jin K. (2009) Involvement of Notch1 signaling in neurogenesis in the subventricular zone of normal and ischemic rat brain in vivo. J Cereb Blood Flow Metab. 2009 Oct;29(10):1644-54. doi: 10.1038/jcbfm.2009.83. Epub 2009 Jun 17.

Wardlaw JM, Murray V, Berge E, del Zoppo GJ. (2014) Thrombolysis for acute ischaemic stroke. Cochrane Database Syst Rev. 2014 Jul 29;(7):CD000213. doi: 10.1002/14651858.CD000213.pub3.

Wetterling F, Chatzikonstantinou E, Tritschler L, Meairs S, Fatar M, Schad LR, Ansar S. (2016) Investigating potentially salvageable penumbra tissue in an in vivo model of transient ischemic stroke using sodium, diffusion, and perfusion magnetic resonance imaging. BMC Neurosci. 2016 Dec 7;17(1):82.

White BC, Sullivan JM, DeGracia DJ, O'Neil BJ, Neumar RW, Grossman LI, Rafols JA, Krause GS. (2000) Brain ischemia and reperfusion: molecular mechanisms of neuronal injury. J Neurol Sci. 2000 Oct 1;179(S 1-2):1-33.

Wiese KE, Nusse R, van Amerongen R. (2018) Wnt signalling: conquering complexity. Development. 2018 Jun 26;145(12). pii: dev165902. doi: 10.1242/dev.165902.

Winkler CC and Franco SJ. (2019) Loss of Shh signaling in the neocortex reveals heterogeneous cell recovery responses from distinct oligodendrocyte populations. Dev Biol. 2019 Aug 1;452(1):55-65. doi: 10.1016/j.ydbio.2019.04.016. Epub 2019 May 6.

Wolterink-Donselaar IG, Meerding JM, Fernandes C. (2009) A method for gender determination in newborn dark pigmented mice. Lab Anim (NY). 2009 Jan;38(1):35-8. doi: 10.1038/laban0109-35.

Woodruff TM, Thundyil J, Tang SC, Sobey CG, Taylor SM, Arumugam TV. (2011) Pathophysiology, treatment, and animal and cellular models of human ischemic stroke. Mol Neurodegener. 2011 Jan 25;6(1):11. doi: 10.1186/1750-1326-6-11.

Wu X, Tu X, Joeng KS, Hilton MJ, Williams DA, Long F. (2008) Rac1 activation controls nuclear localization of beta-catenin during canonical Wnt signaling. Cell. 2008 Apr 18;133(2):340-53. doi: 10.1016/j.cell.2008.01.052.

Xia T, Zhang H, Zhang L, Yang X, Sun G, Chen J, Xu D, Zhao C. (2019) Comparative and evolutionary analysis of the reptilian hedgehog gene family (*Shh*, *Dhh*, and *Ihh*). PeerJ. 2019 Aug 30;7:e7613. doi: 10.7717/peerj.7613. eCollection 2019.

Yang H, Zhu Q, Cheng J, Wu Y, Fan M, Zhang J, Wu H. (2019) Opposite regulation of Wnt/β-catenin and Shh signaling pathways by Rack1 controls mammalian cerebellar development. Proc Natl Acad Sci U S A. 2019 Mar 5;116(10):4661-4670. doi: 10.1073/pnas.1813244116. Epub 2019 Feb 14.

Yang Z, Suzuki R, Daniels SB, Brunquell CB, Sala CJ, Nishiyama A. (2006) NG2 glial cells provide a favorable substrate for growing axons. J Neurosci. 2006 Apr 5;26(14):3829-39.

Yao C, Williams AJ, Cui P, Berti R, Hunter JC, Tortella FC, Dave JR. (2002) Differential pattern of expression of voltage-gated sodium channel genes following ischemic brain injury in rats. Neurotox Res. 2002 Feb;4(1):67-75.

Yao GY, Zhu Q, Xia J, Chen FJ, Huang M, Liu J, Zhou TT, Wei JF, Cui GY, Zheng KY, Hou XY. (2018) Ischemic postconditioning confers cerebroprotection by stabilizing VDACs after brain ischemia. Cell Death Dis. 2018 Oct 10;9(10):1033. doi: 10.1038/s41419-018-1089-5.

Yoo S and Wrathall JR. (2007) Mixed primary culture and clonal analysis provide evidence that NG2 proteoglycan-expressing cells after spinal cord injury are glial progenitors. Dev Neurobiol. 2007 Jun;67(7):860-74.

Zehendner CM, Sebastiani A, Hugonnet A, Bischoff F, Luhmann HJ, Thal SC. (2015) Traumatic brain injury results in rapid pericyte loss followed by reactive pericytosis in the cerebral cortex. Sci Rep. 2015 Sep 3;5:13497. doi: 10.1038/srep13497.

Zhang RL, Chopp M, Roberts C, Liu X, Wei M, Nejad-Davarani SP, Wang X, Zhang ZG. (2014a) Stroke increases neural stem cells and angiogenesis in the neurogenic niche of the adult mouse. PLoS One. 2014 Dec 1;9(12):e113972. doi: 10.1371/journal.pone.0113972. eCollection 2014.

Zhang Y, Chen K, Sloan SA, Bennett ML, Scholze AR, O'Keeffe S, Phatnani HP, Guarnieri P, Caneda C, Ruderisch N, Deng S, Liddelow SA, Zhang C, Daneman R, Maniatis T, Barres BA, Wu JQ. (2014b) An RNA-sequencing transcriptome and splicing database of glia, neurons, and vascular cells of the cerebral cortex. J Neurosci. 2014 Sep 3;34(36):11929-47. doi: 10.1523/JNEUROSCI.1860-14.2014.

Zhang X, Zhu C, Luo Q, Dong J, Liu L, Li M, Zhu H, Ma X, Wang J. (2016) Impact of siRNA targeting of β-catenin on differentiation of rat neural stem cells and gene expression of Ngn1 and BMP4 following in vitro hypoxic-ischemic brain damage. Mol Med Rep. 2016 Oct;14(4):3595-601. doi: 10.3892/mmr.2016.5667. Epub 2016 Aug 24.

Zhang Z, Hartmann H, Do VM, Abramowski D, Sturchler-Pierrat C, Staufenbiel M, Sommer B, van de Wetering M, Clevers H, Saftig P, De Strooper B, He X, Yankner BA. (1998) Destabilization of beta-catenin by mutations in presenilin-1 potentiates neuronal apoptosis. Nature. 1998 Oct 15;395(6703):698-702.

Zhao JW, Raha-Chowdhury R, Fawcett JW, Watts C. (2009) Astrocytes and oligodendrocytes can be generated from NG2+ progenitors after acute brain injury: intracellular localization of oligodendrocyte transcription factor 2 is associated with their fate choice. Eur J Neurosci. 2009 May;29(9):1853-69. doi: 10.1111/j.1460-9568.2009.06736.x. Epub 2009 Apr 28.

Zhao W, Belayev L, Ginsberg MD. (1997) Transient middle cerebral artery occlusion by intraluminal suture: II. Neurological deficits, and pixel-based correlation of histopathology with local blood flow and glucose utilization. J Cereb Blood Flow Metab. 1997 Dec;17(12):1281-90.

Zhu X, Hill RA, Dietrich D, Komitova M, Suzuki R, Nishiyama A. (2011) Age-dependent fate and lineage restriction of single NG2 cells. Development. 2011 Feb;138(4):745-53. doi: 10.1242/dev.047951.

Online sources

Stroke <http://brainmind.com/Stroke.html> [20.3.2020]

Transcription factor Sp1 <https://www.uniprot.org/uniprot/P08047#function> [20.3.2020]

8 ATTACHMENTS

Kriska J, Honsa P, Dzamba D, Butenko O, Kolenicova D, Janeckova L, Nahacka Z, Andera L, Kozmik Z, Taketo MM, Korinek V, Anderova M. (2016) Manipulating Wnt signaling at different subcellular levels affects the fate of neonatal neural stem/progenitor cells. Brain Res. 2016 Nov 15;1651:73-87. doi: 10.1016/j.brainres.2016.09.026. Epub 2016 Sep 19.; **IF 2.746**

Valny M, Honsa P, Waloschkova E, Matuskova H, **Kriska J**, Kirdajova D, Androvic P, Valihrach L, Kubista M, Anderova M. (2018) A single-cell analysis reveals multiple roles of oligodendroglial lineage cells during post-ischemic regeneration. Glia. 2018 May;66(5):1068-1081. doi: 10.1002/glia.23301. Epub 2018 Feb 2.; **IF 5.829**

Honsa P, Valny M, **Kriska J**, Matuskova H, Harantova L, Kirdajova D, Valihrach L, Androvic P, Kubista M, Anderova M. (2016) Generation of reactive astrocytes from NG2 cells is regulated by sonic hedgehog. Glia. 2016 Sep;64(9):1518-31. doi: 10.1002/glia.23019. Epub 2016 Jun 24.; **IF 6.200**